

Study of enhanced oil recovery using polymer-stabilised CO₂-Foam

By: Saham Sherhani



A Doctoral Thesis submitted in partial fulfilment of the requirements
for the award of the degree of

Doctor of Philosophy

2020/2021

Supervisors

Dr. Pedro Diaz

Dr. Suela Kellici

Acknowledgement

First and foremost, I am grateful to Almighty **ALLAH**, who has given me the strength to complete my research.

I would like to acknowledge everyone who played a role in my academic accomplishments.

My family, who supported me throughout the project.

My supervisors, each of whom has provided guidance throughout the research process.

Last but not least, I would like to express my appreciation to the technicians in the School of Engineering for their assistance towards my research. A special thanks to my dear friend Dr. Hassan Zabihi, who has supported me with patience and understanding.

Without you all, I could never have reached this current level of success. Thank you all for your unwavering support.

Abstract

CO₂ is one of the most widely used gases in flooding processes due to solubility of CO₂ in oil that can efficiently reduce oil viscosity at reservoir pressure. However, low viscosity of CO₂ gas, results in early gas breakthrough, poor sweep efficiency, viscous fingering, and channelling that result in low oil recovery. Due to low viscosity, gases tend to have higher mobility than oil and water which leads to gravity override and channelling through oil in the rocks. This decreases the amount of oil being (Xu et. al., 2017).

Foam flooding processes have been used successfully for more than 6 decays, but more work has to be done to better understand and optimize the process for successful field implementation.

Foam is an EOR technique that significantly can improve the macroscopic sweep efficiency by lowering the gas mobility. Due to limited stability of conventional surfactants for foam generation, foam is not being widely used as a common EOR technique. One proposed approach for foam stabilization is the addition of polymers, so called polymer enhanced foam.

Hydrophobically modified polyacrylamide is a type of associative polymers that has been introduced to oil field applications as an alternative to conventional HPAM for the past two decades. The main characteristics of these polymers are their significant enhancement of solution viscosity, salinity tolerance and temperature resistance in comparison with conventional polymers such as HPAM, which would be more important in real applications.

The aim of this project was to study the effect of novel phenyl-polyacrylamide (PPAM)- a hydrophobically modified polyacrylamide- as a potential viscosifier in foam flooding process.

The two main objectives of this work were to study the change in the rheological behavior of polymeric foam in rocks with differing morphological properties, namely permeability and heterogeneity. Also, to study the effect of hydrophobically modified polymer on oil displacement.

Based on the results of sand pack floods, it was concluded that permeability and type of polymer govern the trend of apparent viscosity growth and decay for a given sand

permeability. The permeability of the sand had significantly influenced the foam viscosity, it was concluded that the heterogeneity of a sand pack does affect foam dynamics.

Oil displacement tests were further conducted through consolidated core samples (Bentheimer sandstone). Greater mobility reduction was observed for PPAM foam. This can be due to its larger molecular structure in solution which increases polymer viscosity.

The core flooding results indicated that PPAM-foam resulted in higher oil recovery compared to HPAM-foam and surfactant foam, at the same condition.

Viscosity reduction of PPAM foam in core flood test for sandstone was lower than HPAM foam at the same conditions. Therefore, it can be considered as a good candidate for EOR at reservoir condition.

List of Abbreviations

AM	Acrylamide monomer
API	American petroleum Institute
BPR	Back Pressure Regulator
C*	Critical Aggregation concentration
C ₃ H ₅ NO	Acrylamide monomer Chemical formula
C ₉ H ₉ NO	Phenyl-acrylamide monomer
CMC	Critical Micelle concentration
-CONH ₂ -	Amide group
COO ⁻	Carboxylate group
cp	Centi-poise
E	Overall sweep efficiency
E _d	Microscopic sweep efficiency
E _i	Vertical sweep efficiency
EOR	Enhanced Oil Recovery
E _s	Aerial sweep efficiency
E _V	Volumetric sweep efficiency
FT-IR	Fourier Transform Infra-red Spectroscopy
HMPAM	Hydrophobically modified polyacrylamide
HMPs	Hydrophobically modified polymers

H-NMR	Nuclear magnetic resonance
HPAM	Hydrolyzed polyacrylamide
IPV	Inaccessible pore volume
KO	Oil permeability
Kro	Oil relative permeability
K_{rw}	Water relative permeability
K_w	Water permeability
L	Length
M	Mobility
mD	Milli-darcy
mPa.s	Milli pascal. Second
PPAM	Phenyl polyacrylamide
ppm	Part-per-million
PV	Pore volume
q	Fluid flow rate
RF	Resistance factor (mobility reduction factor)
SDS	Sodium dodecyl sulphate Sor Residual oil saturation
Sor	Residual oil saturation
T	Temperature
UV	Ultra-violet spectroscopy

List of Figures

Figure 2. 1: presentation of symmetric foam (a 2D interface of a bulk foam system) (Schramm,1994).....	11
Figure 2. 2: Mechanism for foam generation via snap-off a) gas invades the pore body, b) gas enters the pore body, and c) wetting fluid moves back to snap off the gas thread	14
Figure 2. 3: Mechanism for foam generation via lamella division (Kovscek and Radke 1994).	15
Figure 2. 4: Mechanism for foam generation via leave-behind (Kovscek and Radke 1994). ..	16
Figure 2. 5: Schematic of a common black film. Surfactant molecules accumulate at gas-liquid interfaces (Farajzadeh et al., 2008).	17
Figure 2. 6: A schematic showing the relationship between disjoining pressure, Π and film thickness, h for (1) stable films; (2) metastable films; (3) unstable films (Kornev et al., 1999).	18
Figure 2. 7: Capillary pressure vs liquid saturation.....	19
Figure 2. 8: Possible fate of an oil drop in solution approaching gas-surfactant solution interface. (Aveyard et. al., 1994)	21
Figure 2. 9: Steady-state pressure drops in a sand pack as a function of superficial phase velocities (Osterloh and Jante, 1992).	24
Figure 2. 10: HPAM molecule structure (Shaohua, 2015).	28
Figure 2. 11: Schematic illustration of the three retention mechanisms in a porous network, namely adsorption, mechanical trapping, and hydrodynamic retention (Sorbie, 2013).	30
Figure 2. 12: Berea sandstone pore with polymer enhanced foam lamellae (Kutay a Schramm, 2004).	31
Figure 2. 13: structure of surfactant molecule	32
Figure 2. 14: Classification of surfactants	34

Figure 2. 15: Relationship between surfactant concentration and surface tension (Shramm, 2000)	35
Figure 3. 1: Experimental flow chart.....	37
Figure 3. 2: Mattson satellite FT-IR.....	39
Figure 3. 3: NMR spectrometer (Pulsar) for High Performance NMR Spectroscopy.....	40
Figure 3. 4: Polymer solution preparation by using a magnet stirrer.	43
Figure 3. 5: Pendant drop set-up.	44
Figure 3. 6: Schematic process of the pendant drop method.	45
Figure 3. 7: a) Schematic solution drop with the parameters needed for surface tension measurement, b) the captured picture from a surfactant/brine solution drop.	45
Figure 3. 8: IFT vs surfactant concentration by pendant drop method.....	46
Figure 3. 9: Bohlin Rheometer	47
Figure 3. 10: Schematic of the foam column set-up used for foam generation and foam stability study.....	48
Figure 3. 11: Sieve analysis of soil.....	50
Figure 3. 12: KDS syringe pump	51
Figure 3. 13: A schematic illustration of the experimental set-up used for permeability and adsorption measurements.....	52
Figure 3. 14: Sand-pack flooding system.	54
Figure 3. 15: ISCO pump.....	56
Figure 3. 16: Mass EL-FLOW meter by Bronkhorst.....	58
Figure 3. 17: EL-PRESS pressure meter by Bronkhorst.	59
Figure 3. 18: Schematic set-up of slim tube.	61

Figure 3. 19: Slim tube set-up	61
Figure 3. 20: Schematics of core holder set-up	65
Figure 3. 21: Core flood system.	65
Figure 3. 22: Core holder cylinder and as dismantled to the right	66
Figure 3. 23: Hydraulic pump.....	67
Figure 3. 24: Vacuum pump for core saturation.....	68
Figure 3. 25: Soxhlet extractor for core cleaning.....	70
Figure 4. 1: Height decay profile of foam in presence of oil (using five different surfactants)	74
Figure 4. 2: Height decay profile of foam in absence of oil (using five different surfactants)	74
Figure 4. 3: The liquid fraction of foam a) Cocobetaine, b) , SDS and c) CocoSDS after 40 min from the onset of the experiments	76
Figure 4. 4: Effect of IOS concentration on foam stability.....	78
Figure 4. 5: FT-IR spectrum of sample of P(acrylamide/phenyl-acrylamide).....	79
Figure 4. 6: H-NMR spectrum of a sample of P (acrylamide/phenyl- acrylamide) containing 1.2 mol % hydrophobe.....	79
Figure 4. 7: Effect of polymers concentration on viscosity	80
Figure 4. 8: Effect of NaCl on viscosity.....	81
Figure 4. 9: Height decay profile of a) IOS foam, b) CocoSDS foam, both with and without polymer in absence of oil.....	82
Figure 4. 10: Height decay profile of a) IOS foam, b) CocoSDS foam, both with and without polymer in presence of oil	83
Figure 4. 11: Pressure drop versus brine flow rate in sand pack.....	86

Figure 4. 12: Absolute pressures (millibar) as a function of time (min) in SP1 (injection of F2)	88
Figure 4. 13: Pressures gradient (millibar/cm) as a function of time (min) in SP1 (injection of F2)	89
Figure 4. 14: Absolute pressures (millibar) as a function of time (min) in SP1 (injection of F4)	91
Figure 4. 15: Pressures gradient (millibar/cm) as a function of time (min) in SP1 (injection of F4)	92
Figure 4. 16: Absolute pressures (millibar) as a function of time (min) in SP2 (injection of F6)	93
Figure 4. 17: Pressures gradient (millibar/cm) as a function of time (min) in SP2 (injection of F6)	94
Figure 4. 18: Absolute pressures (millibar) as a function of time (min) in SP3 (injection of F1, F3 and F5)	95
Figure 4. 19: Pressures gradient (millibar/cm) as a function of time (min) in SP3 (injection of F1, F3 and F5)	96
Figure 4. 20: Oil recovery by continuous water injection (CWI)	101
Figure 4. 21: MMP measurement for initial slim tube experiments	103
Figure 4. 22: MMP measured by using the oil recovery (run 2)	103
Figure 4. 23: Visual cell: (a) clean/empty state, (b) when oil and CO ₂ are present at immiscible pressure and (c) when oil and CO ₂ are present at miscible pressure.	104
Figure 4. 24: Oil recovery by CCI from core samples A and B.	105
Figure 4. 25: Oil recovery comparison of different methods of CGI and CWI in sandstone core samples.	106
Figure 4. 26: Pressure drop in core B (500mD) using CocoSDS and IOS foam	108

Figure 4. 27: Oil recovery in core B (500mD) using CocoSDS and IOS foam108

Figure 4. 28: Oil recovery by surfactant IOS and CocoSDS alternating gas injection in core B.
.....109

Figure 4. 29: Pressure drop in core A (100mD) using IOS foam in presence of HPAM and
PPAM.....111

Figure 4. 30: Oil recovery in core A (100mD) using IOS foam in presence of HPAM and PPAM
.....111

Figure 4. 31: Pressure drop in core B (100mD) using IOS foam in presence of HPAM and
PPAM.....112

Figure 4. 32: Oil recovery in core B (100mD) using IOS foam in presence of HPAM and PPAM
.....113

Figure 4. 33: Pressure drop in cores A&B (100mD &500mD) using IOS foam in presence of
HPAM114

Figure 4. 34: Oil recovery of IOS foam in presence of HPAM in cores A&B (100mD &500mD)
.....115

Figure 4. 35: Pressure drop in cores A&B (100mD &500mD) using IOS foam in presence of
PPAM.....116

Figure 4. 36: Oil recovery of IOS foam in presence of PPAM in cores A&B (100mD &500mD)
.....117

List of tables

Table 3. 1: Foam formula for foam generation	40
Table 3. 2: Foam formulas to be used in sand pack	41
Table 3. 3: Surfactants and polymer properties	41
Table 3. 4: Measured IFT for DTAB and SDS by pendant drop.	46
Table 4. 1: Foam drainage data	77
Table 4. 2: Sand pack properties.....	85
Table 4. 3: Grain size distribution	85
Table 4. 4: Pressure data results for foam and brine injection	87
Table 4. 5: The permeability and the apparent foam viscosity in two sections across sand pack SP1 injecting surfactant foam (F2).....	89
Table 4. 6: The permeability and the apparent foam viscosity in two sections across sand pack SP1 using polymeric foam (F4).....	92
Table 4. 7: The permeability and the apparent foam viscosity in two sections across sand pack SP2 using polymeric foam (F6).....	94
Table 4. 8: Permeability and apparent foam viscosity for SP3	97
Table 4. 9: Core samples (Benthemier sandstone)	99
Table 4. 10: Crude oil injection	99
Table 4. 11: The produced oil vs applied pressure.	102
Table 4. 12: Summary of core flooding tests for surfactant foams	117
Table 4. 13: Summary of core flooding tests for surfactant/polymer foams	118
Table 4. 14: Mobility reduction (RF) results in core B for surfactant foams	119
Table 4. 15: Mobility reduction (RF) results in core A&B for surfactant/polymer foams	120

Table of content

Study of enhanced oil recovery using polymer-stabilised CO ₂ -Foam.....	i
Acknowledgement.....	ii
Abstract	iii
List of Abbreviations.....	v
List of Figures	vii
List of tables	xii
Chapter 1: Introduction.....	1
1. Chapter 1: Introduction.....	2
1.1 Research aims and objectives	4
1.2 Description of chapters	5
Chapter 2: Literature review	6
2. Chapter 2: Literature Review.....	7
2.1 Background.....	7
2.2 Foam flow through porous media.....	9
2.3 Foam Formulation and Stability	11
2.4 Foam Properties	11
2.5 Foam generation mechanism.....	13
2.6 Lamella stability and coalescence	16
2.7 Presence of oil	19
2.8 Steady state foam flow through porous media	23
2.9 Foam stability in Enhanced Oil Recovery	24
2.10 Foam apparent viscosity model	25
2.11 Polymer Enhanced Foam.....	26
2.11.1 Type of Polymers	27
2.11.1.1 Conventional polymer HPAM.....	28
2.11.1.2 hydrophobically modified polymer (PPAM).....	29
2.11.2 polymer retention	29
2.11.3 Surfactant- Polymer Interactions	31
2.12 The Structure of Polymer Enhanced Foam	31
2.13 Surfactant	32
2.14 Surfactant Classification	33
2.14.1 Anionic Surfactants.....	33
2.14.2 Cationic Surfactants.....	33
2.14.3 Non-ionic Surfactants	33

2.14.4	Zwitterionic (Amphoteric) Surfactants	34
2.15	Critical micelle concentration (CMC)	34
Chapter 3: Methodology		36
3.	Chapter 3: Methodology	37
3.1	Foam generation Material and Method	37
3.1.1	Polymer Characterisation	38
3.1.1.1	FT-IR spectroscopy	38
3.1.1.2	H-NMR spectroscopy.....	39
3.1.2	Fluid properties and materials.....	40
3.1.3	Surfactant and surfactant/Polymer solution preparation	41
3.1.4	CMC measurement	43
3.1.4.1	Interfacial tension and surface tension of surfactant solutions	43
3.1.5	Rheological properties measurement	46
3.1.6	Experimental setup.....	47
3.1.7	Foam generation and foam stability procedure	48
3.2	Foam flow behaviour in Sand Pack	48
3.2.1	Material and method	48
3.2.1.1	Sand Pack preparation and analysis.....	49
3.2.1.2	Porosity measurement.....	50
3.2.1.3	Permeability measurement.....	51
3.2.1.4	Adsorption.....	52
3.2.2	Surfactant Foam and polymer enhanced foam procedure by co-Injection	53
3.3	Core flooding for EOR, Method and Material	54
3.3.1	Experimental set-up and apparatus	55
3.3.1.1	ISCO 500D pump	55
3.3.1.2	Floating piston accumulators (FPAs).....	56
3.3.1.3	Pressure transducers.....	56
3.3.1.4	Back pressure regulator (BPR).....	57
3.3.1.5	Air bath (oven)	57
3.3.1.6	Flow meter and wet gas meter	57
3.3.2	Minimum miscibility pressure (MMP) measurements by slim tube	59
3.3.2.1	Slim tube methodology	60
3.3.2.2	Slim tube procedure.....	62

3.3.2.3	Data collection technique	64
3.3.3	Core flooding.....	64
3.3.3.1	Core and core holder.....	66
3.3.3.2	Confining Pressure	67
3.3.4	Core flood Experimental procedure	67
3.3.4.1	Fluid preparation.....	67
3.3.4.2	Core preparation	68
3.3.4.3	Brine injection	68
3.3.5	Steps of Initial water flooding (IWF) procedure	69
3.3.6	Steps of Foam flooding (tertiary oil recovery) procedure	69
3.3.7	Core cleaning process	70
3.3.8	Data collection	70
3.3.9	Source of Errors in the experiments	71
Chapter 4: Results and discussions		72
4.	Chapter 4: Result and discussion	73
4.1	Result and discussion of foam generation and stability	73
4.1.1	Polymer free foam stability in the absence and presence of oil, Bulk scale	73
4.2	Liquid drainage	75
4.2.1	Effect of surfactant concentration on foam stability using IOS.....	77
4.2.2	Polymer enhanced foam stability	78
4.2.2.1	PPAM characterisation.....	78
4.2.2.2	Comparing PPAM with HPAM	80
4.2.3	Effect of Polymer additive on foam stability.....	81
4.3	Foam flow behaviour in sand pack.....	84
4.3.1.1	Permeability of sand pack to brine	85
4.3.2	Surfactant foam flow behaviour in sand pack	87
4.3.3	Surfactant/polymer foam flow behaviour in sand pack.....	90
4.3.4	Surfactant Foam versus Polymer Enhanced Foam	95
4.3.5	Oil displacement tests using foam	98
4.3.5.1	Oil Injection (drainage).....	99
4.3.5.2	Brine injection (imbibition)	100
4.3.6	Continuous Water Injection (CWI) in core A and B	100
4.3.7	Minimum miscibility pressure (MMP) measurement using slim tube:	101
4.3.8	Continuous CO ₂ injection (CCI).....	104

4.3.9	CWI and CCI comparison.....	106
4.3.10	Foam injection	106
4.3.10.1	Surfactant foam injection.....	107
4.3.10.2	Surfactant/polymer foam injection.....	110
4.3.10.3	Comparison of oil displacement results of IOS foam in presence of HPAM (by co-injection) in 100 mD core A and 500 mD core B.....	113
4.3.10.4	Comparison of oil displacement results of IOS foam in presence of PPAM (by co-injection) in 100 mD core A and 500 mD core B.....	115
	<i>Chapter 5: Conclusions and recommendation for future work</i>	121
5.	Chapter 5 Conclusions.....	122
5.1	Conclusions.....	122
	<i>Chapter 6: Recommendation for future work</i>	125
	<i>Chapter 7: References</i>	128
7.	References.....	129

Chapter 1: Introduction

1. Chapter 1: Introduction

Fast depleting oil reserves coupled with ever increasing demand for energy is pushing companies to develop techniques to make energy recovery and consumption more efficient. As it is witnessed today, the rate of replacement of produced reserves by new discoveries has been declining steadily (IEA 2015). This scenario leads to the conclusion that the demand for oil may not only be met by putting more efforts in exploration alone but also by improving the production techniques from known and existing reservoirs.

Oil covers approximately 35% of the primary energy supply (IEA 2015). New sources, such as renewables, have not been demonstrated to be reliable yet as they account for only 12 % (projected to reach 15% by 2035) of the total world energy consumption (IEA 2015). Therefore, to guarantee the supply of energy and provide a transition period between current sources and the renewables ones, current sources have to be exploited in a more efficient manner.

Implementation of enhanced oil recovery (EOR) techniques is a crucial contribution to address the global need for energy. Today, the oil recovery around the world lies between 30-40% and considering the increasing world population and the global energy demand, this recovery efficiency is not satisfying. An increase in efficiency of the recovery process above 60% will be more adequate (Brame, 2019- Kasimbazi, 2014).

Enhanced oil recovery comes into picture when primary and secondary recovery techniques have been applied and a considerable portion of the original oil in place (OOIP) still resides in the reservoir.

Primary recovery process involves displacing oil from porous rocks in the reservoir towards the production well using the reservoir's own energy, such as natural water drive, gas-cap drive, or reservoir pressure. In secondary recovery, a fluid (water or gas) is injected into the reservoir in order to maintain reservoir pressure, and to continue oil displacement into the wellbore.

CO₂ flooding is one of the most widely used gas flooding processes. Over 75% of the incremental oil production in 2010 in the US from gas flooding processes comes from CO₂ flooding (Brame, 2019- Ashoori et al., 2011). As per the Oil and Gas Journal (2010), CO₂

flooding (miscible) produced 272,109 bbl/d from 109 projects and CO₂ flooding (immiscible) 9,160 bbl/d from 5 projects. The other advantage of CO₂ flooding is in its ability to store CO₂ in the subsurface formations reducing the global carbon footprint. CO₂ is used as an injectant to interact with the crude oil to change its properties and cause the oil to flow. Upon mixing with oil, pure CO₂ has the property to swell the oil, detach it from the rock surfaces, makes it lighter and allows it to flow more freely within the reservoir (Muhammad Sagir et. al., 2014).

Despite the fact, that gas floods are popular and widely used for enhanced oil recovery, the low viscosity of gas results in early gas breakthrough, poor sweep efficiency, viscous fingering, and channelling that result in low oil recovery. Due to low viscosity, gases tend to have higher mobility than oil and water which leads to gravity override and channelling through oil in the rocks. This decreases the amount of oil being contacted by gas and leads to early gas breakthrough, causing poor sweep efficiency.

To overcome this problem, foam has been proposed. Foam demonstrates great potential for displacing fluids in porous media. Foam decreases the relative permeability of gas by blocking the pores through which the gas can flow. Consequently, it diverts the flow from higher permeability zones to lower permeability zones (upswept zone). Since foam is a dispersion of discontinuous gas in a liquid film, it increases the apparent viscosity of the gas phase. In addition, foam improves oil recovery by reducing the capillary forces due to lower interfacial tensions resulting from the presence of a surfactant (Schramm, 1994; Rossen, 2010; Osei-Bonsu, 2017).

The major drawback associated with CO₂ injection is its poor volumetric sweep efficiency, because of which the gas does not contact a lot of oil, and incremental recovery is low (Xu et. al., 2017- Ramadhan, 2018).

The dynamics of oil-foam interaction especially in porous media is not fully understood and is a topic of ongoing research. There are many open questions regarding the nature and the dynamics of foam generation and propagation in porous media that need to be addressed such as how exactly the confined pore geometry of porous media influences the dynamics of foam-oil interaction or how the properties of foam affect its sweep efficiency in oil saturated porous media (Faragzadeh, 2012- Alfakher, 2019).

Despite the fact that foams have been extensively studied, many challenges still remain such as: the oil recovery mechanisms involved in CO₂ foam flood, the complex flow behaviour of the system, the foam stability, and the adverse influence of oil on foam stability.

Some works have evaluated the effects of various surfactants and hydrocarbons with well-defined properties on foam stability. These studies concluded that the selection of appropriate surfactant plays an important role in foam stability. Also, addition of polymer to the foam liquid phase has been frequently studied to enhance foam performance for enhanced oil recovery (Xu et. al. 2017).

(Shen et al., 2006) have found the use of low concentration of polyacrylamide, for instance, showed higher foam resistance and longer foam persistence. Foam stability increases as polymer enhances the viscosity of the liquid phase by slowing the rate of drainage and gas diffusion (Shen, et. al. 2006). Therefore, this project aims to study the use of polymer to enhance foam stability for enhanced oil recovery. In this regards an experimental investigation of foam stability using different type of surfactants and polymers will be employed.

1.1 Research aims and objectives

This project aims to experimentally study the use of polymer-stabilised foams in sandstone core flooding to enhance oil recovery.

For this purpose, sandstone core and CO₂-foam were employed. To formulate the foam, different types of surfactants/polymers and brines were used.

The objectives are:

- To design an optimal foam formulation.
- To study the stability of foam in bulk and bubble scale.
- To study the effect of a hydrophobically modified polymer (modified polyacrylamide) on foam stability (bulk and bubble size).
- To investigate oil displacement in porous media using formulated foam.

Chapter 1: Introduction

1.2 Description of chapters

This thesis contains 7 chapters.

Chapter 1 is an introduction to this project.

Chapter 2 includes background information about chemical EOR and a literature review of foam flooding. This chapter reviews the fundamental information on foam in porous media, which include foam generation mechanisms and contributing factors to foam stability. In addition, this chapter discusses polymer-enhanced foam along with its benefits and limitations.

Chapter 3 describes the materials and methods used in this project including all three phases of the study. The first section of the chapter presents the process of foam generation, study its stability in presence and absence of oil and investigates the rheological properties of formulated foam in bulk solution. The second part is to study the effect of rock permeability on foam rheological behaviour using sand pack. The last session explains the method and material used in core flooding to investigate the effect of using polymeric foam on oil displacement in porous media.

Chapter 4, the experimental results, and the outcome are presented in this chapter. Chapter 4 is divided into three phases. First phase includes visual observations and results from the foam generation tests. The second part discusses the results from the co-injections of surfactant and surfactant+polymer in the sand pack. As well as basic sand pack properties from routine analysis which are followed by experimental results and discussions. In part 3 Oil displacement results in sandstone cores are shown and discussed.

Chapter 5 includes a brief conclusion of the thesis. All the key results and the achieved results are shown in this chapter.

Chapter 6, include ideas of possible future work, and recommendation.

Chapter 7, the references are presented in this chapter.

Chapter 2: Literature review

2. Chapter 2: Literature Review

2.1 Background

Successful field applications of any enhanced oil recovery (EOR) technique require mobility control for the displacing phase to maximize sweep efficiency. Gas-mobility control in porous media plays an important role in maximizing oil recovery by increasing the volume of oil-in place contacted by the injected gas (Green and Willhite, 1998).

The gas displacement process can be improved with the reduction of the mobility ratio.

Mobility ratio, M , is defined as the mobility of the displacing phase, gas, divided by the mobility of the displaced phase, oil, as seen in the equation below:

$$M = \frac{\frac{K_{rg}}{\mu_g}}{\frac{K_{ro}}{\mu_o}} = \frac{K_{rg} \cdot \mu_o}{K_{ro} \cdot \mu_g} \quad (2.1)$$

The mobility ratio can be decreased by increasing the gas viscosity or decreasing the relative permeability of gas, both of which can be achieved through foam generation.

Aqueous foam flooding is an effective technique to control gas mobility in permeable porous media with successful applications to improving volumetric sweep efficiency in gas flooding and steam flooding (Schramm, 1994; Rossen et. al, 2010).

The overall displacement efficiency can be expressed as the product of microscopic and volumetric displacement efficiencies:

$$\left(E = \frac{ED}{Ev} \right) \quad (2.2)$$

The overall efficiency (E) is the ratio of oil recovered by EOR process and oil present before the process (OOIP). Microscopic displacement efficiency (ED) measures the effectiveness of the displacing fluid in mobilizing the oil at the local pore-level where displacing fluid contacts the oil whereas the volumetric displacement efficiency (Ev) measures the effectiveness of displacing fluids sweeping out the reservoir in a volumetric sense.

Volumetric displacement efficiency (E_v) is the product of areal and vertical sweep efficiencies where the areal sweep efficiency is the fractional area of the pattern that is swept by the displacing fluid (Lake et al., 2014).

Low sweep efficiency can happen due to channelling (flow through high permeability layers), viscous fingering (viscosity difference between oil and gas) and gas overriding (density difference of the injected gas and the reservoir oil). So, mobility and conformance issues are the most serious concerns which diminish the effectiveness of a CO₂ flood (Sagir et. al., 2014).

CO₂ and oil are not miscible on first contact, their miscibility occurs through multiple contacts, which is called multi-contact miscibility (MCM). First contact miscibility (FCM) refers to a condition where two fluids become miscible and form a single phase when they are first brought into contact at a specific pressure and temperature. There are two mechanisms for MCM, vaporising gas drive (VGD) and condensing gas drive (CGD) (Al Wahaibi and Al Hadhrami, 2011).

Minimum Miscibility Pressure (MMP) is the lowest pressure at constant composition and temperature, at which multiple or first-contact miscibility can be attained. Interfacial tension is present at such pressure and there exists no interface between the fluids.

Haugen et. al (2014) study shows immiscible foam is less efficient (30 pore volumes injected) compared to miscible foam (2 pore volumes injected) to reach ultimate recovery.

In this study MMP was investigated through some experiments in order to choose an appropriate injection pressure to maximise the recovery efficiently.

2.2 Foam flow through porous media

A promising cost-effective EOR process is to combine surfactant flooding with gas injection to generate foam. This method provides better mobility control and utilizes less chemicals (Nguyen et al., 2018- Li et al., 2012).

Aqueous foam is a dispersion of gas phase within a continuous aqueous phase, which is stabilized by surfactant molecules at the gas-liquid interface and could be generated by co-injection or alternate injection of gas and foaming agent (Osei-Bonsu, 2017- Vassenden et al., 2000).

In porous media, gas bubbles are separated by liquid-filled films called lamellae. Each individual lamella has a certain capillary resistance to gas flow. Foam reduces gas mobility greatly, both by trapping a large fraction of the gas in place and by increasing the resistance to flow of the gas that does flow (Falls et al. 1989- Ballan, 2013). The efficiency of foam is believed to be the result of the high apparent viscosity of the foam and its penetration into the high permeability layers and/or fractures (Li et al., 2012; Hematpur, H et. al., 2018).

The recovery mechanisms in foam flooding are related to the effectiveness in reducing interfacial forces that hold residual oil in place, and the capability of altering flow distribution and fluid conductivity (Li et al., 2012). As a result, it is important to understand foam performance in a foam assisted surfactant gas flooding process.

The flow of foam through porous media is much different than two-phase flow of gas and water. In the latter one, mobility of each phase strongly depends on its own saturation. In the former one, however, foamed gas is a discontinuous phase, and its mobility strongly depends on foam texture, which is the number of lamellas per unit gas volume (Falls et al., 1988). The finer the foam texture, the higher the flow resistance to gas flow (Ettinger and Radke, 1992). Aqueous phase in foam, however, flows through its continuous liquid network. Therefore, the relationship between the water relative permeability and water saturation is not affected by the presence of foam in porous media (Huh and Handy, 1989). However, the high amount of trapped gas developed during foam flow decreases the aqueous phase mobility by blocking the available area to flow (Ballan, 2013).

Many experimental studies (Xu et al. 2017- Lee et al., 1991) showed that foam reduces the gas mobility more in high permeability cores than in low permeability cores. This leads to a crossflow of gas from high- to low permeability layers if the layers are in capillary equilibrium. Therefore, the foam front moves through each layer at the same rate. If there is no capillary equilibrium between layers, however, foam plugs the high-perm layer and diverts flow to low-perm layer. Therefore, foam is relatively stronger in high-perm layers than in low-perm layer, which is the driving mechanism for cross flow (Tanzil et al., 2002).

2.3 Foam Formulation and Stability

Foam is defined as a dispersion of gas in a continuous liquid phase where the gas flow paths have been made discontinuous by thin liquid films called lamellae (Ganglitz et al., 2002). These lamellae are defined as a thin liquid film with interfaces on both sides of the liquid phase.

Foam, containing surfactants dissolved in the liquid phase to stabilize the gas dispersion in liquid (Tang and Kovscek, 2006), can improve conformance in gas-injection improved oil recovery (Nguyen et al., 2018).

Foam can be formed in bulk by flowing gas into a bulk liquid solution. However, in the application of the oil and gas industry, foam must be formed to displace oil in porous media. Thus, the generation, destruction, and transport of foam have been greatly studied. The rheology of foam films is also important for stability.

The dispersion of the gas phase in foam can be stabilized using nanoparticles and polymers. Foaming agents (surfactant) lower the surface tension and provide a protective film to prevent the gas bubbles from collapsing (Schramm 1994). Bulk foam, defined as dispersion of gas in a liquid phase without the presence of a porous medium, liquid phase at the bottom and gas phase at the top, as shown in Figure 1, which is a 2D interface of a bulk foam system.

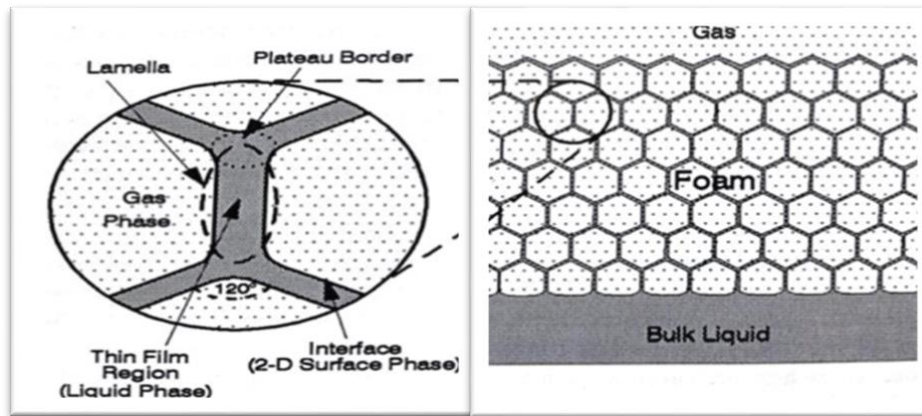


Figure 2. 1: presentation of symmetric foam (a 2D interface of a bulk foam system)
(Schramm,1994)

2.4 Foam Properties

Foams can be categorized based on the following three properties: texture, quality, and rheology.

- **Foam Texture**

Foam texture plays a significant role in understanding the foam strength and its ability to provide mobility control in porous medium. It determines the generation of foam as bulk foam or as a chain of bubbles separated by an individual lamella, the number of lamellae per unit length of capillary, and the radius of curvature of the gas-liquid interface (Hirasaki and Lawson, 1985- Ghosh, 2016). Texture also gives a measure of average bubble size and bubble size distribution. Bubble size affects the foam strength and the viscosity of the foam phase.

Nguyen (2018) has suggested that finer bubble sizes result in more stable foam. It is believed that as the foam texture gets finer, the foam provides better resistance to flow in rock matrix and reduces mobility of gas by a significant amount (Kovscek and Radke, 1994).

Bulk foam with a broad gas bubble size distribution is found to be less stable because of the gas diffusion from small to large gas bubbles. Bulk foam is formed when the capillary radius is larger than the equivalent radius of the bubble and individual lamellae are formed when the capillary radius is smaller compared to the radius of the bubbles (Hirasaki and Lawson, 1997).

The resistance to flow imparted by foam will be higher for homogeneous bubble size distribution (Schramm 1994) with discrete bubbles in comparison to the continuous gas phase. Friedmann (1991) found that bubble size and bubble size distribution range decrease with an increase in surfactant concentration and increase in system pressure. Foam texture depends on the type of surfactant, pore network, and foam quality.

• Foam Quality

Foam quality is defined as the gas volume percentage within foam at a specified pressure and temperature. In the bulk phase, foam quality is expressed by the following equation:

$$F_g (\%) = V_g / (V_g + V_l) \times 100 \quad (2.3)$$

Where V_g and V_l are gas volume and liquid volume respectively.

In core flood experiments, foam quality is defined by the following equation:

$$F_g (\%) = Q_g / (Q_g + Q_l) \times 100 \quad (2.4)$$

Where Q_g and Q_l are gas injection rate and liquid injection rate respectively.

Bulk foam having high foam quality is referred to as “dry foam” (Schramm 1994). High foam quality leads to the reduction of mobility due to discontinuous gas bubbles in the liquid films. Marsden (1966) found that foam mobility increases with decreasing foam quality due to decreasing foam viscosity, whereas Lee (1991) found that foam mobility decreased with decreasing foam quality (Xu et. al. 2017)

The effect of foam quality to change the radius of curvature of the liquid, an important variable in the thickness of the liquid film wetting the solid and affecting the resistance to flow, is significant at high qualities (Hirasaki and Lawson, 1985). Foam qualities can exceed 97%. Studies have shown that foam is unstable below quality 40% and above 95% quality; not much research has been done at these extreme low and high-quality values (Ghosh, 2016).

• Foam Rheology

The study of foam rheology describes the behaviour of foam as a phase in the porous media and the impact of its petrophysical properties like viscosity on the transport

processes. Foams are shear thinning fluids whose viscosity decreases with increasing shear rate (Marsden, 1986).

It is difficult to measure absolute foam viscosity directly. Alternatively, the term “apparent foam viscosity” is used, defined from Darcy’s law. The apparent foam viscosity varies with rock permeability non-linearly and approaches asymptotic values at both high and low permeabilities, with viscosity being higher for high permeability rocks (Lee, 1991).

Foam mobility, ease with which foam flows in a porous medium, is defined as the ratio of the effective permeability to apparent viscosity. For a water-wet system, the relative mobility of a liquid phase is calculated as a function of the saturation and is independent of whether the gas exists as foam (Falls et al., 1988). For a continuous gas, no reduction in relative permeability is observed because the cross-sectional area to the flow of gas phase inside a porous medium is not reduced. However, if the gas phase is discontinuous, the relative permeability reduces, and the foam has a larger apparent viscosity, reducing the gas mobility.

In porous media, the apparent foam viscosity depends on the bubble size. The resistance to flow increases with decrease in foam bubble size because the foam viscosity increases (Hematpur et al., 2018).

Falls (1988) suggested that the apparent gas viscosity increases by an order of magnitude when the ratio of bubble size to average pore size decreases by two-fold.

2.5 Foam generation mechanism

Foam generation in porous medium is governed by the operating conditions such as pressure gradient, and pore network in the reservoir. Studies of different gases and surfactant formulations have shown that a minimum pressure gradient is required for foam generation, which varies inversely with rock permeability (Gauglitz and Friedmann 2002). Foam generation depends only on pore throat radius and length of the pore cluster and not on length of the medium.

The mechanisms governing foam generation in porous media are snap-off, lamella division, and leave behind. These mechanisms have been thoroughly studied and are important to the fundamental understanding of foam behaviour in porous media (Nguyen D. et. al, 2018).

- **Snap Off mechanism**

Snap-off is a process of creating several discontinuous gas bubbles of smaller size from a larger gas film at the pore throats. It is one of the most important mechanisms for foam generation in porous media.

The necessary conditions for snap-off to occur in porous media are that the body-to-throat ratio must be larger than two (Kovscek and Radke, 1994) the capillary pressure must be low, and the liquid saturation must be high (Nguyen D. et. al, 2014).

Snap-off occurs when the capillary pressure is larger than the entry pressure, and gas enters the pore body, as seen in Figure 2. The bubbles formed by snap-off are not stable in the absence of the surfactant, and tend to coalesce quickly, forming a continuous gas phase. Figure 2 illustrate the snap-off mechanism, gas enters the liquid filled pore throat forming a gas finger and a wetting collar and a bubble is formed after snap-off.

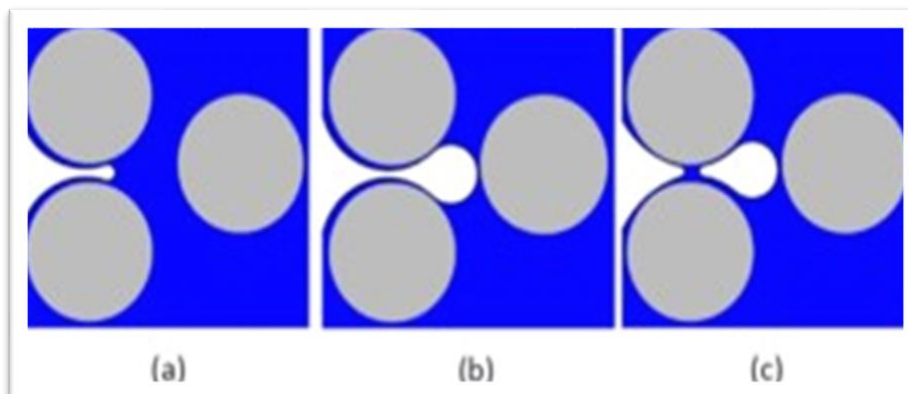


Figure 2. 2: Mechanism for foam generation via snap-off a) gas invades the pore body, b) gas enters the pore body, and c) wetting fluid moves back to snap off the gas thread

- **Lamella division mechanism**

Mast (1972) first identified another kind of lamellae generation called lamellae division in an etched glass micromodel study.

Division is one means by which flowing foam can reproduce lamellae as they break. It is especially efficient where more than two bubble trains converge on a single pore.

Typically, when a bubble reaches a branch point in a flow channel, the bubble may divide into two rather than simply following one of the two available pathways. As the translating foam bubble encounters a point where the flow branches in two directions, the interface stretches around the branch point and enters both flow paths as two separate lamellae. For this process, surfactant is the necessary condition.

The frequency of lamella division is dependent on many parameters, of which the number of branch points and bubble sizes were found dominant (Kovscek and Radke, 1994). Availability of division sites in turn depends on occupancy of trapped bubbles (or stationary lamellae) or presence of a third phase such as oil droplets.

Moreover, a local capillary pressure fluctuation is required during stretching of the parent bubble around the branch point. The lamella, otherwise, may be ruptured before dividing, due to liquid drainage.

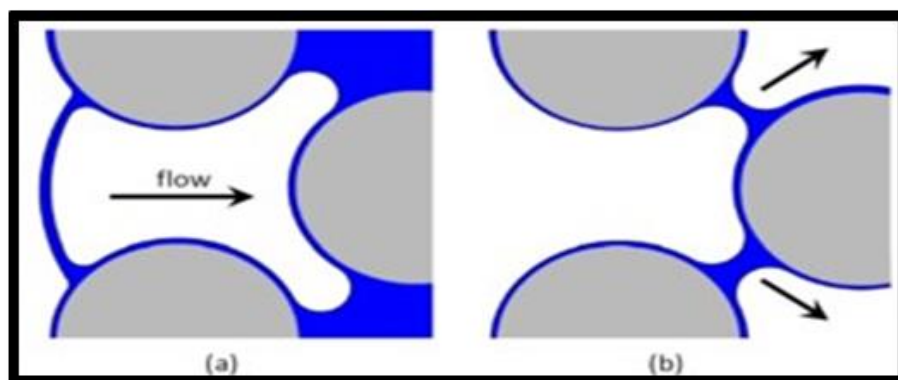


Figure 2. 3: Mechanism for foam generation via lamella division (Kovscek and Radke 1994).

- **Leave behind mechanism**

Either snap-off or lamella-division produce additional lamellae perpendicular to the flow direction. Lamellae, however, can also be created parallel to the flow direction.

The process called “leave behind” can only occur during drainage and generate the bubble parallel to the flow direction, when gas saturation is rising.

As the gas invades a porous medium initially saturated with surfactant solution, large numbers of lamellae are created. These lamellae are created in the throats between adjacent pore bodies when the pore bodies are entered by gas from separate directions. Lenses are then left behind between grains in the porous medium as menisci converge downstream.

If the capillary pressure of the medium is not too high and the pressure gradient not too large, stationary stable lenses emerge. Later, these lenses may drain to thin films.

Snap-off and lamella-division may be considered the controlling mechanisms of gas viscosity since increased gas viscosity arises primarily from pushing lamellae through constrictions.

On the other hand, the leave-behind mechanism contributes principally to a further reduction of gas permeability by giving rise to blocked flow paths to gas and applies only to drainage processes (Osei-Bonsu, 2017; Hematpur, H et. al., 2018).

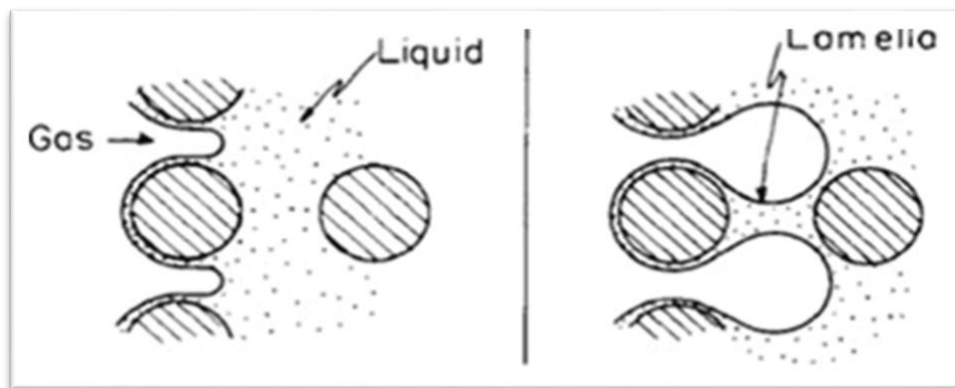


Figure 2. 4: Mechanism for foam generation via leave-behind (Kovscek and Radke 1994).

2.6 Lamella stability and coalescence

The stability of foam in porous media is governed by the stability of individual foam lamellas, which depends on many factors such as capillary pressure, surfactant concentration and adsorption, gas diffusion through a lamella, presence of oil phase, salt concentration, surface forces and mechanical fluctuations (Aronson et al., 1994).

There are three distinct forces acting on a foam lamella: repulsive positive electrostatic forces (Π_{EL}), attractive negative Van Der Waals forces (Π_{VW}) and capillary forces between gas and liquid phases (Exerowa and Kruglyakov, 1998- Balan, 2013). Surfactant molecules absorbed at gas-liquid interfaces create charged surfaces repulsing each other and stabilize lamella. Surfactant molecules consist of a polar portion called “head”, and a nonpolar portion called “tail”. In common black film surfactant molecules accumulate at gas-liquid interfaces, since the head (polar) and tail (nonpolar) portions are attracted by water and gas molecules, respectively (Figure 2.5) (Green and Willhite, 1998- Ghosh, 2016). An increase in surfactant concentration in aqueous phase increases the stability of foam lamellas, therefore gas

mobility decreases and gas trapping increases (Simjoo et al., 2013). Moreover, repulsive forces increase with salt concentration in liquid phase since surfactant concentration at gas-liquid interface increases with salt concentration.

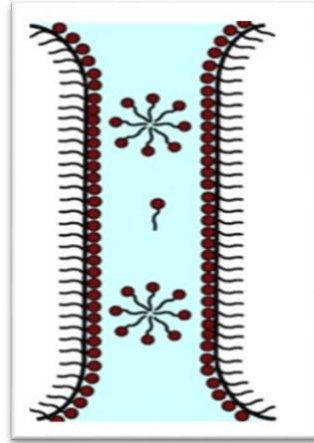


Figure 2. 5: Schematic of a common black film. Surfactant molecules accumulate at gas-liquid interfaces (Farajzadeh et al., 2008).

Attractive Van der Waals forces make the charged surfaces closer and destabilize lamella. The criteria for lamella stability are that the difference between repulsive and attractive forces, which is called as disjoining pressure (Π) in DLVO theory (Balan, 2013), must be positive to balance capillary forces (P_C) (Eq. 2.5). Disjoining pressure strongly depends on the film thickness (h), which decreases with increasing capillary pressure. Figure 2.6 shows the relationship between disjoining pressure and film thickness for stable films, metastable films, and unstable films.

$$\Pi(h) = P_C = \Pi_{EL} - \Pi_{VW} \quad (2.5)$$

Π : disjoining pressure

Π_{EL} : Electrostatic pressure

Π_{VW} : Van der Waals pressure

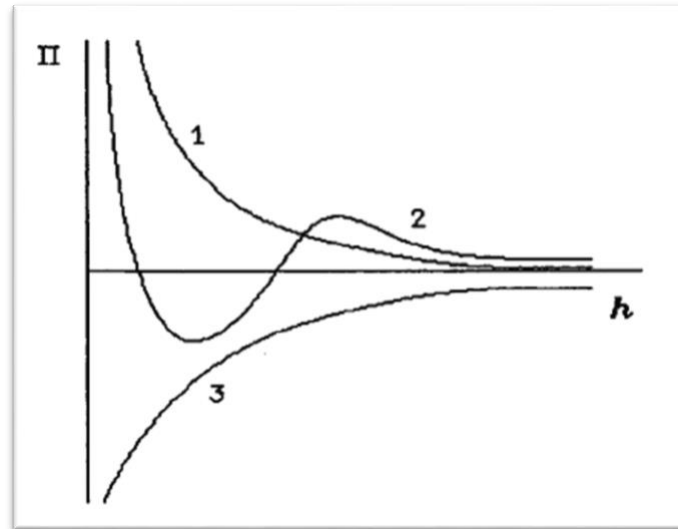


Figure 2. 6: A schematic showing the relationship between disjoining pressure, Π and film thickness, h for (1) stable films; (2) metastable films; (3) unstable films (Kornev et al., 1999).

As the fraction of gas in foam (f_g) increases at a fixed gas velocity, capillary pressure increases and approaches a critical capillary pressure (P_C) (Figure 2.7). A further increase in the fraction of gas does not increase capillary pressure, however foam texture coarsens, and capillary pressure drops (Khatib et al., 1988). Water saturation at P_C , which is called critical water saturation (S_W), remains constant. Therefore, the foam mobility at P_C depends on the ratio of gas/liquid fractional flow and the liquid mobility at P_C . Based on this observation and the fractional flow theory, some investigators (Zhou and Rossen, 1995) attempted to model foam mobility in porous media at P_C . An increase in surfactant concentration makes foam lamellas more stable, which leads to higher P_C . Surfactant type and electrolyte concentration in liquid phase also control the magnitude of P_C (Khatib et al, 1988).

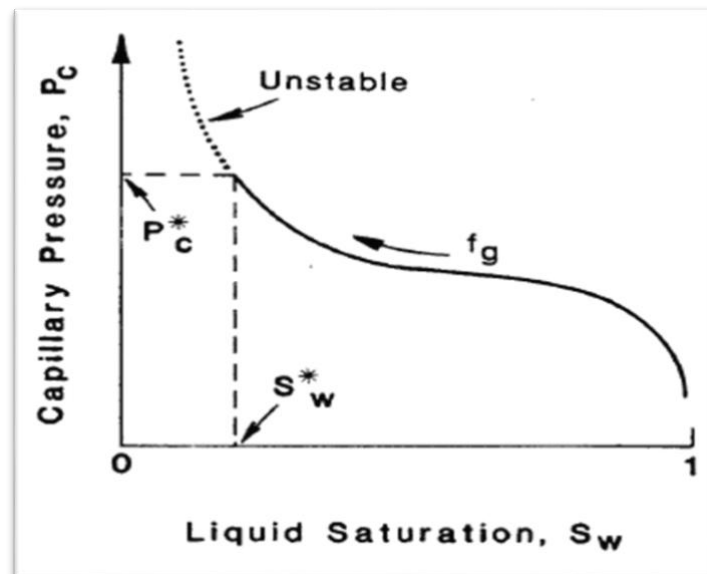


Figure 2. 7: Capillary pressure vs liquid saturation

The presence of oil, especially light oil, in porous media has a detrimental effect on foam lamella stability (Andrianov et al., 2012). It decreases the effectiveness of foam by reducing gas and water mobility in porous media. When foam lamella contacts with oil, oil droplets enter lamella and spread on the gas-liquid interface. Therefore, gas-liquid interface becomes a gas- liquid- oil interface, which changes interfacial forces and makes the lamella unstable (Schramm et al., 1994).

Moreover, foam lamella generation requires a water-wet porous medium. Foam formation in oil-wet formations requires a surfactant which can change wettability from oil-wet to water-wet (Alfakher, 2019).

2.7 Presence of oil

The addition of crude oil is detrimental to both the generation and the stability of foam. Experimental studies have demonstrated the detrimental impact of oil on foam stability (Osei et. al., 2015; Andrianov et. al., 2012). The effect of the presence of oil on foam destabilization depends on the oil, surfactant solution, and aqueous-phase compositions (Osei et. al., 2015). Ideally, it is possible to make surfactant foams that last over months and years (Schramm, 1994).

The effect of oil on foam stability has been studied by many investigators at bulk and bubble-scale (Farajzadehet. al., 2012; Osei et. al., 2015; Hematpur, H et. al., 2018). In many cases, a

bulk foam test has been used to determine the ability of a surfactant to generate stable foams in the presence of oil in porous media. In these experiments, the surfactant, gas and oil are generally mixed in a column to produce a fixed volume of foam. The foam is then observed for a period and the rate of foam height decay or the half-decay time (i.e. the time taken for foam to reach half of its original height) has been considered as the measure of the foam stability. Results from these experiments (Andrianov et. al., 2012) have shown that light oils are more detrimental to the stability of the foam. It has also been demonstrated that foam can be generated effectively in the presence of heavy oil (Osei et. al., 2017). While many of the conclusions drawn from these experiments may be valid for bulk foams, direct translation of the outcomes to foam flow in porous media may be inadequate due to the complexity of the interaction between foam and oil within confined geometries (Osei et. al., 2017).

Aveyard et. al. (1994), have conducted a systematic series of experiments using a well characterised porous medium manufactured by 3D printing technique to evaluate the influence of oil on the dynamics of foam displacement under different boundary conditions. The effects of the type of oil, foam quality and foam flow rate were investigated. Their results reveal that generation of stable foam is delayed in the presence of light oil in the porous medium compared to heavy oil. Additionally, it was observed that foams with high gas fraction appeared to be less stable in the presence of oil lowering its recovery efficiency. Farajzadeh et. al. (2012) results demonstrated that oil displacement efficiency by foam is strongly influenced by the surfactant formulation. Their pore-scale investigation shows that the stability or instability of foam at bulk scale does not necessarily determine its effectiveness in porous media.

Friedmann et. al. (1991) demonstrated that the oil saturation was more influential upon the stability of foams than the type of oil in porous media. The presence of oil reduces the foam mobility reduction factor of different surfactant to different degrees. This observation was also reported by Mannhardt et. al. (1998) in their study of the effect of oil saturation on foam performance in porous media. They observed that oil become detrimental to foam at oil saturation above 5% to 20%.

The destabilizing effects of oil on foam are believed to be a result of direct surface interactions between oil and foam which are determined by various physiochemical properties

(Farajzadeh et. al, 2012). It is widely accepted that these interactions are governed by three main mechanisms: entry of oil droplet into gas-liquid interface (Osei et. al., 2015), spreading of oil on the gas-liquid interface and formation of an unstable bridge across lamella (Garret, 2013).

According to Osei et. al. (2015) the thermodynamic feasibility of oil destroying foam can be determined by evaluating the entering coefficient (E), spreading coefficient (S) and bridging coefficient (B). The stability of foams in the presence of oil depends on the spreading, entering, and bridging coefficients of the gas/surfactant/oil interactions and oil emulsification.

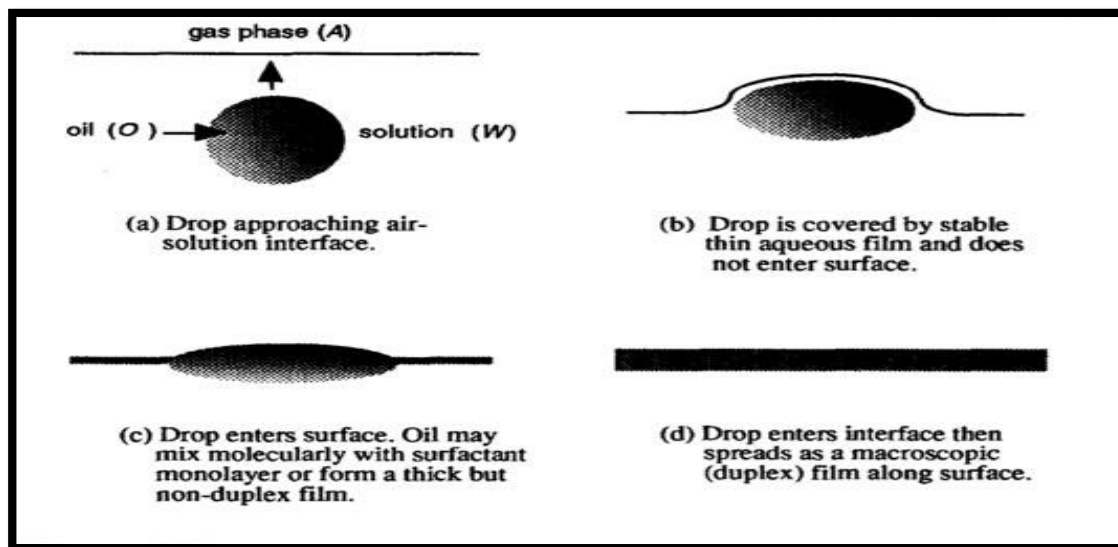


Figure 2. 8: Possible fate of an oil drop in solution approaching gas-surfactant solution interface. (Aveyard et. al., 1994)

- Entering (E), Spreading (S) and Bridging (B) Coefficients

The mathematical expressions for E, S and B are given by:

$$E = \sigma_{gw} + \sigma_{ow} - \sigma_{og} \quad (2.6)$$

$$B = \sigma_{gw}^2 + \sigma_{ow}^2 - \sigma_{og}^2 \quad (2.7)$$

$$S = \sigma_{gw} - \sigma_{ow} - \sigma_{og} \quad (2.8)$$

Where, σ_{wg} is the surface tension between surfactant solution and the gas, σ_{ow} is the interfacial tension between oil and surfactant solution and σ_{og} is the surface tension between the oil and gas.

The most stable foams are formed when the entering coefficient is negative, and the lamella number is low (Farajzedah et. al., 2012; Hematpur, H et. al., 2018).

The first condition to be satisfied for oil to destroy foam is that the oil droplet must be able to invade the gas–water interface (Osei et. al., 2015). This condition is met when $E > 0$. It is worth noting that, entering is not possible until oil is present in the form of emulsified oil, i.e., droplets with sizes smaller than the thickness of the foam lamella. Once an oil droplet has entered the gas-liquid interface, it will spread on the surface of the film.

This occurs when $S > 0$ (Osei et. al., 2017 - Osei et. al., 2015- Farajzadeh et. al., 2012). The spreading of the oil droplet over the film interface forces liquid out of the film into the plateau borders which causes the film to thin and eventually rupture. Also, it has been suggested that the spreading of oil alters the film interfacial rheology which could change the rate of film drainage (Vitasari et. al., 2013).

Simjoo et. al. (2013) suggested that both the entry and spreading condition must be satisfied for oil droplet to act as antifoam. On the contrary, when $S < 0$ (no oil spreading), oil forms a lens at the interface between the gas and liquid and may eventually destroy the foam film if it makes its way into the lamella surface (bridging mechanism where $B \geq 0$). Vikingstad et. al. (2005) conducted a systematic static bulk foam test to investigate the factors that affect foam stability. Their results showed that a negative spreading coefficient is not a prerequisite for stable foam formation (Bonsu et. al., 2015).

- Pseudo-emulsion Film

A pseudo-emulsion film is a thin liquid film between the oil droplet and the gas phase.

Mannhardt et. al. (1998) found that the stability of foam is related to the stability of pseudoemulsion film. When the pseudoemulsion film (formed between the oil droplet and gas phase) is stable, oil spreading is suppressed which means the oil will stay in the lamella. Oil will only spread or bridge gas-liquid interface when the pseudoemulsion film ruptures, the

oil may form a lens at the gas-water interface, and this can break the foam down. It has been observed that mixing surfactants can significantly improve the stability of foams and potentially reduce the destabilizing effect of oil on foam.

2.8 Steady state foam flow through porous media

Steady-state flow of foam through porous media can exist either in high-quality or low-quality flow regimes (Cavalcante, 2016 - Osterloh and Jante, 1992). Foam quality is defined as the fraction of gas in the foam. In the low-quality flow regime, steady-state pressure gradient is dependent on gas velocity but is independent of liquid velocity (Figure 2.8). Capillary resistance and gas trapping are the main mechanisms controlling the flow behaviour in this regime. Furthermore, foam texture does not change much, and shear-thinning behaviour is observed in the low-quality regime (Alvarez et al., 2001).

In the high-quality regime, however, steady-state pressure gradient is dependent on liquid velocity but is independent of gas velocity (Figure 2.8). At high foam qualities, capillary pressure and coalescence are the dominant mechanisms defining the foam behaviour (Osterloh and Jante, 1992; Alvarez et al., 2001). Moreover, there exists a transition zone between high-quality and low-quality foam-flow regimes, which depends on critical capillary pressure at a specific permeability, gas velocity, surfactant formulation and concentration (Alvarez et al. 2001). Bubble size in high-quality foam regime is larger than in low-quality foam regime.

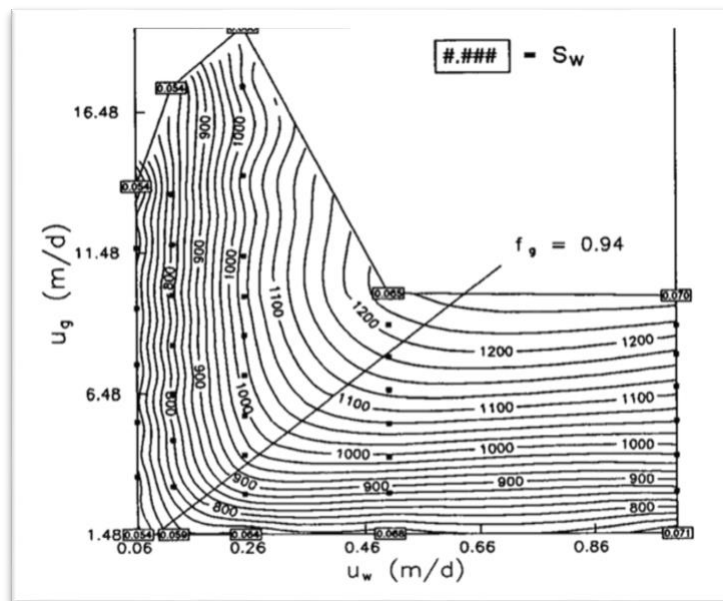


Figure 2. 9: Steady-state pressure drops in a sand pack as a function of superficial phase velocities (Osterloh and Jante, 1992).

2.9 Foam stability in Enhanced Oil Recovery

A major concern with the application of foam as an EOR method is the stability - the longevity of foam in contact with crude oil (Osei-Bonsu, 2017). The foam (i.e., foam films) must remain stable in the porous media to perform as an effective gas blocking agent. The stability of foam is controlled by the competing processes of foam generation and foam destruction.

Once foam has been generated, it can be destroyed by two general mechanisms: capillary suction coalescence and gas diffusion. Capillary suction coalescence occurs when two bubbles come into contact causing the liquid film separating them to thin and eventually collapse. Capillary suction coalescence, which is primarily responsible for lamella destruction, depends on liquid saturations, rock permeability, and surfactant concentration.

Gas diffusion primarily affects trapped bubbles and is less common in porous media because the bubble radius of curvature is related to the pore throats and pore bodies rather than bubble volume. Gas on the concave side of a foam bubble has a lower potential than the gas on the convex size of a foam bubble. Therefore, gas dissolves through the liquid film and diffuses to the concave side.

Eventually, the bubble shrinks until it disappears (Ghosh, 2016). The stability of a single foam lamella is a representation of the coalescence in porous media, which depends on the type or mixture of surfactants, the chemical composition of the brine, the capillary pressure, and the movement of mechanical disturbances (Friedmann, 1991). The stability of foam in porous

medium is affected by the addition of crude oil as suggested in the literature (Farajzadeh et al., 2012).

2.10 Foam apparent viscosity model

Darcy law (Equ. 2.9) gives a linear relationship between flow rate (q) and pressure drop (ΔP), to define permeability (k) as a measured parameter for conductivity of porous media as:

$$K = \frac{\mu q L}{A \cdot \Delta P} \quad (2.9)$$

Where A and L are cross sectional area and length respectively, μ is Newtonian viscosity of fluid flowing through porous media which means viscosity is constant and does not change at different shear rate. The relationship between flow rate and pressure drop is linear.

A polymer solution used in EOR is a non-newtonian fluid; therefore, the

viscosity term (μ) is not constant. In situ apparent viscosity (μ_p) is often used in foam flooding and is defined as follow:

$$\mu_{app} = \frac{A \cdot \Delta P \cdot k}{q l} \quad (2.10)$$

Apparent viscosity is not constant and changes with shear rate, also the relationship between pressure drop and flow rate is not linear.

It is not possible to measure the apparent viscosity during core flooding experiments. Instead, the apparent viscosity is determined by equations that depend on the mobility reduction (RF), by applying Darcy's law (Equation 2.11) for water and foam:

Initial water flow:

$$q_w = \frac{A \cdot \Delta P_w \cdot k}{\mu_w L} \quad (2.11)$$

Foam solution flow:

$$q_f = \frac{A \cdot \Delta P_f \cdot k}{\mu_f L} \quad (2.12)$$

The resistance factor (Mobility reduction) RF (Equ. 2.13) can be expressed:

$$RF = \frac{k_w / \mu_w}{k_f / \mu_f} = \frac{q_w / \Delta P_w}{q_f / \Delta P_f} \quad (2.13)$$

Where μ_p is the apparent viscosity of the surfactant solution. If the same flow rate is used for water and polymer, RF can be simplified as:

$$RF = \Delta P_f / \Delta P_w \quad (2.14)$$

2.11 Polymer Enhanced Foam

It has been suggested that the addition of a polymer to the surfactant foaming solution improves foam's efficacy as a gas mobility control agent (Kutay and Schramm, 2004). Polymer/surfactant interaction can be broadly divided into two categories: a strongly interacting polymer/surfactant system (due to opposite charges) and a weakly-interacting polymer/surfactant system (due to like or neutral charges). For oil field applications, one general requirement is to minimize the adsorption of the surfactant and polymer components to the rock matrix. To achieve this objective, the polymer and surfactant used must be of the same charge. Based on this assumption, the following discussion only pertains to weakly-interacting polymer/surfactant system.

The addition of polymer to a surfactant foaming solution typically increases the foam liquid phase viscosity due to polymer chain (Bureiko et al., 2014). From the perspective of foam generation, an addition of polymer to the surfactant solution seems to decrease the rate of foam generation events. A study (Kovscek, 1994) found the rate of snap-off frequency may be expressed as linearly proportional to liquid velocity and to gas velocity. Assuming a constant pressure gradient, a higher liquid phase viscosity could translate to lower liquid and gas phases velocity. The lower liquid and gas velocities could lead to fewer foam generation events and potentially limit foam generation to the near well-bore region.

From the perspective of foam stability, the addition of polymer seems to reduce the occurrence of lamellae destruction. Polymer improves the stability of thick foam film by increasing its viscosity and reducing the rate of film drainage. In thin films, polymers resist

thinning forces by forming a mesh-like structure. This structure creates a steric repulsion between adjacent film surfaces (Shehzad et al., 2017).

The addition of polymer to surfactant solution typically increases the foam apparent viscosity. This phenomenon can be attributed to the increase in the viscosity of the foam's liquid phase due to polymer chain entanglement (Beltran et al., 2003). The effect of polymer addition to foam interface Gibbs elasticity is less clear. This component of foam viscosity is a function of interface viscoelasticity, which itself is controlled by the rate of surfactant exchange between the interface and the bulk solution. This exchange phenomenon is quantified by a term called dynamic surface tension. Effect of polymer addition on trapped foam saturation has not been investigated. However, increased foam apparent viscosity and stability could very well lead to an increase in trapped foam saturation in porous media. Despite the previously discussed benefits, incorporating polymer into the surfactant foaming solution does have several drawbacks and limitations. One of the drawbacks is a reduced injectivity due to the high viscosity of the liquid slug. Moreover, additional surface facility is required to mix the polymer into the surfactant foaming solution. The application of polymer-enhanced foam is also confined by several limitations. One of these limitations is that polymers typically have a low temperature ceiling, above which the polymer molecules are hydrolyzed (Shehzad et al., 2017). Additionally, polymers tend to be unstable in high salinity conditions. A study (Pope et al., 1982) has shown that polymer and surfactant co-exist only below a certain critical salinity, beyond which polymer-rich and surfactant-rich phases are formed. Moreover, high-molecular-weight polymers are known to be shear sensitive (Bureiko et al., 2014). Polymer macromolecule breaks down beyond certain critical shear rate. This event is irreversible and leads to a severe loss of miscodifying power. Polymer stabilizers are commonly used to extend the operating window of polymers into higher temperature and higher salinity conditions. However, these stabilizers, most notably formaldehyde, are highly toxic and heavily regulated (Xu and Saeedi, 2016).

2.11.1 Type of Polymers

One of the most general polymer types used in the EOR process is a synthetic material, polyacrylamide in its partially hydrolysed form (HPAM). In addition to that, in this thesis, another modified polyacrylamide named phenyl polyacrylamide (PPAM) is used.

2.11.1.1 Conventional polymer HPAM

The polyacrylamide used in polymer flood application is in its hydrolysed form (HPAM). HPAM is a straight-chain polymer that has the amide group (CONH₂) as the monomer and carboxylic group (COO⁻) in their structure as shown in Figure 2.9. Acrylamide monomer is reacted with sodium hydroxide (NaOH) and partial hydrolysis can occur in some of these monomers. The carboxyl groups dissociate and leave negatively charged ions leading to polyelectrolyte properties in aqueous solution. Typical degrees of hydrolysis are 25% - 35% chosen to optimize the specific properties of the polymer solutions. If the degree of hydrolysis is too low, the polymer will not be water soluble. If it is too high, its properties are overly sensitive to salinity and hardness (Ren et al., 2011).

The typical molecular weight of HPAM used in polymer flood is within the range of 2-20 × 10⁶ g/mol. The viscosity-increasing feature is derived from the repulsion between polymer molecules and between the segments of the same molecule.

As a result of these molecular arrays, the viscosity of polymer increases and causes the lower mobility of the polymer solution (Shaohua 2015).

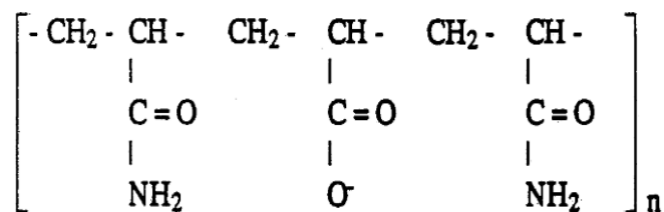


Figure 2. 10: HPAM molecule structure (Shaohua, 2015).

HPAM polymers are inexpensive, excellent viscosifier and more bacteria resistant than biopolymers, but they cannot be used in water with high salinity (> 30000 ppm), especially at raised temperature (> 80°C). Other disadvantages associated with HPAM are low thermal and shear stability, and injectivity problems of high molecular weight and high concentration solutions used for flooding (Nodar 2009; Sochi 2010).

2.11.1.2 *hydrophobically modified polymer (PPAM)*

Essentially, hydrophobically modified polymers (HMPs) consist of a hydrophilic long-chain backbone, with a small number of hydrophobic groups localized either randomly along the chain or at the chain ends (Lara-Ceniceros et al., 2007). When these polymers are dissolved in water, hydrophobic groups aggregate to minimize their water exposure. In aqueous solutions at a basic pH, hydrophobic groups form intramolecular and intermolecular associations that give rise to a three-dimensional network (Caram et al., 2006). These networks significantly increase the viscosity of the polymer solution. Another important factor is that the functional groups on these kinds of polymers are less sensitive to brine salinity compared to a conventional polymer, as polyacrylamide, whose viscosity dramatically decreases with increasing salinity.

In this study copolymer phenyl polyacrylamide (PPAM) which is a hydrophobically modified polyacrylamide, made of acrylamide (AM) as a hydrophile monomer and phenyl-acrylamide (PA) as a hydrophobe monomer has been used. PPAM is polyacrylamide (C_3H_5NO) hydrophobically modified with a low amount (1-3 mole %) of phenyl-acrylamide.

2.11.2 *polymer retention*

Polymer retention includes all mechanisms causing removal of polymer molecules from solution during flow through a porous network. Polymer molecules can be retained by the porous rock during polymer flooding due to interactions between the two of them. Consequently, the efficiency of the polymer flooding is reduced since polymer molecules will be removed completely or partially from the injected fluid leading to a lower viscosity compared to the original polymer solution (Sorbie, 2013). The loss of this mobility control effect is significant at low polymer concentrations. In addition, polymer retention can cause a delay in the velocity of the polymer front and create oil bank propagation (Lara-Ceniceros et al, 2007). A positive consequence of polymer retention is that the permeability of the porous rock can be reduced in areas where retention occurs (Sorbie, 2013). The permeability reduction causes additional reduction of the mobility of polymer and water which will contribute to increased oil recovery (Zolotukhin and Ursin, 2000). Despite the permeability reduction, polymer retention generally has a negative impact on the oil recovery. Polymer retention depends on polymer type, molecular weight, rock composition, brine salinity, brine

hardness, flow rate and temperature (Lake, 2010). Polymer retention will normally be lower during polymer flooding under reservoir conditions compared to experimental tests due to lower flow rates (Chang, 1978).

Polymer retention is caused by the following mechanisms (Sorbie, 2013):

- • Adsorption on solid surfaces
- • Mechanical trapping in pores
- • Hydrodynamic retention

The three retention mechanisms are illustrated in Figure 2.10.

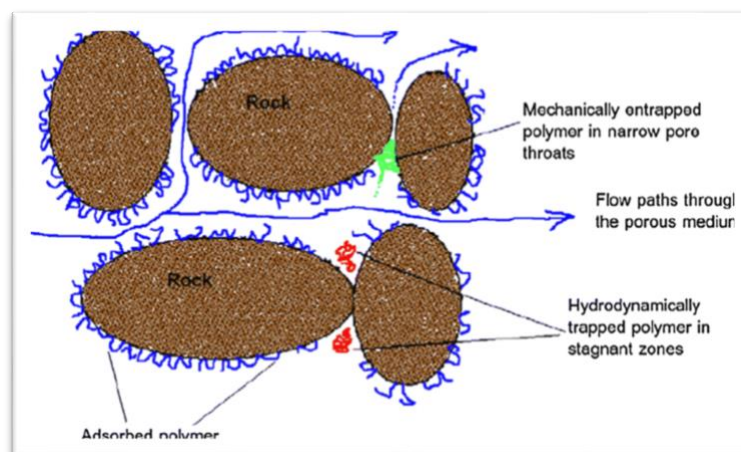


Figure 2. 11: Schematic illustration of the three retention mechanisms in a porous network, namely adsorption, mechanical trapping, and hydrodynamic retention (Sorbie, 2013).

Hydrodynamic retention and mechanical trapping can only occur when a polymer solution flows through a porous network (Sheng, 2013; Hematpur, H et. al., 2018). Hydrodynamic retention is observed as increasing polymer retention with increasing flow rate during experimental polymer flooding of cores. Adsorption of polymer on solid rock surfaces and mechanical trapping in pores are important mechanisms behind the overall polymer retention in a reservoir (Chang, 1978). Mechanical trapping in pores occur when large polymer molecules flow through narrow pore throats (Sheng, 2013). Polymer adsorption onto the solid surface of the porous rock is caused by interactions between the polymer molecules and the porous rock (Sorbie, 2013).

2.11.3 Surfactant- Polymer Interactions

The interaction between surfactant and polymer in bulk and at the interface between gas and lamellae in foam are complex. Electrostatic and/or hydrophobic forces control the interactions. Factors such as salt, surfactant or polymer concentration, molecule structure, the degree of branching, charge density and backbone rigidity affect the forces between surfactant and polymer (Bureiko et al., 2014). Surfactants adsorb to polymer to achieve a more energetically state than they do in micelles (Jenkins and Bassett, 1997).

2.12 The Structure of Polymer Enhanced Foam

Knowledge about the structure of polymer enhanced foam is required to understand how it will behave when flowing in a porous network. In a porous rock, if the lamellae are parallel to the flow direction, they can stretch over several pores. Lamellae can also span across multiple pores. The structure of polymer enhanced foam lamellae flowing in a porous medium matches the structure of bulk foam. In a pore space the polymer enhanced foam is lamellar and is orientated three-dimensionally. The thickness of lamellae is 1-12 μm . An anionic surfactant is used during the polymer enhanced foam by co-injection in sand packs in this thesis. The lamellae of polymer enhanced foam obtained from anionic surfactant have dimensions that are of the order of and smaller than pores. These lamellae appear as thin films, rod-like filaments and sheets aligned with the flow direction. The shape of these lamellae is illustrated in Figure 2.11. In enhanced oil recovery these lamellae can be used for mobility control since they effectively reduce the permeability of pores to injected fluids.

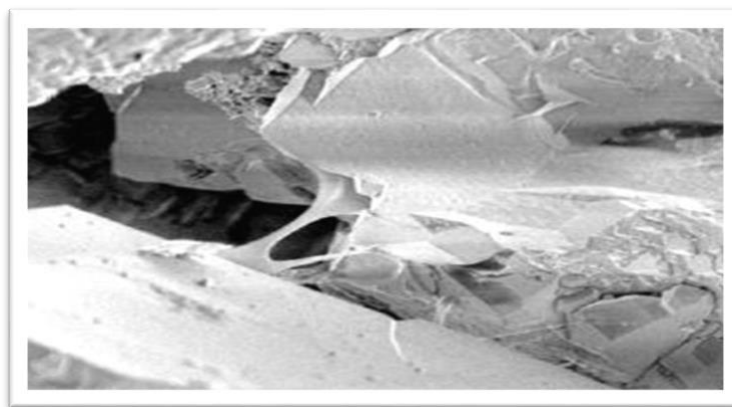


Figure 2. 12: Berea sandstone pore with polymer enhanced foam lamellae (Kutay a Schramm, 2004).

2.13 Surfactant

The surfactant term is a contraction of surface-active agent. Surfactants are chemical substances that adsorb on or concentrate at surfaces or interfaces between phases. In their most common form, surfactants consist of a nonpolar (hydrocarbon chain) portion and a polar (ionic) portion. Surfactants are amphiphilic which means that they contain both hydrophilic and hydrophobic groups. The polar portion is usually called the head, and the hydrocarbon chain is often called the tail of the molecule (Shramm, 2000).

Figure 2.12 is a simplified sketch of the surfactant molecule. The hydrophobic tail is the water-insoluble component while the hydrophilic head is the water-soluble component. In aqueous solution, the hydrocarbon portion interacts with water molecules very weakly. Water molecules try to extract hydrocarbon out of the water. Therefore, the tail is called hydrophobic. On the contrary, since the head (polar portion) interacts strongly with water, this portion of the surfactant is called hydrophilic (Figure 2.12). As shown in the figure, surfactant molecules (head and tail) tend to attach and form a layer at surfaces or between interfaces with the hydrophilic head residing in the water medium while the hydrophobic tail residing in the non-polar oil medium. Thus, surfactants significantly alter the interfacial properties between two surfaces or interfaces (Ren et al., 2011).

Surfactants decrease the interfacial forces between two surfaces, reduce the surface tension, or interfacial tension (IFT) between two phases (Delshad *et al.*, 2006).

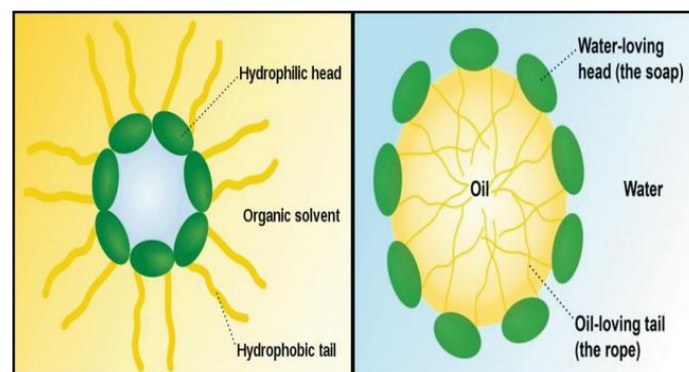


Figure 2. 13: structure of surfactant molecule

2.14 Surfactant Classification

Surfactants are classified as anionic, cationic, non-ionic, and zwitterionic (amphoteric) with respect to the ion charge of the surfactant head group.

2.14.1 Anionic Surfactants

Anionic surfactants have a negative charge on its head group. In aqueous solution, the molecule ionizes, with the metal cation separated from the head group. Anionic surfactants have been most widely used in Enhanced Oil Recovery (EOR) applications. Because they have low adsorption on the rock matrix. Since they can be produced economically, they have a low cost on EOR processes. They are relatively stable. Sulfates, sulfonates, carboxylates, etc. are some examples of anionic surfactants (Ghosh and Mohanty, 2018).

2.14.2 Cationic Surfactants

These surfactants are classified as cationic because of the negative charge on their polar head group. In aqueous solution, ionization occurs, and the head has a positive charge (cationic). Due to the high adsorption rate on the rock surface, cationic surfactants are rarely used in EOR applications. These surfactants are generally more expensive than anionic surfactants. Pyridinium, piperidinium, etc. are some examples of cationic surfactants (Hirasaki *et al.*, 2011).

2.14.3 Non-ionic Surfactants

A non-ionic surfactant does not have any charged group on its hydrophilic head. When it is dissolved in aqueous solution, ionization does not occur. The head group is larger than the tail group in this structure. Non-ionic surfactants are mainly used as cosurfactants to improve phase behaviour and increase solubility. Although they have high salinity tolerance than anionic surfactants, non-ionic surfactants cannot have a considerable influence on IFT reduction as well as anionic surfactants. Polyoxymethylene, alkanolamides are some examples (Sandersen, 2012).

2.14.4 Zwitterionic (Amphoteric) Surfactants

Zwitterionic surfactants have both positive and negative charges (opposite charge) on their head. They dissociate in water into cationic and anionic parts. These surfactants contain two or more of the other classes. Figure 2.13 exhibits the surfactant classification with their examples and structures (Farn, 2006).

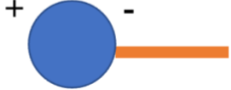
Class	Examples	Structures
Anionic Negatively charge head group	Sulfonates Sulphates Carboxylate Phosphate	
Cationic Positively charge head group	Quaternary ammonium organics Amines Sulfonium compounds piperidinium	
None-ionic Molecule does not ionize	Polyol ethers alkanol amides	
Zwitterionic With two or more of other classes	Amino carboxylic acids trimethyl glycine	

Figure 2. 14: Classification of surfactants

2.15 Critical micelle concentration (CMC)

The surfactant used should be suitable for the reservoir conditions (lithology, temperature, and pressure) in order to improve oil recovery. Critical micelle concentration (CMC) is the term that is used to describe the ability of a surfactant to reduce IFT. At CMC, the surfactant molecules, group into a structure that is known as a micelle. By adding a surfactant into a two-phase system, the surfactant will initially partition into the interface of the system, thus reducing the energy of the interface and removing the hydrophobic part of the surfactant from water. The increase in surfactant concentration will increase the surface coverage, which decreases the surface free energy, and the surfactant starts aggregating into micelles, resulting in a further reduction in energy at the interface and removing the hydrophobic part from water (Figure. 2.14). After reaching CMC, an increase in surfactant concentration will

not reduce surface tension (Shramm, 2000). Surfactant concentration should be higher than CMC to produce the lowest possible IFT.

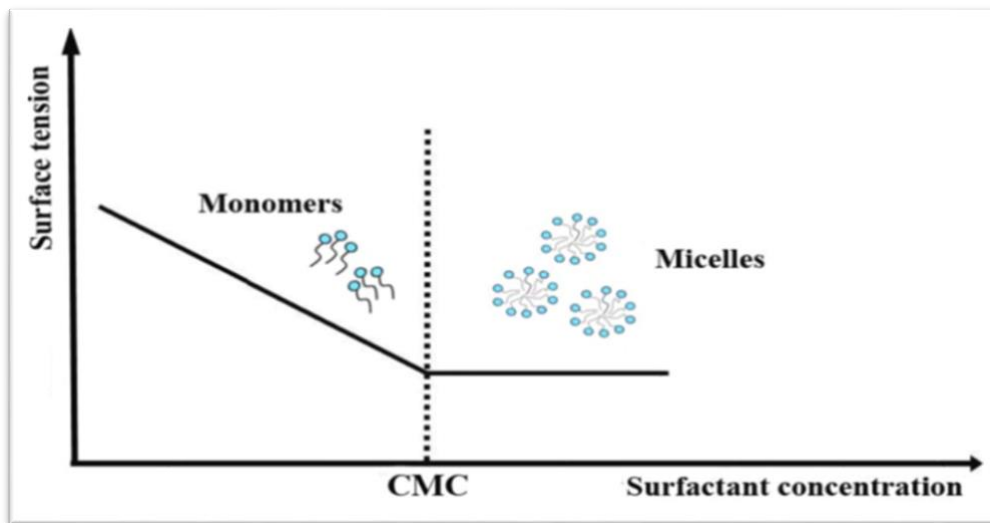


Figure 2. 15: Relationship between surfactant concentration and surface tension (Shramm, 2000)

Chapter 3: Methodology

3. Chapter 3: Methodology

This chapter is divided in three sections:

The first section shows the foam generation process, study of foam stability in presence and absence of oil and investigates the rheological properties of generated foam in bulk solution. The second part investigates the effect of rock permeability on foam rheological behaviour using sand pack. The last session shows the method and materials used in core flooding processes to investigate the effect of using polymeric foam on oil displacement in porous media.

A flow chart for the experiments is shown in Figure 3.1.

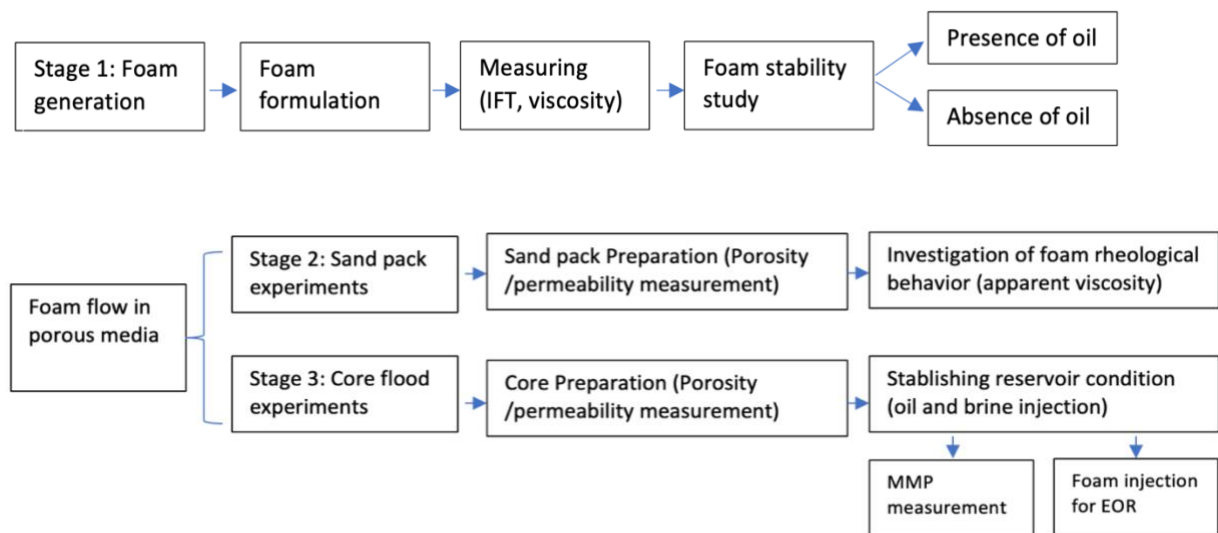


Figure 3. 1: Experimental flow chart

3.1 Foam generation Materials and Method

Experimental investigations have been carried out to examine the mechanism of foam generation in presence of Sodium Dodecyl Sulphate (SDS) and Internal Olephin sulfonate (IOS) as anionic surfactants, Betain, Dodecyltrimethylammonium bromide (DTAB) and Cocobetain as cationic surfactants. A mixture of dissimilar surfactants is more effective in achieving ideal microemulsion phase behaviour for oil recovery applications. Therefore, a mixture of anionic and cationic surfactants was used for some of the experiments. Two surfactants were created by mixing 1:1 ratio of Cocobetaine/SDS and SDS/DATB which is referred to as CocoSDS and SDS_DATB hereafter.

in addition, two polymers named Hydrolysed polyacrylamide (HPAM) and hydrophobic modified polyacrylamide (Phenyl polyacrylamide PPAM) are used, by using the CO₂ as gaseous component.

The half-decay was used as the measure to quantify foam stability the half-decay time defined as the time taken to reach half of the initial height of the foam, the longer the half-decay time the more stable is the foam and vice versa. This criterion was used in several previous studies (Simjoo et. al., 2013).

The surface tensions of the surfactant solutions and the oils were measured by a tensiometer at 25 ° C. The interfacial tensions were also measured with a spinning drop.

3.1.1 Polymer Characterisation

Polymer characterisation tests were carried out using two analytical techniques, Fourier transform infrared spectroscopy (FT-IR) and nuclear magnetic resonance spectroscopy (HNMR).

3.1.1.1 *FT-IR spectroscopy*

An FT-IR spectrometer (Mattson Satellite 5000 FT-IR) was used for the Fourier transform infrared (FTIR) spectroscopic analysis (Figure 3.2). In infrared spectroscopy, IR radiation is passed through a sample; some of the infrared radiation is absorbed by the sample and some of it is passed through (transmitted). The resulting spectrum represents the molecular absorption and transmission, creating a molecular fingerprint of the sample. Like a fingerprint no two unique molecular structures produce the same infrared spectrum. Infrared spectroscopy was used for qualitative analysis of the polymer.



Figure 3. 2: Mattson satellite FT-IR

3.1.1.2 *H-NMR spectroscopy*

NMR (Figure 3.3) analysis is used to confirm the chemical structure of an organic compound. Different functional groups are distinguishable, and identical functional groups with differing neighbouring substituents still give distinguishable signals. The principle behind NMR is that many nuclei have spin, and all nuclei are electrically charged. If an external magnetic field is applied, an energy transfer is possible between the base energy to a higher energy level (generally a single energy gap). The energy transfer takes place at a wavelength that corresponds to radio frequencies and when the spin returns to its base level, energy is emitted at the same frequency. The signal that matches this transfer is measured and processed to yield an NMR spectrum for the nucleus concerned.

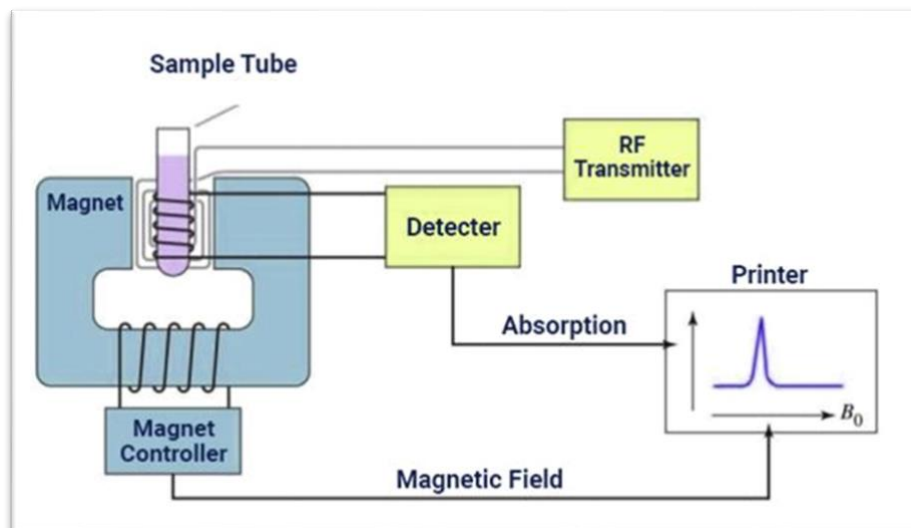


Figure 3. 3: NMR spectrometer (Pulsar) for High Performance NMR Spectroscopy

3.1.2 Fluid properties and materials

The surfactant solution was specially made to perform the foam coalescence tests. All formulated foams are presented in Table 3.1 and Table 3.2. The preparation of all solutions during this thesis, regardless of the type of surfactant, polymer, and solvent, followed the American Petroleum Institute (API) standard procedure (Dupuis, 2010).

Foam formula for foam generation
4%wt surfactant+ 2%wt NaCl + Distil water+ CO ₂ . (Polymer free foam)
2%wt surfactant+ 0.04% wt polymer+ 2%wt NaCl + Distil water+ CO ₂ . (Polymeric foam)

Table 3. 1: Foam formula for foam generation

Foam formula to be used in sand pack & core flooding	
F1	2%wt IOS+ 2%wt NaCl + Distilled water
F2	2% wt COCOSDS+2% wt NaCl + Distilled water
F3	F1+ 0.04% wt HPAM
F4	F2+ 0.04% wt HPAM
F5	F1 + 0.04% wt + PPAM
F6	F2+ 0.04% wt +PPAM

Table 3. 2: Foam formulas to be used in sand pack

The material used in this project are presented in Table 3.3.

Surfactants and polymer properties	
IOS	$C_{16}-C_{18}$
SDS	$Na C_{12} H_{25} SO_4$
Cocobetaine	$C_{19} H_{38} N_2 O_3$
DTAB	$C_{15} H_{34} Br N$
HPAM	$C_3 H_5 NO$
PPAM	$C_9 H_9 NO$

Table 3. 3: Surfactants and polymer properties

3.1.3 Surfactant and surfactant/Polymer solution preparation

To prepare a surfactant solution without polymer the procedure is as follows:

- Fill a suitable open beaker with 500g of brine/distilled water.

Chapter 3: Methodology

- Drop a suitable magnet into the container.
- Use a magnetic stirrer to create a vortex (Figure 3.4) almost reaching the bottom of the container.
- Add the surfactant to brine/distilled water and stir for one hour.

At this point the solution is ready to be used.

To prepare the surfactant/polymer solution, here is an example of preparation of 4000 ppm polymer solution in brine/distilled water.

- Fill a suitable open glass container (e.g., beaker) with 500g of brine/distilled water.
- Drop a suitable magnet into the container.
- Use a magnetic stirrer to create a vortex almost reaching the bottom of the container.
- Carefully sprinkle 2.5 g of polymer powder into the wall of the vortex, not the bottom. This careful sprinkling process was carried out for 30 seconds.
- Right after the addition of the polymer granulate, the stirring speed was reduced to the lowest possible rotation to avoid any mechanical degradation of polymer and to prepare a homogeneous polymer solution.
- Turn the magnetic stirrer down to the lowest, yet smooth turning level.
- The polymer solution was left on adequate stirring overnight and then the surfactant was added to it and left to stir for one hour. At this point the stock solution is ready to use.
- The polymer solutions were filtered through a 3 μ m Millipore fiberglass filter to remove any microgels or high molecular weight clumps that may have formed during the polymer preparation.

The stock solution was diluted when solutions with lower concentrations were prepared, using the magnetic stirrer at low speeds to avoid possible mechanical degradation. Solutions

older than a couple of weeks, especially lower concentrations, were disposed and replaced by a freshly made solution.

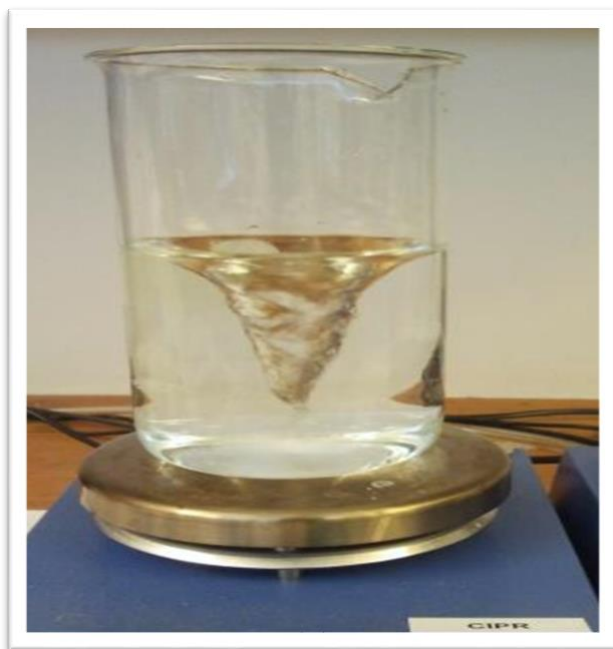


Figure 3. 4: Polymer solution preparation by using a magnet stirrer.

3.1.4 CMC measurement

The formation of foam in the presence of surfactant is a strong function of the critical micelle concentration (CMC) of the surfactant and the corresponding surface tension. The surface tension of the surfactants at different concentrations was measured to determine their CMC values. CMC was calculated by using a pendant drop method to create a solution in which micelles can be created. In the pendant drop method, the IFT between the surfactant solution at different concentrations with air was measured (Figure 3.5). The point where an increase in concentration doesn't lower the IFT anymore is the CMC.

3.1.4.1 Interfacial tension and surface tension of surfactant solutions

For all surfactants used in this project, the CMC was provided by the supplier. Only DTAB (which was used in combination with SDS) needed CMC measurement.

Chapter 3: Methodology

To calculate the CMC for DTAB, 4 wt% (wt refers to weight per cent) of surfactant solution is prepared and diluted with brine at various ratios to create 1 wt%, 0.5 wt%, 0.25 wt% and 0.125 wt% solutions.

A syringe is used to collect a sample from each of these concentrations. Then, a drop of the solution is forced out of the syringe needle, and a picture of the solution drop is captured while it is still connected to the tip of the needle (the needle diameter is 0.68 mm). Each drop has a unique shape in air. First Ten Angstroms software is used to calculate the CMC by measuring d_e and d_s from the captured pictures (Figure 3.7). The maximum diameter d_e is measured from the drop profile and the diameter d_s at a horizontal plane at a distance d_e from the bottom of the drop.

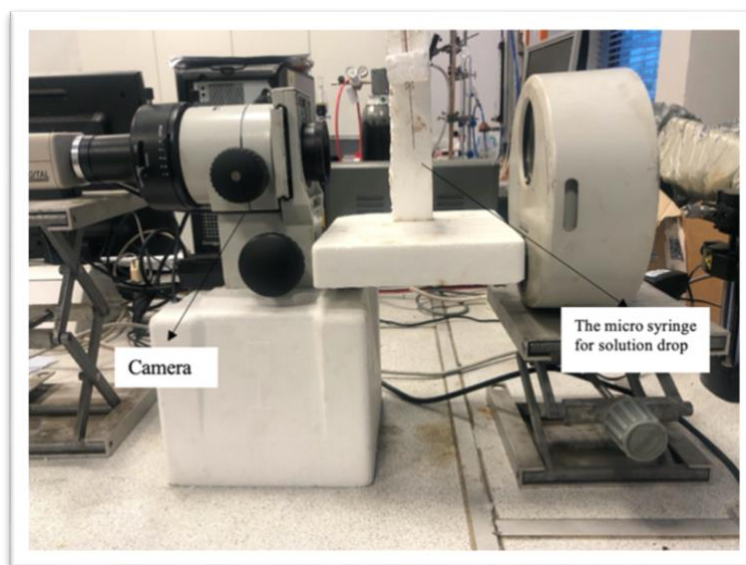


Figure 3. 5: Pendant drop set-up.

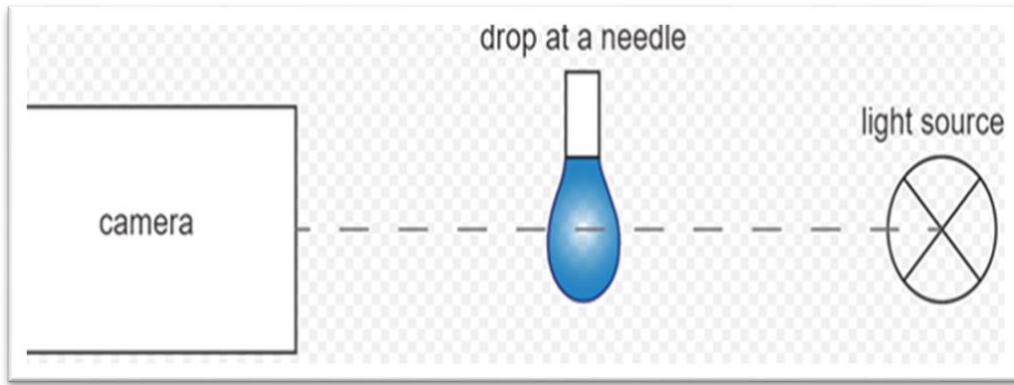


Figure 3. 6: Schematic process of the pendant drop method.

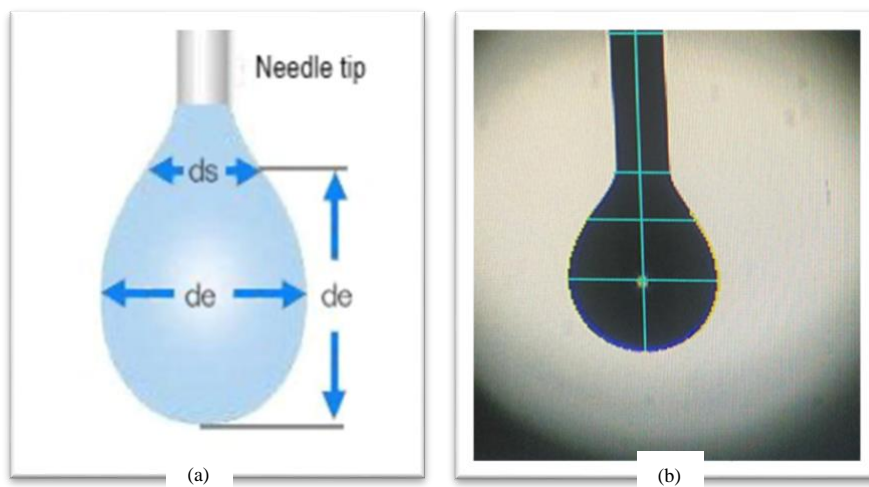


Figure 3. 7: a) Schematic solution drop with the parameters needed for surface tension measurement, b) the captured picture from a surfactant/brine solution drop.

The software calculates the surface tension through the following equation:

Surface tension:

$$\gamma = \Delta\rho g h (d_e)^2 1/H \quad (3.1)$$

where:

$\Delta\rho$: density difference

g : gravity acceleration.

$1/H$: correction factor determined from d_s/d_e

Table 3.4 shows the IFT measured by First Ten Angstroms software. By plotting surfactant concentrations versus their IFT, CMC was measured (Figure. 3.8).

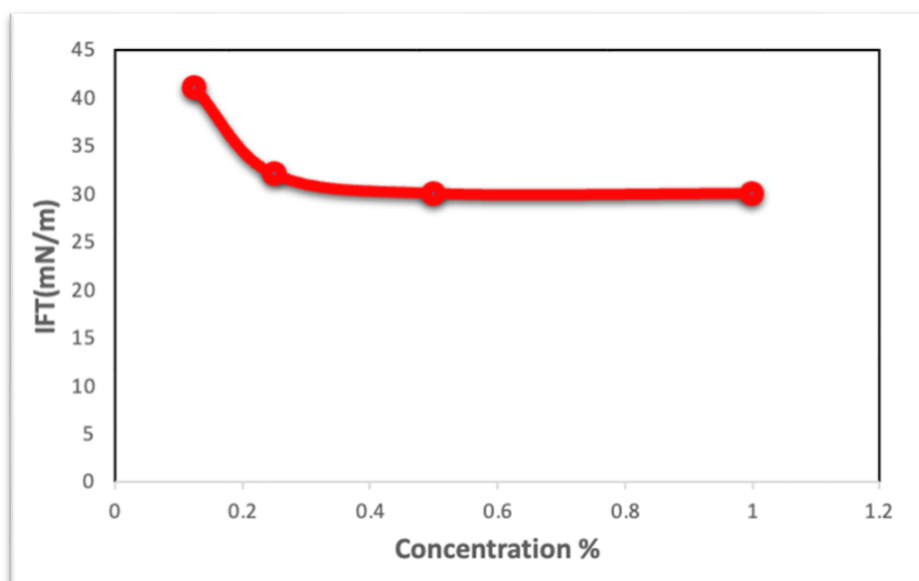


Figure 3. 8: IFT vs surfactant concentration(wt%) by pendant drop method.

The results are presented in Table 3.4,

Surfactant concentration (%)	IFT (DTAB)
0.125	41
0.25	32
0.5	30
1	30

Table 3. 4: Measured IFT for DTAB by pendant drop.

3.1.5 Rheological properties measurement

Rheological measurements were carried out by using a BOHLIN 200 Rheometer shown in Figure 3.9. The viscosity of the surfactant and surfactant/polymer solution is measured at different shear rates ranging from (0.1 s^{-1} to 1000 s^{-1}) and the effect of salinity on the viscosity is determined by loading the solution into the plate of the viscometer and leave it

Chapter 3: Methodology

for 1-2 minutes to settle before turning on the viscometer. The measuring system consists of a cone and a plate with 4° angle and 40 mm diameter of plate.

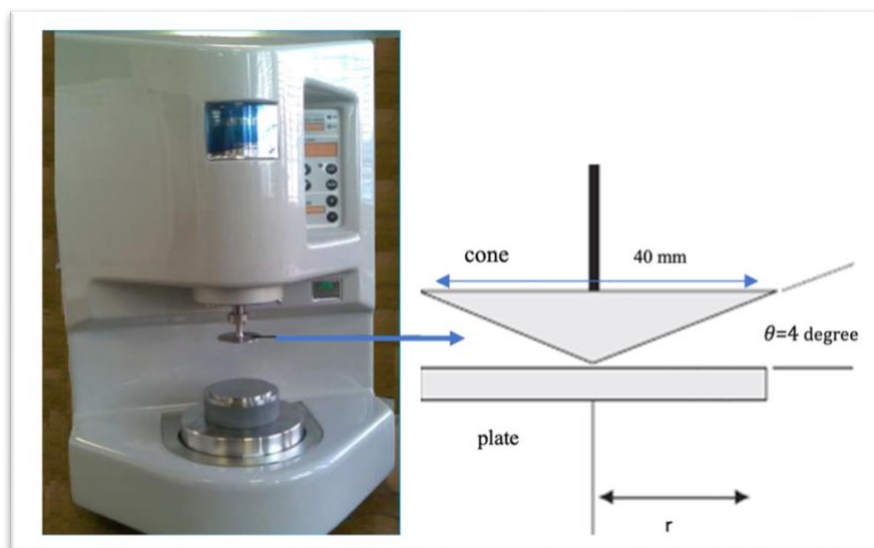


Figure 3. 9: Bohlin Rheometer

3.1.6 Experimental setup

An experimental setup was designed and developed to quantify the bulk foam height as a function of time for determining foam stability at bulk-scale as shown in Figure 3.10.

For the bulk-scale experiment, a chromatography column with an inner diameter and height of 4 cm and 60 cm respectively was used. Fitted to the bottom was a sintered disk with a pore size distribution of $40\text{--}100\ \mu$. The function of the sintered disk was to enable gas sparging.

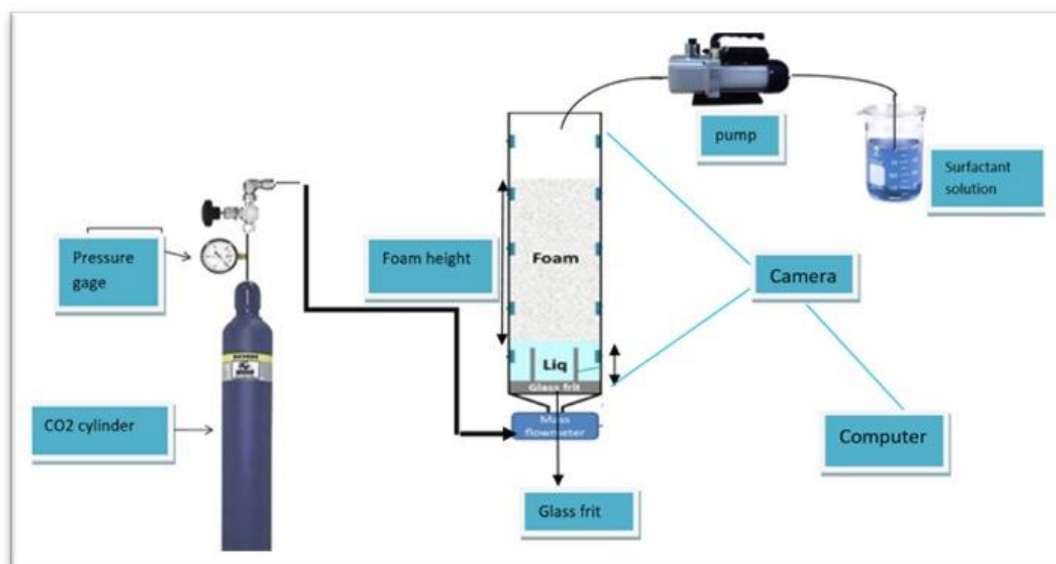


Figure 3. 10: Schematic of the foam column set-up used for foam generation and foam stability study

3.1.7 Foam generation and foam stability procedure

In this study, CO₂ was used to make foam which was injected into the chromatography column containing 100 cm³ of the surfactant or surfactant/polymer solution at a volumetric flow of 100 cm³/min (± 0.1 cm³/min) using a mass flow controller to provide CO₂ at a constant flow rate; the gas was passed to the base of the column through a pressure regulator and gas flowmeter. The gas injection flow rate was kept at 100 ml/sec for surfactant systems whereas for the same systems with added polymer the gas flow rate was kept at 120 ml/sec to obtain uniform and stable foam. Foam was generated by sparging gas through the surfactant solution via the sintered disk. After generating a bulk foam, gas injection was stopped to allow the drainage of foam. The time when gas injection was stopped is referred to as initial time for foam drainage and it corresponds to maximum foam height. Continuous reading of foam height at different time intervals were noted. Foam height is the measure of net foam generated during foaming process. At any instant of time, the foam height (h) can be calculated as the difference between height of foam level and liquid level in the column. In foam stability study, the half-decay time ($t_{1/2}$) is defined as the time taken by foam to reach half of its initial value. It describes the foam stability such that a longer $t_{1/2}$ corresponds to more stable foam.

3.2 Foam flow behaviour in Sand Pack

Foam flow tests were carried out in both sand packs and sandstone cores.

This part covers the second phase of the project which is to investigate the effect of rock permeability and heterogeneity on foam/polymeric foam behaviour and rheology using sand pack. It includes a detailed description of the methodology used for pore-scale characterization of foam in porous media.

3.2.1 Material and method

As discussed, the purpose of this part of the project was to study the effect of rock heterogeneity and permeability on foam and polymeric foam rheological behaviour. The first

step to approach this work was to conduct experiments using unconsolidated sand packs, henceforth referred to as sand pack flood experiments. The objective was to use specific mixtures of sands to create specifically designed porous environments to study foam and polymeric foam rheological behaviour in controlled systems. Four sand mixtures were designed (heterogeneity) within two sand packs, in addition to one homogenous sand pack. In this way, the effect of permeability and heterogeneity could be investigated.

3.2.1.1 Sand Pack preparation and analysis

The sand used for the sand packs, is crushed Berea sand. The sand is sieved, washed with distilled water, and dried before use. The particle size distribution of the sand was measured by means of sieve analysis. Three sands with average size of 50-110 μm ,110-280 μm and 280-355 μm were used for sand pack flooding tests. Figure 3.11 shows sieves and shaker. Table.2 shows the sand size distribution for each sand pack.

The sand pack was packed vertically, filling the column with sequences of 1 cm of sand at the time. Between each 1 cm of sand filling the cylinder was shaken and moved back and forth horizontally 20 times to improve the packing of sand. The sand was packed from the inlet towards the outlet and was completed when the packed sand column reached 20 cm from the inlet. The three pressure taps along the cylinder were closed during sand filling. After each experiment all the parts of the sand pack were disconnected, cleaned with water, and dried with air.



Figure 3. 11: Sieve analysis of soil

3.2.1.2 Porosity measurement

The sand pack was vacuumed for 15-20 minutes to remove air in order to have a better brine saturation. When saturation was completed, the porosity was calculated using the following equation (Zhang 2013):

$$\text{porosity } (\phi) = \frac{V_p \text{ (Pore volume)}}{V_b \text{ (Bulk volume)}} \quad (3.1)$$

$$\text{Pore volume } (V_p) = \frac{\text{Saturated weight} - \text{Dry weight}}{\text{density of brine}} \quad (3.2)$$

$$\text{Bulk volume } (V_b) = \left(\frac{\text{Sand weight}}{\text{Grain density}} \right) + \text{Pore volume} \quad (3.3)$$

The dry weight was measured after the sand was packed and the wet weight was recorded after the sand pack was completely saturated. The grain density was measured by filling a volumetric flask with a known weight of sand and then filling the rest of the volume with water.

A syringe pump (KDS 210) (Figure 3.12) was used for the sand-pack flooding experiments. It had a maximum injection rate capacity of 20 ml/min.

A low-pressure transducer Omega (PX2300), with a measuring interval 0 to 1.7 bar was used to measure differential pressure across the sand pack holder.

Pressure data are recorded on a data acquisition system as a function of current intensity versus time.



Figure 3. 12: KDS syringe pump

3.2.1.3 Permeability measurement

Permeability tests were done with brine injection only. The syringe pump was used to determine permeability because of its ability to accurately change the volumetric flow rate in small increments. The air was evacuated from the sand pack by using a vacuum pump to ensure fully saturation of sand pack. The sand pack holder was weighed before and after saturation to determine sand pack porosity and then brine injection was performed at different flow rates. Each flow rate was maintained long enough to fully reach a steady state pressure drop. The pressure drops were measured by the pressure transducer and the effluents were collected in the fraction collectors. The injection rate could be checked by the effluent volume because the samples were taken on a time basis. Once the brine injection was completed at different flow rates, the data from the experiment were collected and the permeability was determined using Darcy's law. A schematic diagram is shown in Figure 3.13.

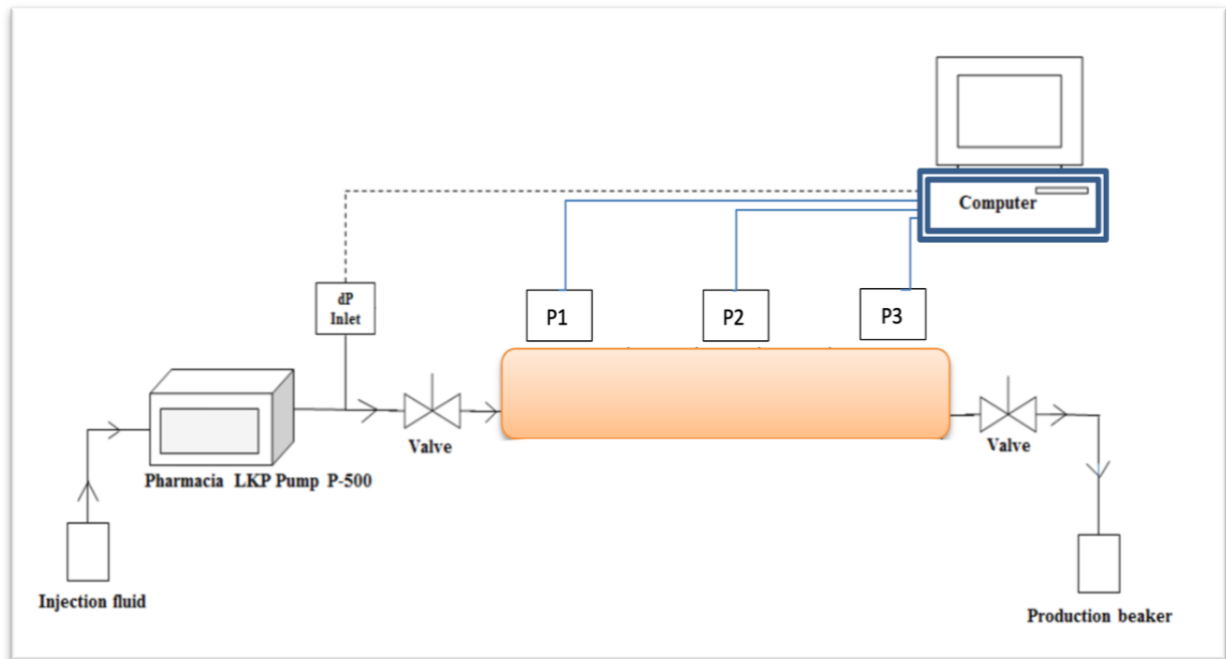


Figure 3. 13: A schematic illustration of the experimental set-up used for permeability and adsorption measurements.

3.2.1.4 Adsorption

Prior to conducting the surfactant co-injection or the surfactant+polymer co-injection experiments, the sand packs were pre-flooded with 2 PV of the appropriate foam agent (surfactant solution or surfactant+polymer solution) to satisfy adsorption of surfactant and polymer on the sand grains. Note that during surfactant+polymer 2 PV of each fluid (surfactant solution and polymer solution) was injected, 4 PV in total. It is important to satisfy adsorption to avoid the experimental results obtained from the co-injections being affected by unwanted mechanisms of surfactant loss and polymer loss due to adsorption on the sand grains and retention by the porous medium. A lower surfactant concentration due to loss of surfactants can reduce the foaming ability of the surfactant solution and surfactant+polymer solution as well as the stability of the foam. Complete or partial removal of polymer molecules due to interactions with the porous medium can result in a lower viscosity compared to the original surfactant+ polymer solution and hence reduced stability of the foam. The experimental set-up used to satisfy adsorption is shown in Figure 3.13.

3.2.2 Surfactant Foam and polymer enhanced foam procedure by co-Injection

This part provides a detailed overview of the experimental set-up (Figure 3.14), the list of equipment and the procedure for the surfactant foam and polymer enhanced foam by co-injections.

The sand pack flood experiments consisted of different sand packs that mimicked different reservoir rock qualities. These were high and low permeability sands, with a fine to coarse grain size distribution. Sand pack floods were conducted at 25°C. Foam performance was determined by the measured pressure drop across the sand pack. The pressure drops (or pressure gradient $\Delta P/L$) is an indication of foam strength and propagation and was used to calculate the apparent foam viscosity (μ_{app}) using equation 3.4.

$$\mu_{app} = KA\Delta P/L \quad (3.4)$$

The sand pack flood experiments were conducted in the absence of oil, as the effect of rock heterogeneity was targeted, without the interference of the destabilizing effects that oil has on foam. Sand pack flood was conducted at 90% foam qualities.

The sand pack was placed horizontally, and the mass flow controller and the pump were connected to the inlet via two separate fittings. Inlet valve and outlet valve were opened prior to the co-injection. Polymer enhanced foam by co-injection of CO₂ and surfactant+polymer solution experiments were conducted at a constant total volumetric injection rate of 200 ml/h, and gas fractional flow at $f_g=0.9$. A production beaker at the outlet collected produced fluids. The pressures were monitored using 3 absolute pressure transducers located along the sand pack during the co-injection. The surfactant foam by co-injection experiments followed the same procedure as the polymer enhanced foam by co-injection experiments, but the foaming solution contained only surfactant.

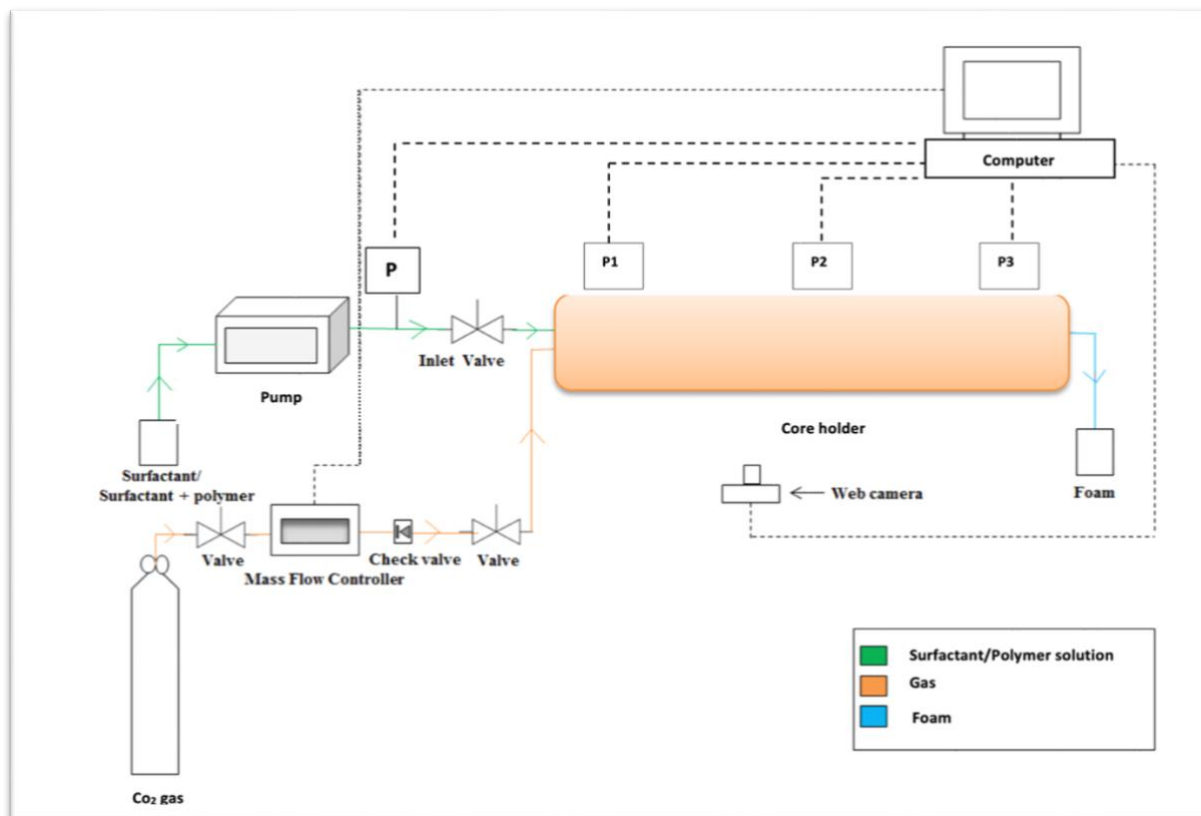


Figure 3. 14: Sand-pack flooding system.

3.3 Core flooding for EOR, Method and Material

In this section, a series of oil displacement experiments were conducted on sandstone core samples. Two Bentheimer sandstone cores with absolute permeability of 100 mD and 500 mD were used.

A complete high pressure core flooding apparatus was used to conduct the experiments. It is composed of a core holder, pressure transducers, pumps and piston cylinders for fluids, a back pressure regulator, sample fraction collector and data acquisition system.

However, the first step was to measure the MMP to avoid the effect of injection pressure on data readings and analysis. The Injection pressure has an impact on the oil production results. Above miscibility pressure, oil recovery reaches a plateau, and exceeding that pressure will not increase oil recovery. Therefore, MMP was determined through a series of oil production tests with CO₂ using a slim tube.

After MMP determination using a slim tube, a series of core flood experiments were conducted using continuous CO₂ injection (CCI), continuous water injection (CWI) and foam injection.

3.3.1 Experimental set-up and apparatus

Equipment used in core flooding and slim tube is listed below:

3.3.1.1 ISCO 500D pump

A D-Series ISCO digital syringe pump with a cylinder capacity of 266.05 ml was used. The pump flow rate was set on a panel with a range from 0.01 ml/min to 100 ml/min (this pump is capable of any injection rate at different pressures up to 10,000 psi). The pump controller regulates all pumping functions. Programming and set-up were performed using the keypad on the front panel (Figure 3.15). The ISCO injection pump is capable of constant injection rates over a wide pressure range, as well as a constant pressure flow over a wide range of flow rates. The ISCO pump can inject test fluids directly or indirectly into the system. In the indirect mode (used in this study), the pump injects the driving fluid (distilled water) exclusively into the accumulators placed in the oven and then the substance on the other side of the piston (brine, oil, gas, toluene/acetone, or surfactant solution) was fed into the injection lines. For CO₂ injection, the ISCO pump was used to keep the pressure constant. For fluids injection, the ISCO pump was used to keep the injection rate constant. So, the role of the ISCO pump for any liquid was to keep the injection rate and the pressure constant for any injection.

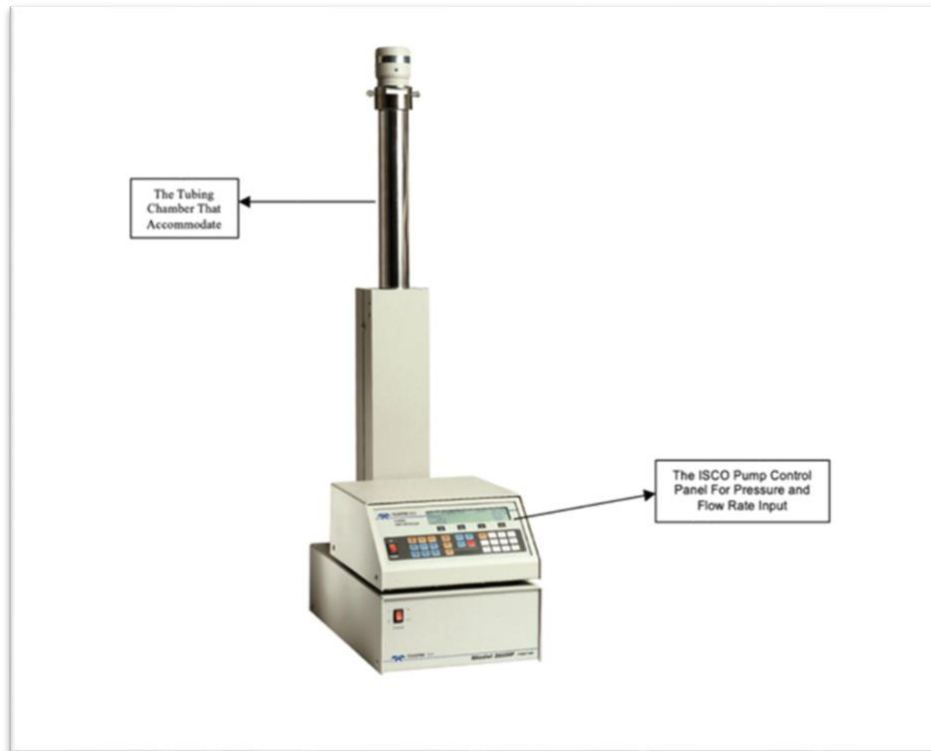


Figure 3. 15: ISCO pump.

3.3.1.2 Floating piston accumulators (FPAs)

The accumulators maintained the test fluids at reservoir conditions during the experiment. The accumulators were basically cylinders equipped with two end plugs and one floating piston, separating the cylinder into two different chambers: a driving chamber and a test chamber. The driving chamber contained the driving fluid (distilled water) coming from the pump, while the test chamber contained the fluids that were injected into the core holder (brine, oil, CO₂, and solvent).

3.3.1.3 Pressure transducers

Pressure transducers were used to measure the pressure of the core inlet, core outlet, pump, back pressure regulator, and overburden. One differential pressure transducer was connected to the core inlet and outlet for the measurement of pressure drop across the core. The pressure transducer and pressure gauges were supplied by Bronkhorst pressure controller Inc with a range of $\pm 0.25\%$ accuracy for the transducer and $\pm 1\%$ accuracy for the

pressure gauges, respectively. The pressure transducer was connected to a data acquisition system for converting the electrical signals into pressure readings.

3.3.1.4 *Back pressure regulator (BPR)*

A back pressure regulator (BPR) was used to control and maintain the pressure inside the system and reduce the pressure drop to a minimum. An accurate BPR was necessary in these experiments, as the pressure needed to remain constant throughout the flooding experiments. The BPR set the outlet pressure (P₂) at a level where production did not happen until P₂ was increased to that pressure. The nitrogen cylinder provided the pressure for the BPR and was located outside the oven.

3.3.1.5 *Air bath (oven)*

Measurements were taken at reservoir temperature using an oven (air bath), which heated up the core sample (in the core holder) and the fluids. The oven maintained a high temperature throughout the different processes of the experiments.

3.3.1.6 *Flow meter and wet gas meter*

A Bronkhorst model F-230M mass flow controller (MFC) was used in this experiment; it was suitable for accurate volume measurement and control flow ranges between 0.2–10 ml/min at operating pressures up to 5,800 psi. The MFC consisted of a thermal mass flow sensor, a precise control valve and a microprocessor-based pc-board with a signal. As a function of a set point value, the flow controller swiftly adjusted the desired flow rate. The MFC was equipped with a digital pc-board, offering high accuracy, excellent temperature stability and fast response. The main digital pc-board contained all the general functions needed for measurement and control. The MFC was used to set the injection rate for the pressurized CO₂ flowing from the FPA. The flow meter (Figure 3.16) was also capable of measuring the volume of CO₂ flowing to keep the volume of the injecting cycles consistent. All functions were controlled through different software: FlowDDe, FlowPlot, FlowView and FlowAd.



Figure 3. 16: Mass EL-FLOW meter by Bronkhorst.

Apart from the gas flow meter, a gas pressure meter was mounted downstream just after the collectors to record the time of gas breakthrough (Figure 3.17). A wet gas meter and a sight glass were used alongside each other to confirm achieving miscibility for MMP experiments. For instance, miscibility was achieved if only one phase was flowing through the sight glass, but the wet gas meter was detecting CO₂. The wet gas meter allowed precise measurements of gas produced at the ambient conditions.



Figure 3. 17: EL-PRESS pressure meter by Bronkhorst.

3.3.2 Minimum miscibility pressure (MMP) measurements by slim tube

Miscibility is an important factor in the design of any EOR project that involves gas injection. It has been widely agreed that at miscibility pressure, optimal oil recovery occurs. To measure the miscibility between oil and gas, different methods for slim tube measurements, rising bubble technique, vanishing interfacial tension and numerical simulation, have been introduced. Slim tube displacement is often referred to as the industry's most common method for determining MMP (Alshuaibi *et al.*, 2018). However, slim tubes differ in size and porosity. The justification for using a long slim tube is to minimise the effect of the transition zone (Fig. 2.6). The transition zone is part of the reservoir where the saturation is graded from 100% water in the water zone to an irreducible water saturation (Masalmeh, 2000). In a slim tube MMP measurement process, a transition is where both gas and oil are present but due to the long tubing, enough time is provided for both oil and gas to become miscible and generate one phase. A slim tube can provide accurate data as actual fluids are used in the procedure (Amao *et al.*, 2012). A slim tube is packed with uniform sand or glass beads and housed in an oven.

3.3.2.1 *Slim tube methodology*

To understand how the whole process of a slim tube experiment led to MMP calculation, the system set-up is described in the section below. Every part of the slim tube design was necessary to keep errors to a minimum. In this study, 2 PV of injected CO₂ was used based on the slim tube manufacturer's suggestion.

3.3.2.1.1 Slim tube set-up

The slim tube set-up included: floating piston high pressure accumulator for oil, floating piston high pressure accumulator for gas, floating piston high pressure accumulator for solvents, high pressure positive displacement pump (ISCO pump), stainless steel coil tube (slim tube by Vinci), oven, precise back- pressure regulator, wet gas meter (by Bronkhorst), high pressure visual cell (sight glass), CO₂ cylinder and N₂ cylinder for back pressure build up (Figure 3.18).

The slim tube itself was located inside the oven and was connected to upstream accumulator, one accumulator was used to pressurize the CO₂ to the planned injection pressure, one to keep the solvent (toluene and acetone) to clean up the slim tube after each run, and another one for oil injection. These accumulators were connected to the ISCO pump, whose injection rate and injection pressure were controlled and stabilized.

The CO₂ accumulator (Figure 3.19) was connected to the CO₂ cylinder (located outside the oven). The CO₂ cylinder was bought from BOC and had an internal pressure of 50 bars (725 psi). The injected CO₂ was fed to the Bronkhorst flowmeter before entering the slim tube. The injection rate and pressure were controlled through FlowPlot, FlowView and FlowDde software.

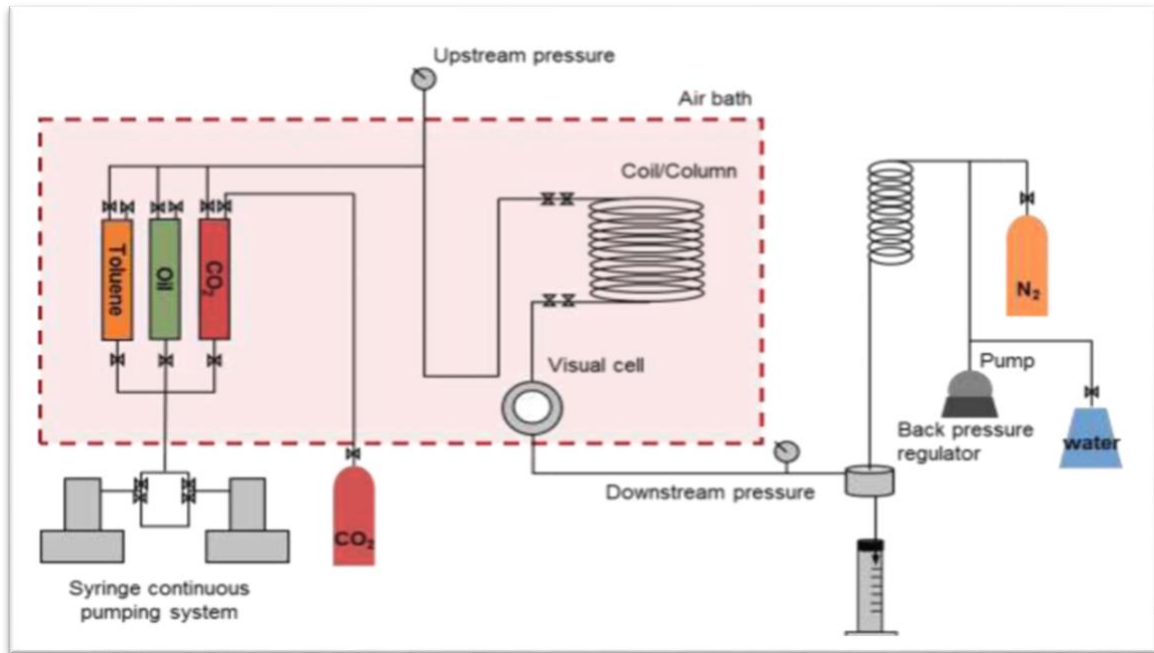


Figure 3. 18: Schematic set-up of slim tube.

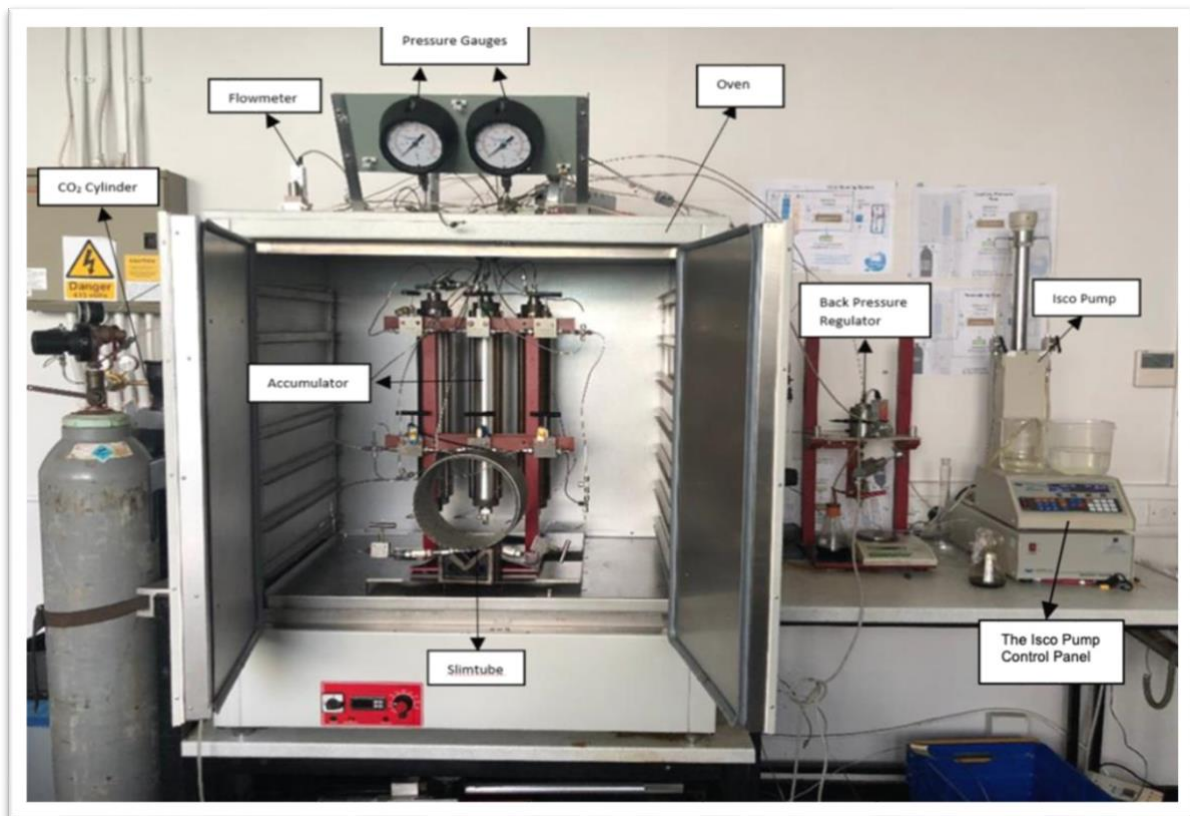


Figure 3. 19: Slim tube set-up

3.3.2.1.2 Slim tube

The slim tube was a one-dimensional narrow tube packed with sand. The tube was initially saturated with oil at a reservoir temperature. The oil was then displaced by injecting CO₂ into

the tube at a constant outlet pressure. The slim tube was 12m long, with a high permeability of 15 Darcy, and an approximate porosity of 35%. The high-pressure tubing of the slim tube was made from stainless steel capable of standing pressure up to 10,000 psi and a temperature of 150 °C. Two Butech hand valves were also used, one at the inlet and one at the outlet of the slim tube, to isolate the system at times of failures, e.g., leakage.

3.3.2.2 Slim tube procedure

Before and after each procedure, the slim tube underwent a process of preparation, which included cleaning, drying, and filling the slim tube to 100% oil saturation. The same process of preparation was followed at each run to clean the slim tube of any unwanted fluids and make it ready for the next experiment. The slim tube was cleaned with toluene, the toluene was washed out with acetone and dried after each experiment. The middle accumulator was used for cleaning under pressure. About 2-3 PV of toluene was injected through all tubing and valves to clean any remained oil, and to remove any wax. Then, 2 PV of acetone was injected. The system was also heated to dry out. A vacuum pump was used at the end of the cleaning process to seal the slim tube for oil injection. This process was repeated after each run. In this study, removing and reassembling different parts was kept to a minimum to reduce the chance of leakage. The fewer times a fitting was removed and replaced, the longer the fitting remained leak-free. If there was leakage or valve failure, the sealing and valve were replaced with new ones.

To start an MMP test, the temperature was raised to 70°C. After the temperature stabilised, oil was injected into the slim tube to 100% saturation. After saturation of the slim tube with oil, filling the FPA with CO₂ and pressurizing it to the injection pressure, and confirmation of no leakage, the oven doors were shut, and CO₂ injection took place for 2 PV.

The pressure inside the CO₂ cylinder was 50 bars (725 psi), but CO₂ and oil were not miscible at this pressure; therefore, the CO₂ pressure needed to be increased to higher pressures until miscibility occurred. This was done through the first accumulator located inside the oven on the left-hand side. At first, the accumulator was filled with CO₂ at 725 psi by connecting it to the gas cylinder. Then, the connection between the CO₂ cylinder and accumulator was stopped using the valve placed on top of the accumulator. After sealing the CO₂ accumulator,

the chamber piston was pushed up with the help of the ISCO pump. The ISCO pump created the extra pressure needed inside the accumulator. After increasing the pressure inside the accumulator to the desired level, the valve was reopened, and CO₂ was ready to be injected into the system. The injection rate of the CO₂ was controlled through FlowDde and FlowView.

The flow meters and pressure transducers were connected through FlowDDE software to the system. After a connection was made between the slim tube system and the computer, data were read using FlowPlot and FlowView. FlowPlot had overall control of the system, and readings were taken as values other than exact numbers. FlowView was used to control and read the exact numbers for injection rate, pressure, and volume of CO₂ produced. Channel 1 was connected to EL-FLOW, which was logging the flow meter readings at the upstream of slim tube (core holder). Channel 2 was connected to EL-PRESS at downstream to read the volume of gas produced. Channels 3 and 4 were P1 and P2, respectively.

FlowDDE handled all communications to the instruments and sent data to the applications. Through FlowView, the injection rate was controlled to avoid any high flow injection rate or CO₂ pressure drop. As mentioned, there was an option available to measure the amount of CO₂ injected, which for the slim tube experiment was set to stop at 230 ml (after 2 PV to measure the recovered oil). This means CO₂ injection was stopped after 2 PV and oil recovery was measured after that amount of CO₂ injection.

After finishing the test, the back pressure was released to let the system pressure drop to atmospheric pressure. This happened gradually and the liquids produced were collected at downstream. Visual observation of the flow through a visual cell helped in determination of the miscibility condition. The achievement of miscibility was expected to be accompanied by a gradual change in colour of the fluid flowing from that of oil to clear gas. On the other hand, observation of two-phase flow was symptomatic of immiscible displacement. Although a colour change in the oil produced was not visible, bubbles at immiscible pressures were observed through the sight glass. On the other hand, at the time of miscibility, one phase was observed through the sight glass.

It was planned to have six displacements at pressures of 1000, 1500, 1750, 2000, 2250 and 2500 psi. These six pressures were chosen to estimate the oil recovery trend on a plot of

pressure vs oil recovery. Oil recovery at 2 PV was measured at different pressures to predict MMP. The dead volume of 62.15 ml was measured by oil injection. The slim tube pore volume was 52.85 ml, which makes the total pore volume 115 ml. Therefore, based on the Vinci manual's recommendation, 230 ml (2 PV) of CO₂ was injected to measure oil recovery. The crude oil used in this project was provided by the Maersk Oil Company, it had a density of 0.8016 g/ml, and an API of 45° with 6 cp viscosity at room temperature.

FlowDDe was used to measure the amount of CO₂ injected as well as to maintain a low flow rate of 0.4 ml/min. BPR was also set at the desired pressure, so after P₁ exceeded P₂, production began. FlowDDe was set to shut the valves after 230 ml of CO₂ was injected.

3.3.2.3 Data collection technique

The MMP calculation procedure was based on a two-phase displacement where the whole system was saturated with oil and then oil was displaced by CO₂ at a constant pressure. Since there was no water in the system, the oil volume inside the tubing was added to the system to make a total of 115 ml of PV.

For each experiment at a set pressure, 2 PV of CO₂ was injected into the system. Then injection stopped, the system was de-pressurized, and oil was collected downstream. The weight of the recovered oil was measured through the difference in weight of the container before and after oil production. By using the density of the oil, the volume of recovered oil was measured. For example, at 1750 psi, 40.5g of oil was recovered and as the density of the oil was 0.8016 g/ml, the volume of recovered oil was 50.5 ml, which was equal to 44% of OOIP.

3.3.3 Core flooding

Core floods are the most representative experiments that can be conducted for reservoir conditions. Foaming capacity in core floods is influenced by pressure, temperature, surfactant formulation, surfactant concentration, injection strategy, oil saturation, and a few more properties.

In this part of experimental study, a series of core flood tests were carried out for both surfactant and surfactant/polymer foam and parameters such as mobility reduction and oil recovery.

Chapter 3: Methodology

A complete high pressure core flooding apparatus shown in Figure 3.20 and Figure 3.20 was used to conduct the experiments. It is composed of a core holder, pressure transducer, pumps, and piston cylinder for fluids, back pressure regulator, sample fraction collector and a data acquisition system.

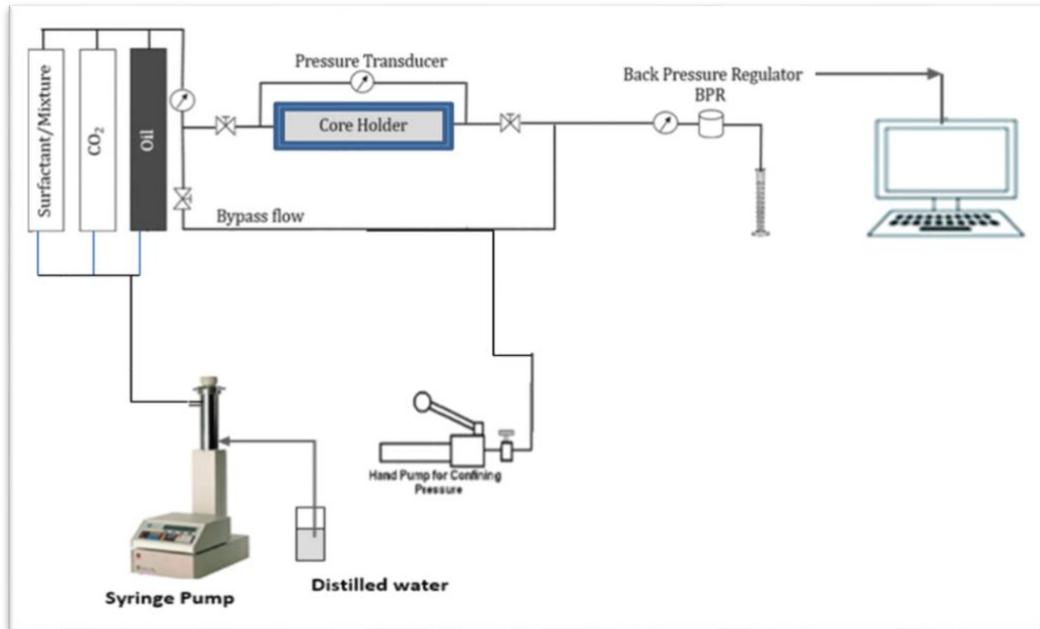


Figure 3. 20: Schematics of core holder set-up

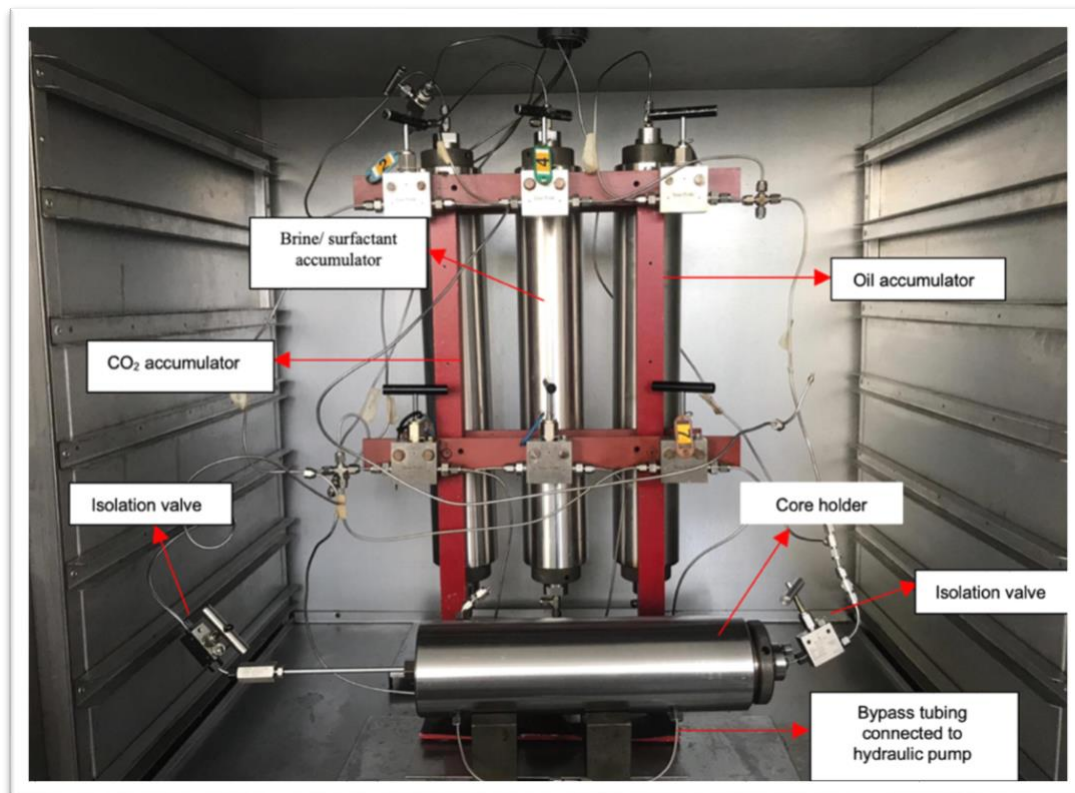


Figure 3. 21: Core flood system.

The initial reservoir condition needs to be applied on the core sample to determine oil recovery. After cleaning the core and measuring its porosity, brine was injected at low flow rate to estimate the brine permeability of the core, followed by oil injection to establish reservoir condition for the core. At this stage, the original volume of oil in the core sample can be calculated by measuring the effluent volume. The test was further carried out by initial water flooding (IWF) into the core sample and the volume of recovered oil was measured. Irreducible water saturation (S_{wi}) and residual oil saturation (S_{or}) can be calculated through the measurement of the volume of effluent samples. Then, foam flooding (tertiary oil recovery) was deployed to produce more oil. Hence the effect of surfactant and surfactant/polymer solutions on oil recovery was investigated.

3.3.3.1 Core and core holder

The core holder used has both inlet and outlet mandrels as shown in Figure 3.22. One mandrel on the left was attached to the cap and the mandrel on the right can slide inside the core holder barrel to accommodate cores of different lengths. The dismantled core holder can be seen on the right in Figure 3.22 and shows the sleeve, a sandstone core and the two inner end pieces.

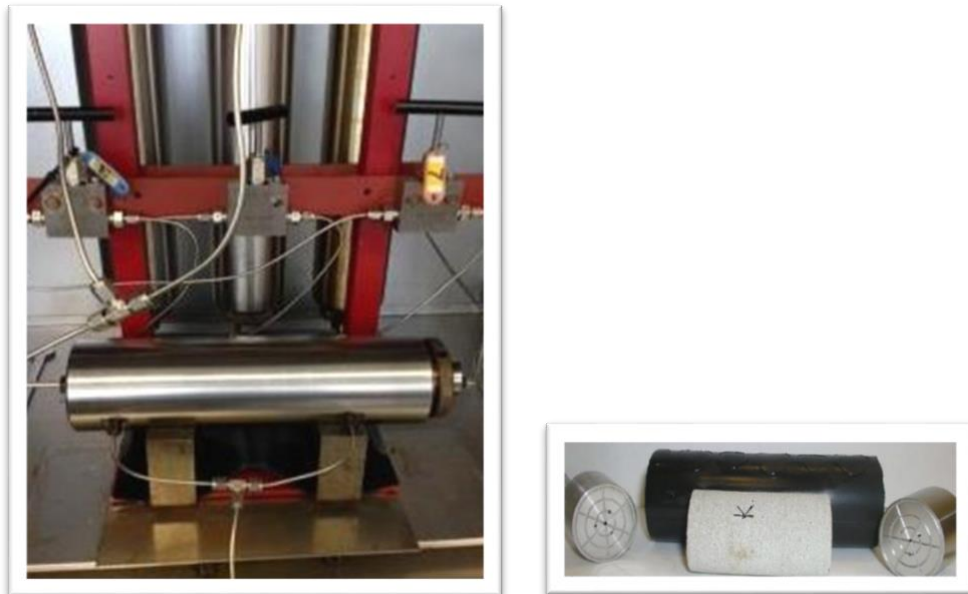


Figure 3. 22: Core holder cylinder and dismantled on the right

3.3.3.2 Confining Pressure

After the core was placed into the core holder, the sleeve was pressurised to simulate the 3D axis stresses that the core was under in real reservoir conditions. Some of these stresses are caused by the weight of the material above the core which is called “overburden” pressure. In this experiment hydraulic oil was used to provide an overburden pressure of around 2000 psi (Figure 3.23).



Figure 3. 23: Hydraulic pump.

3.3.4 Core flood Experimental procedure

Details of the experimental procedure are as follows:

3.3.4.1 Fluid preparation

This step involved filling the accumulators with appropriate fluids and pressurizing the CO₂. One accumulator was used for oil drainage. The other accumulator accommodated brine, surfactant, or surfactant/polymer solution. The third accumulator used for pressurizing and injecting CO₂.

3.3.4.2 Core preparation

- The core was soaked in methanol using a vacuum pump (Figure 3.24) for at least 24 hours. This allows any air trapped in void spaces of the core to escape.
- Remove the core from methanol and allow it to air dry for at least 48 hours.
- Submerge the core in distilled water in a vacuum pump for at least 24 hours, then remove it and wipe it off gently before measuring its wet weight.
- Place the core in a vacuum oven set to 70 °C for 8 hours and then measure the dry weight to be able to calculate the pore volume of the core sample.

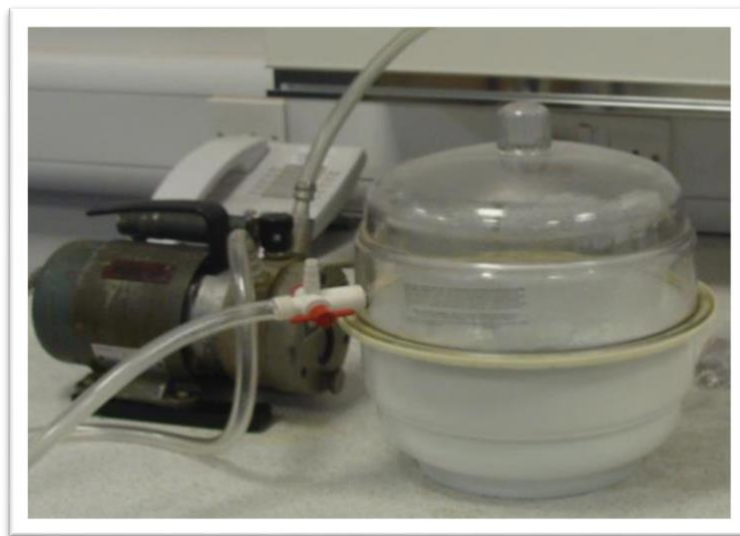


Figure 3. 24: Vacuum pump for core saturation.

3.3.4.3 Brine injection

The same brine for sand pack flooding was used in the core flooding experiment. The prepared brine was filtered through a 0.45 μm Millipore filter paper and then transferred to the injection cylinder (accumulator). The brine was then injected into the core sample at different flow rates by using ISCO syringe pump.

Steps of oil injection procedure:

- Fill in the accumulator with oil, attach all lines and purge oil into the line to make sure there is no air in the system before use.
- Apply the confining pressure in the system by closing the hand pump valve first. Then start pumping hydraulic oil until the confining pressure reaches 2000 psi.

- Increase the back pressure by opening the nitrogen tank valve and set the regulator to 2 bar.
- Ensure all lines have been purged and pressure is monitored during the experiment.
- Apply a low flow rate of maximum 0.5 ml/min to make sure a homogeneous propagation of oil in the core sample for better saturation. Oil injection carried on until a constant pressure drop across the core achieved. At this point the original oil in place (OOIP) that is the total volume of oil in the sample and the volume of brine displaced can be determined.
- After this the pump is shut off and the oil valve should be closed to stop any further flow of oil into the core.

3.3.5 Steps of Initial water flooding (IWF) procedure

- The brine accumulator must be filled with brine solution. Then the lines must be properly reattached to ensure there is no loss of pressure or fluid during the experiments.
- Set the pump flow rate to 0.5 ml/min and make sure the pressure data was recorded on the computer.
- The brine was injected at constant flow rate and the effluent is collected in 10 ml graduated cylinders.
- Brine injection continued until the pressure drop across the core sample remains constant.
- The volume of oil recovered by brine injection can then be determined after completing these steps.

3.3.6 Steps of Foam flooding (tertiary oil recovery) procedure

The same sequence of brine injection was followed for foam injection. Two types of surfactant solution were used in this experiment, PPAM and HPAM were added to the solutions. However, a lower flow rate is required to keep the inlet pressure constant due to the high viscosity of the solution (0.1- 0.2 mL/min). surfactant or surfactant/polymer injection continued until the pressure drop across the core remains constant. For each trial roughly two pore volumes of polymer are injected as the final phase to represent the tertiary oil recovery step.

Chapter 3: Methodology

After the polymer injection is completed, the trial is finished, and the system can be cleaned and reset for a new core.

3.3.7 Core cleaning process

The field cores contained residual oil and brine which needed to be removed for subsequent experiments. The cores were cleaned by a Soxhlet extractor (Figure 3.25) with toluene for the oil/water removal and acetone/methanol for the salt removal. Sufficient time (~one week) was allowed for both the toluene and acetone/methanol cleaning.

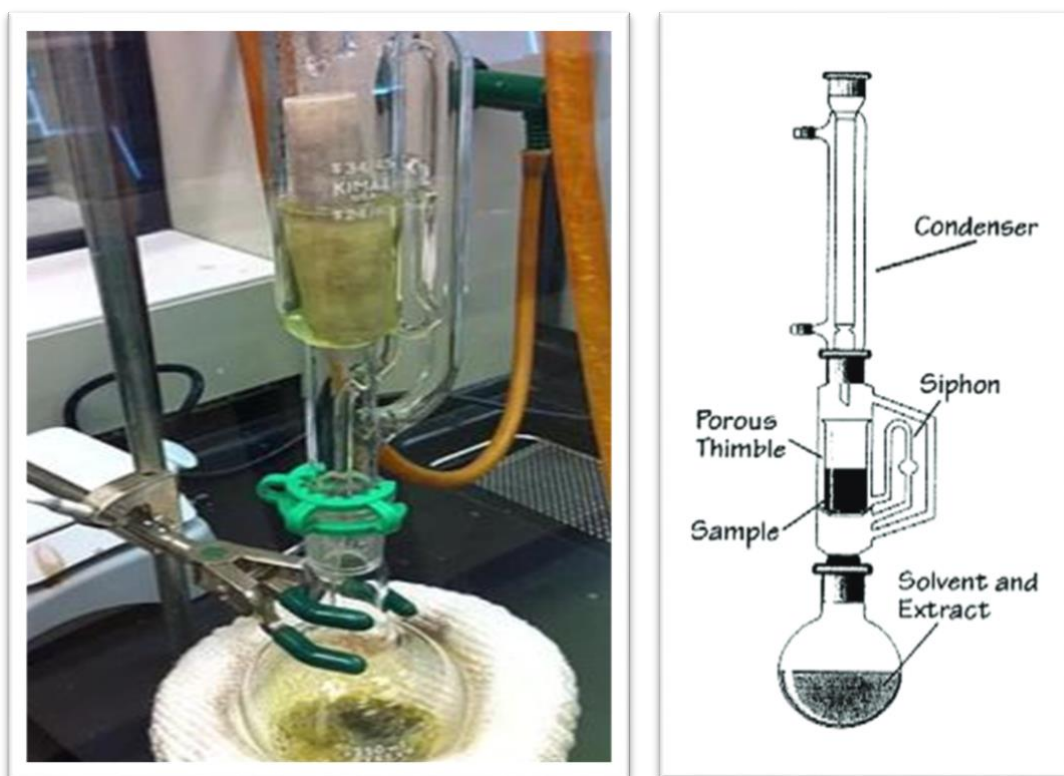


Figure 3. 25: Soxhlet extractor for core cleaning

3.3.8 Data collection

Since the core flood system involved three-phase flow, it was possible to flush the oil in the tubing after establishing S_{iw} in the core using the bypass tubing. After removing the oil in the tubing and disconnecting the bypass path, the core holder was connected to the accumulators for injection. Via this method, any oil that was produced downstream was extracted from the core sample. Unlike the slim tube data collection method, oil recovery was observed throughout the injection and was measured after each injected cycle in a metric scale cylinder.

3.3.9 Source of errors in the experiments

The following factors could cause errors during the experiment:

- Air could get trapped in the apparatus and affect the flow of the fluids and the displaced volume.
- Misreading the volume of the produced fluids on the graduated cylinders.
- The existence of “dead volume” in the system could cause errors in the final calculations.
- Assurance of no liquid residual, especially oil, left in the system which could cause errors in experiments.

Chapter 4: Results and discussions

4. Chapter 4: Result and discussion

In this chapter the results of experimental work are presented and discussed. This chapter is divided into three parts. Part one includes visual observations and results from the foam generation tests. The second part discusses the results from the co-injections of surfactant and surfactant+polymer in the sand pack as well as basic sand pack properties from routine analysis which are followed by experimental results and discussions. In part 3 oil displacement results in sandstone cores are shown and discussed.

4.1 Results and discussion of foam generation and stability

As discussed earlier, in the first part the experimental results, visual observations from the foam generation tests are presented and discussed. The tests were designed to visually investigate the stability of foam in the presence and absence of oil by measuring the half-life of decay foam height in chromatography column. The literature describes that foam stability is the ability of foam to resist bubble collapse and coalescence (Romero-Zeron and Kantzas, 2007).

4.1.1 Polymer free foam stability in the absence and presence of oil, bulk scale

After the column was filled to a height of 60 cm (± 1 cm), the CO₂ sparging into the cylindrical foam column was terminated. Then foam height reduction was monitored over time. Figure 4.1 and Figure 4.2 show the foam decay profiles of six surfactants used in the experiments in the presence and absence of oil.

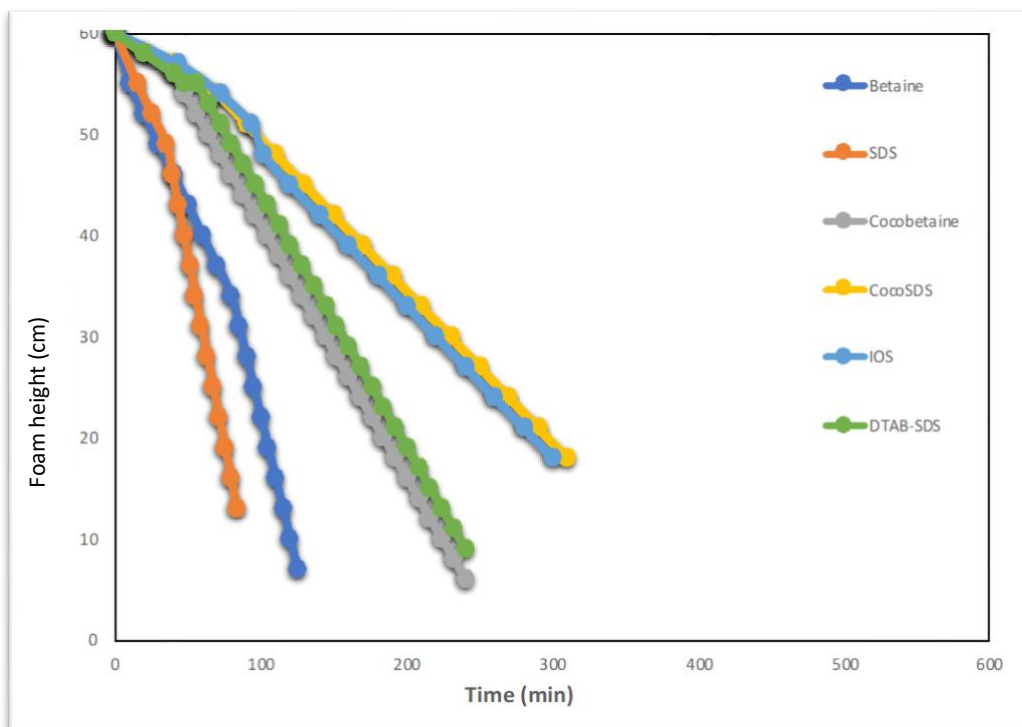


Figure 4. 1: Height decay profile of foam in the presence of oil (using six different surfactants)

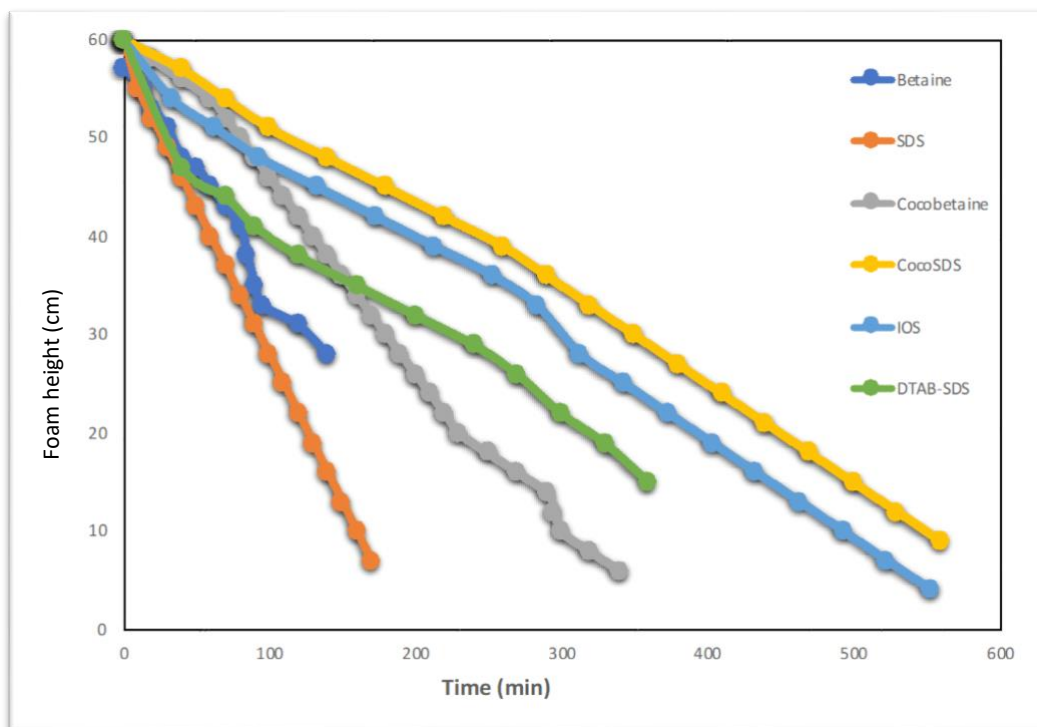


Figure 4. 2: Height decay profile of foam in the absence of oil (using five different surfactants)

As it can be seen in Figure 4.1. and Figure 4.2 the results show that the SDS foam is the least stable foam with a half-decay time of 180 min and 83 min and the Cocobetaine foam has the highest stability with a half-decay time of 550 min and 310 min in the absence and presence of oil respectively. The high stability of CocoSDS can be explained as follows. The mixture of ionic surfactants forms more stable foams due to the strength of the electrostatic double layer effect resulting from charge interactions at the film interface (Myers, 2005). The short lifetime and stability of the generated foams could be interpreted by the rapid spreading of oil droplets that have low surface tension over the lamellae. The spreading oil, by augmenting the curvature radius of the bubbles, decreases the surface elasticity and surface viscosity.

Foam generated by SDS is usually unstable probably because the surfactant molecules do not interact sufficiently at the interface leading to a low interfacial elasticity. In the CocoSDS case, the dimethylaminopropylamine reduces the interfacial tension between the surfactant solution and oil and increases the lateral chain interactions between the surfactant molecules resulting in improvement of surface viscosity and film elasticity which lead to foam stability enhancement.

The stability of Betaine, Cocobetaine and SDS-DTAB and IOS was approximately between 200 min and 570 min in the absence of oil and between 100 min and 300 min in the presence of oil.

4.2 Liquid drainage

Another factor that affects foam stability is liquid drainage. This phenomenon governs the primary phase of foam destabilisation as mentioned earlier; CocoSDS produced the most stable foam among the four surfactants. At shear rate 10 (1/s), the viscosity of CocoSDS is 0.35 (Pa.s) compared to 9.35×10^{-4} for SDS and 8.19×10^{-4} for Cocobetaine. The viscous nature of the surfactant solution results in slow drainage of liquid through the plateau borders.

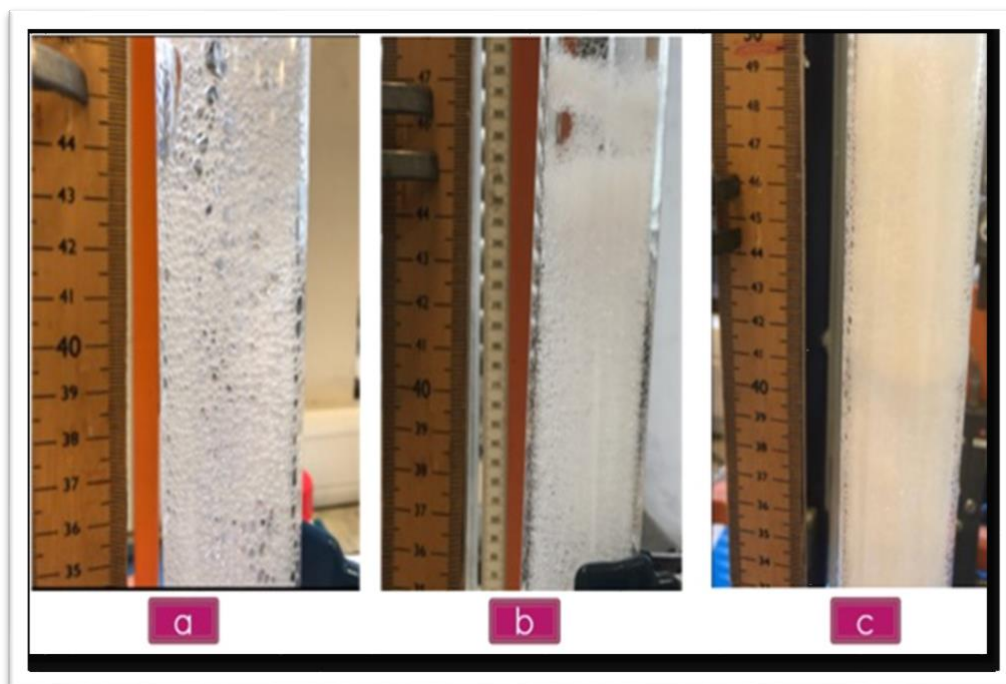


Figure 4. 3: The liquid fraction of foam **a)** Cocobetaine, **b)** SDS and **c)** CocoSDS after 40 min from the onset of the experiments

Figure 4.3 confirms that CocoSDS has more resistance to liquid drainage and higher stability. The order of stability was however reversed in the case of SDS and Cocobetaine for the drainage test. In other words, although the foam generated by Cocobetaine was more stable than SDS the rate of liquid drainage from the foam in the primary decay stage was greater in Cocobetaine than SDS after a given time from the onset of the experiment. It is observed from Figure 4.3 that Cocobetaine foam is much dryer than the SDS foam. During the initial stages of foam decay, there is rapid and uniform drainage of liquid from the Cocobetaine foam. Though it is likely that diffusive foam coarsening may be occurring during this period, bubble collapse does not occur simultaneously due to the stability of the foam films. On the contrary, the reduction in foam height, despite slower liquid drainage rate in SDS suggests that bubbles are rupturing even during the first stage of foam decay. The foam is still wet according to the intensity of the foam in Figure 4.3 suggesting that the coarsening is occurring at a very slow rate in this foam. This explains the faster collapse time in the SDS foam compared to the Cocobetaine foam in Figure 3.1 and Figure 4.2, even though more liquid has drained from the latter. Moreover, the Cocobetaine foam may have higher critical capillary pressure (which

corresponds to a lower critical film thickness before rupture) compared to the SDS causing higher stability after rapid liquid drainage (Hadjiiski et. al., 2003).

Foam	Stability	Drainage
SDS	Not stable	Medium resistance
Betaine	Semi stable	–
Cocobetaine	Stable	Low resistance
DTAB-SDS	Stable	Low resistance
IOS	Very stable	High resistance
CocoSDS	Very stable	High resistance

Table 4. 1: Foam drainage data

It was concluded that CocoSDS and IOS foams are the most stable foams in the presence and absence of hydrocarbon. Therefore, these two foams were used to investigate the effect of polymer on foam stability.

4.2.1 Effect of surfactant concentration on foam stability using IOS

Figure 4.4 shows the results for the IOS concentration on the half-decay time of foam in the presence and absence of oil. The results indicated that, the half decay time of the foam in the presence of oil is systematically lower than in the absence of oil for all of the experiments for all concentrations and increases with surfactant concentration. Increasing surfactant concentration results in reduced gas diffusion due to the formation of thicker interfacial films around the bubbles which affect the surface tension and improve foam stability by reducing the liquid flow within the lamellae region.

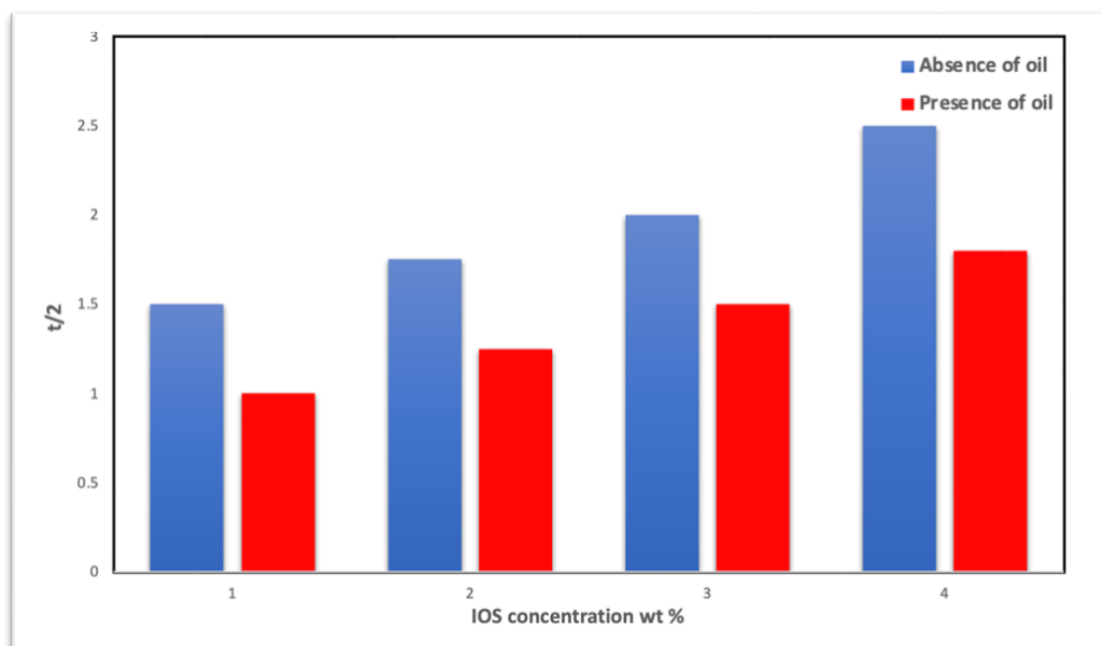


Figure 4. 4: Effect of IOS concentration on foam stability.

4.2.2 Polymer enhanced foam stability

The use of polymer in conjunction with surfactant has been proposed to increase the stability of foam. Hence the effect of two polymers (hydrolysed polyacrylamide (HPAM) and hydrophobic modified polyacrylamide (PPAM) on foam stability at bulk scale is presented. PPAM is polyacrylamide (C_3H_5NO) hydrophobically modified with a low amount (1-3 mole %) of phenyl-acrylamide.

4.2.2.1 PPAM characterisation

- **FT-IR spectroscopy**

The FT-IR spectrum of the synthesized polymer is displayed on Figure 4.5. The PPAM structure is made up of carboxylate functional group ($C=O$), amide group ($N-H$) and phenyl group (C_6H_5). The peak observed at 2982 cm^{-1} is assignable to the $C-H$ stretching from the phenyl group. The IR spectrum also indicated the existence of the carboxylate ($C=O$) and amide ($N-H$) groups through the absorption peaks at 1623 cm^{-1} and 3356 cm^{-1} , respectively. Therefore, the PPAM composition analysis is right according to FT-IR. The Handbook of polymer (1999) was used to extract functional groups relationship with wavelength.

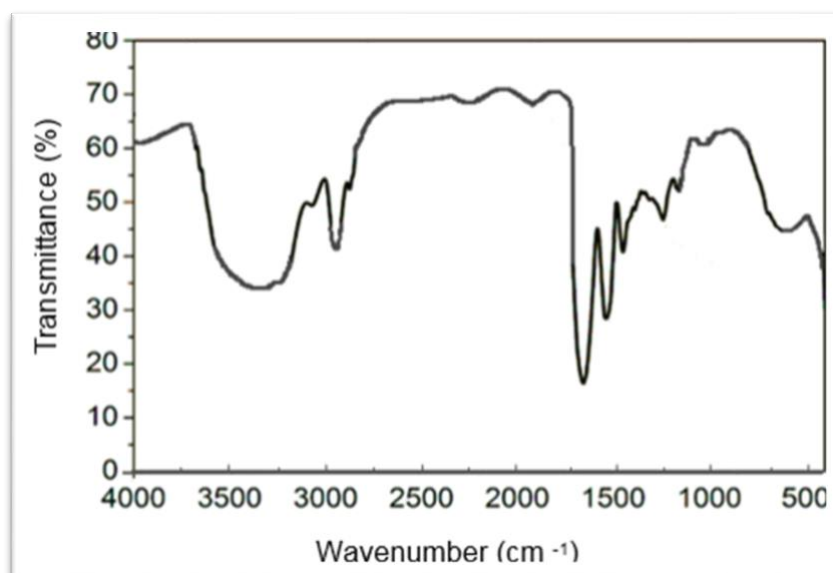


Figure 4. 5: FT-IR spectrum of sample of P(acrylamide/phenyl-acrylamide).

- **H-NMR spectroscopy**

The H-NMR spectrum for PPAM is presented on Figure 4.6. This indicates the presence of methylene CH₂ group (A), CH (B) and phenyl (C) group. Data also confirm the absence of any surfactant molecule after drying the polymer as no more peaks were observed in the spectrum. This observation supports the formation of multi-block copolymers including long sequence of acrylamide and short sequence of the hydrophobic monomers.

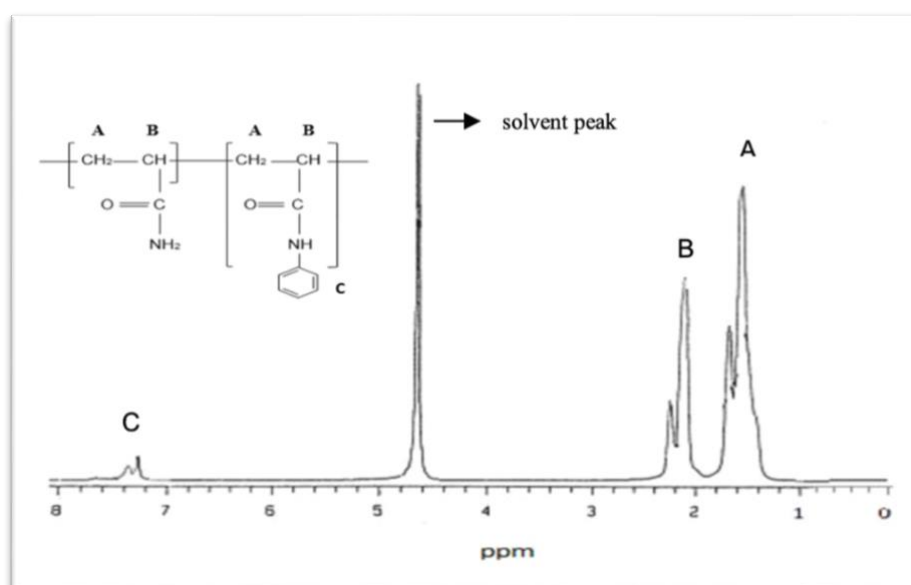


Figure 4. 6: H-NMR spectrum of a sample of P (acrylamide/phenyl- acrylamide) containing 1.2 mol % hydrophobe.

4.2.2.2 Comparing PPAM with HPAM

- **Concentration effect**

Different polymer solutions of HPAM and PPAM at different concentrations are prepared in distilled water. The viscosity of these solutions is measured with a rheometer at fixed shear rate (10 1/s) and the results are shown on Figure 4.7. The results indicate that at low polymer concentration (< 200 ppm) the viscosity of both polymer solutions is almost the same, however, the viscosity of PPAM solutions begins to increase faster than HPAM solution after 200 ppm. In other words, a higher concentration of HPAM solution is required to obtain the same viscosity value as for the PPAM solution. This higher viscosity for PPAM is due to the entanglement of hydrophobic regions and intermolecular association whereas in HPAM the repulsion of negative charges causes the polymer chain to stretch and increase the viscosity (Pandey et al 2008).

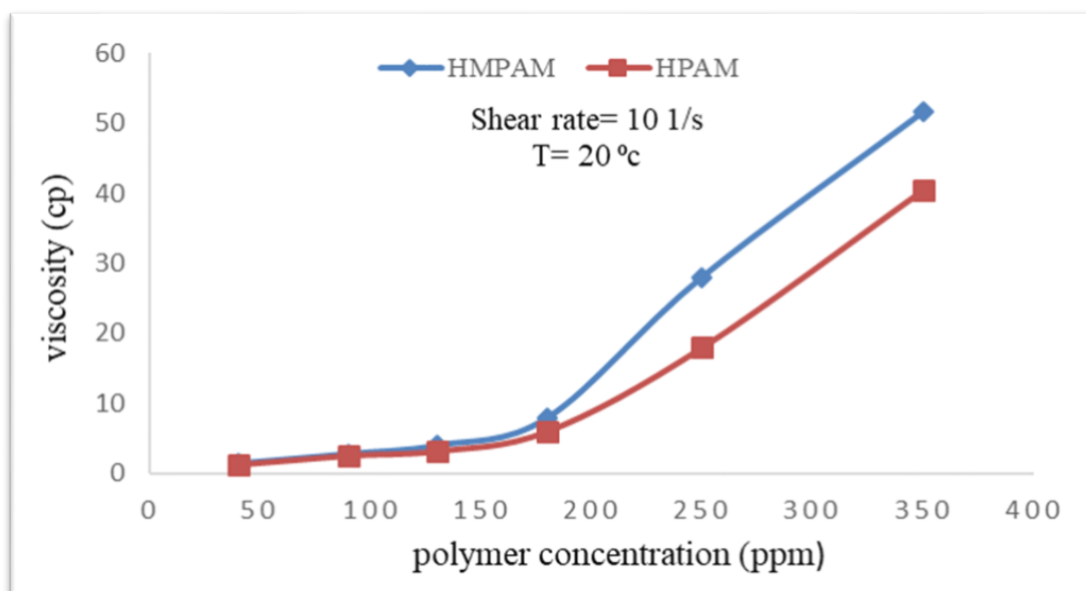


Figure 4. 7: Effect of polymers concentration on viscosity

- **Effect of NaCl concentration**

Figure 4.8 shows the effect of NaCl concentration on the viscosity of PPAM and HPAM solutions. As can be seen adding NaCl concentration causes a reduction in the viscosity of both polymer solutions. The reduction in viscosity of PPAM solution is due to an enhancement in the intramolecular hydrophobic associations compared to inter-molecular associations which reduces the hydrodynamic volume of the polymer (Wever et. al., 2011). However, viscosity reduction in HPAM solution is due to the electrolyte in the salt forming a layer that

shields the repulsion between the negative charges (-COO-) of the polymer backbone which makes the polymer less stretched as it used to be (Mansri et. al., 2007). The PPAM solution shows a higher salinity resistance in the presence of NaCl than the HPAM solution.

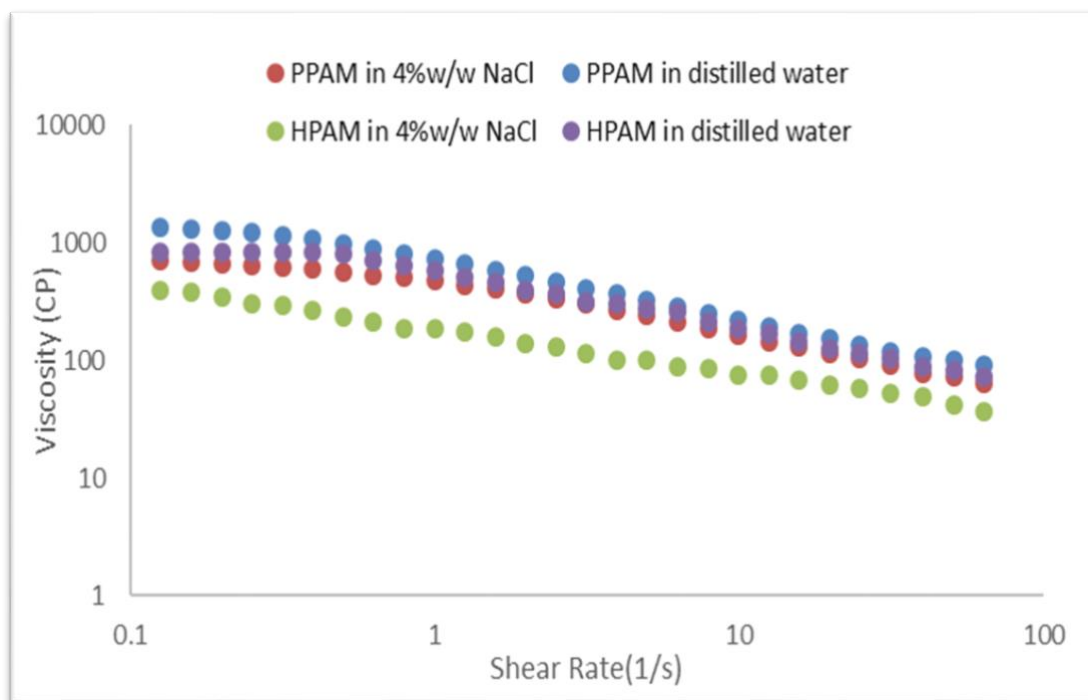
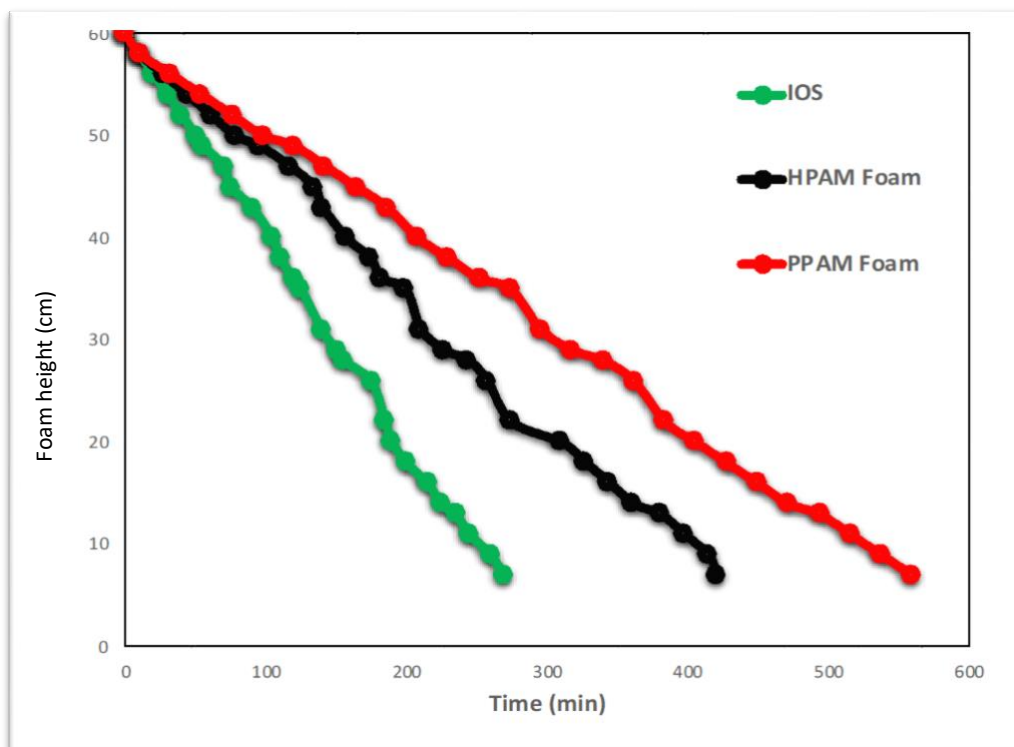


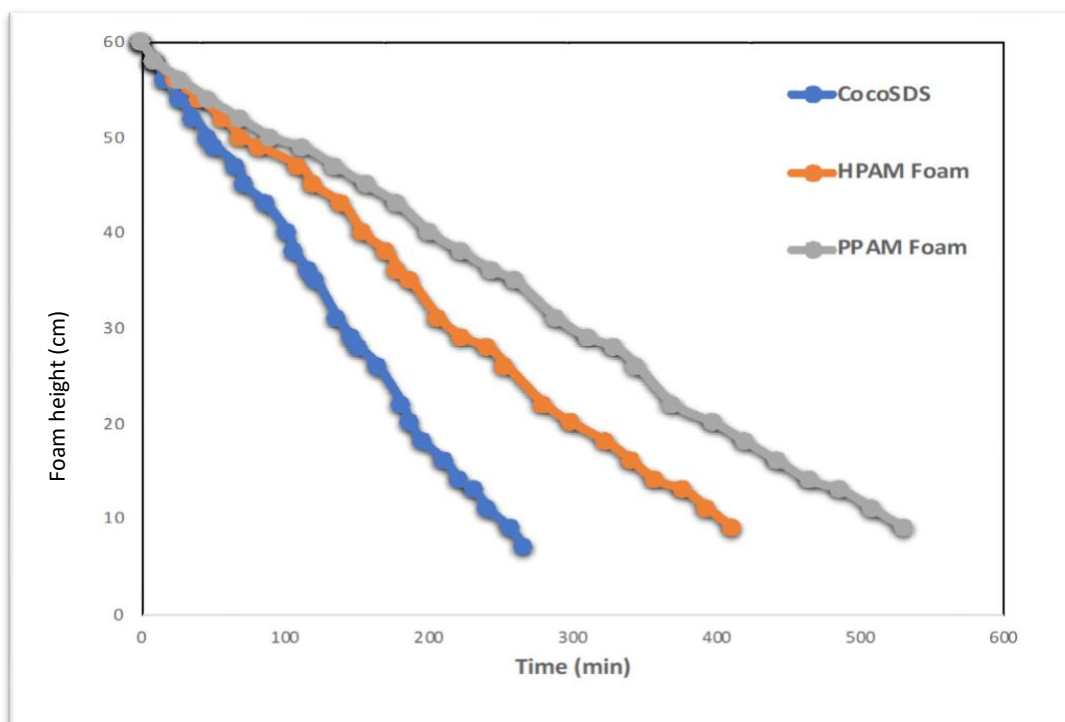
Figure 4. 8: Effect of NaCl on viscosity

4.2.3 Effect of Polymer additive on foam stability

The polymeric foam was prepared using either 2% wt of Internal Olefin Sulfonate (C_{16} - C_{18}) (IOS) or 2% CocoSDS and 2% wt NaCl in distilled water. Then 0.4% wt of PPAM or HPAM was added to the surfactant solutions to generate the polymeric foams.

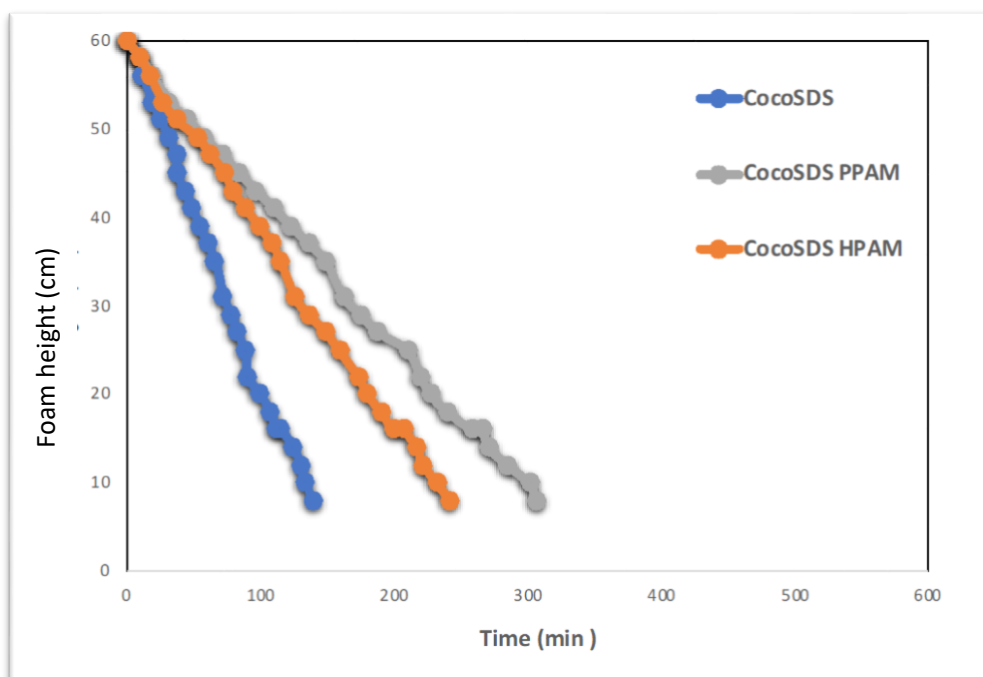


a)

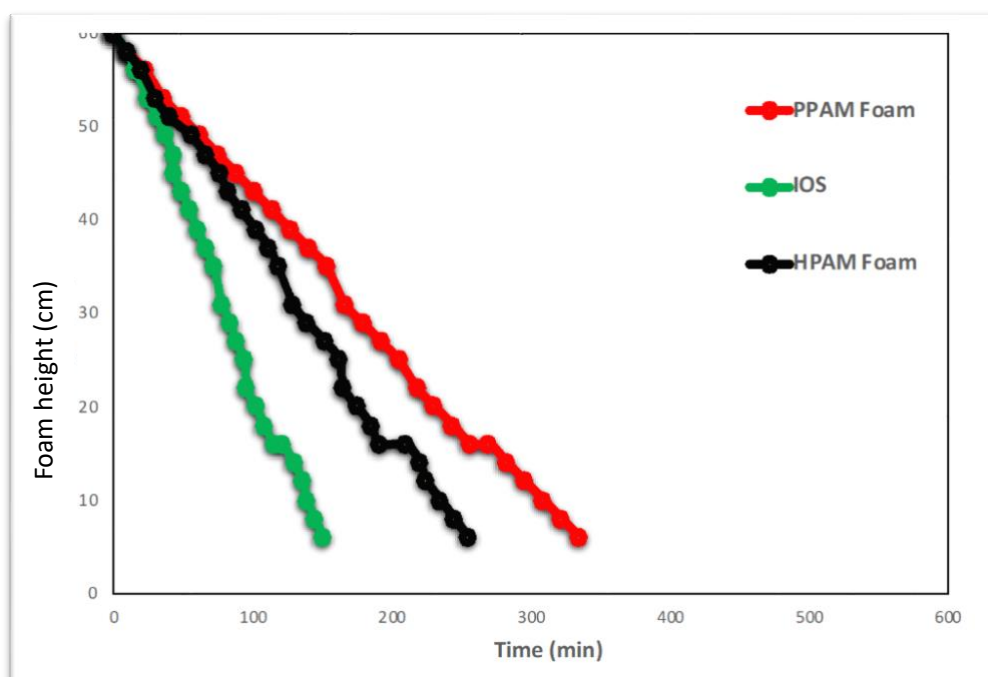


b)

Figure 4. 9: Height decay profile of a) IOS foam, b) CocoSDS foam, both with and without polymer in the absence of oil



a)



b)

Figure 4. 10: Height decay profile of a) IOS foam, b) CocoSDS foam, both with and without polymer in the presence of oil

The polymer free foam was found to be the most unstable due to rapid liquid drainage because of the low solution viscosity, which causes thinning of the lamellae. As can be seen in Figure 4.9. a) and Figure 4.10 a) the results show that in a) the IOS foam is the least stable foam with a half-decay time of 150 min and 280 min, whereas the IOS/PPAM foam has the

highest stability with a half-decay time of 320 min and 580 min in the presence and absence of oil respectively. On Figure 4.9 b) and Figure 4.10 b) the results show the CocoSDS foam to be the least stable foam with a half-decay time of 135 min and 267 min, whereas CocoSDS/PPAM foam has the highest stability with a half-decay time of 318 min and 531 min in the absence and presence of oil respectively. The viscous nature of the surfactant/polymer solutions could regulate the liquid drainage. Incorporation of polymers change the solution properties by increasing the foaming solution viscosity and reducing the drainage rate of liquid which significantly stabilizes the foam lamellae. The addition of conventional polymer exhibited a significant increase in stability; however, the highest longevity of foam was observed in the case of presence of PPAM polymer.

To compare the two different foaming agents, as was shown in Figures 4.9 and Figure 4.10, IOS performs slightly better in low concentration in comparison to CocoSDS in the absence and presence of oil. However, the stability of the generated foams using these surfactants was significantly higher compared to the other surfactants. therefore, both of these foaming agents were employed in the sand pack flooding and core flooding.

4.3 Foam flow behaviour in sand pack

As discussed, the purpose of this part of the work was to study the effect of rock permeability on foam rheological behavior. The objective was to use specific mixtures of sands to create specifically designed porous environments in order to study foam rheological behavior in a controlled system.

The sand packs properties are shown in Table 4.2. The porosity, permeability and density of the sand pack were calculated using equations 3-2 and 3-3. Three sand packs of crushed Berea sand were prepared and were used for different experiments.

Sand Pack	Length (cm)	Section Area (cm ²)	Sand Density (g/cm ³)	Permeability (mD)	Φ %
SP1 (A)	10	4.9	2.67	1710	42.8
SP1 (B)	10	4.9	2.67	2910	42.8
SP2 (A)	10	4.9	2.74	1820	43.2
SP2 (B)	10	4.9	2.74	2530	43.2
SP3	15	4.9	2.65	3100	42.9

Table 4. 2: Sand pack properties

Table 4.3 shows the particle size distribution in 3 sand pack 1 (SP1) and sand pack 2 (SP2).

Grain size (μm)	SP1		SP2	
	A	B	A	B
5-110	10%	70%	20%	70%
110-280	70%	10%	70%	20%
280-355	20%	20%	10%	10%

Table 4. 3: Grain size distribution

Sand pack porosity ($\approx 43 \pm 0.5\%$) is normally very high compared to core samples which provide a high porous environment to avoid polymer trap in porous media. Therefore, it is much easier to investigate foam solutions flow properties.

4.3.1.1 Permeability of sand pack to brine

The permeability of the sand packs was experimentally measured as explained in chapter 3. Local heterogeneities caused by permeability variations within the sand packs were observed by calculating the permeability across different sections of the sand packs. How these permeability variations affect foam will be presented and discussed in this chapter. At pore level foamed gas will tend to flow through high permeable and high porosity areas (Apaydin

and Kovscek, 2001). Permeability variations in a porous medium can influence the ability of the foam has to control gas mobility, foam stability and foam generation. Foam reduces the gas mobility more efficiency with higher permeability. This quality improves the ability of the foam to control channelling due to permeability variations (Hirasaki, 1989). Foam stability is better in high permeable zone where the lamellae are more stable since the capillary pressure is lower than the critical capillary pressure (Khatib et al., 1988). Foam generation by the snap-off is the most dominant mechanism in heterogeneous porous medium and is dependent on the degree of permeability contrast (Tanzil et al., 2000).

Figure 4.11 shows a sample of pressure drop data versus flow rates in SP3 (homogeneous); permeability is calculated to be 3100 mD across the sand pack, from the slope of the line by using Darcy equation.

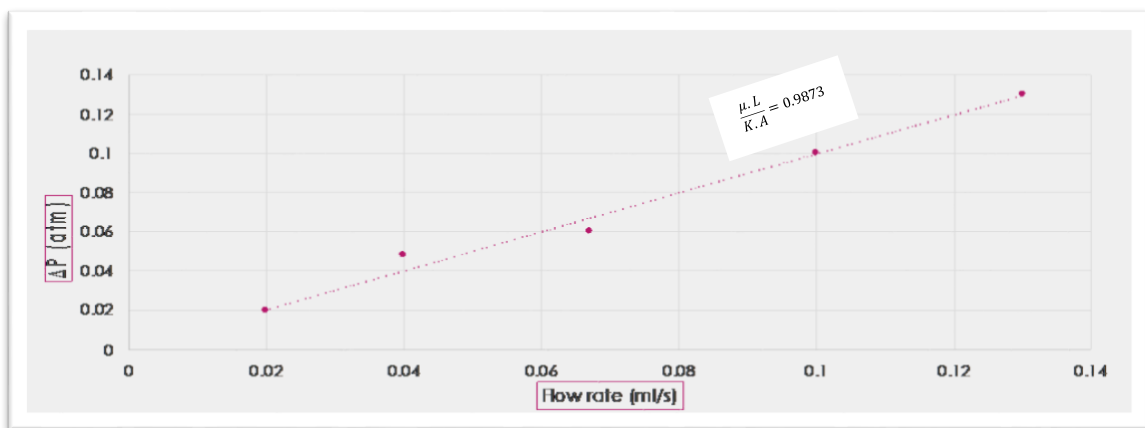


Figure 4. 11: Pressure drop versus brine flow rate in sand pack.

Sand pack is used as an unconsolidated core sample with greater porosity and permeability to investigate the foam flow behaviour in porous media and investigate the interaction of fluid with porous media such as mobility reduction factor which is shown below:

Table 4.4 presents experimental pressure drop data for foam injection (ΔP_F) and brine injection before foam injection (ΔP_B), which are used to calculate the mobility reduction factor (MRF).

Flow rate (ml/min)	ΔP_B	ΔP_F	Mobility reduction (MRF)
0.05	21.55	47.84	2.22
0.2	24.78	43.59	1.76
0.4	31.24	38.28	1.22
0.8	35.55	51.03	1.43
1.2	40.94	57.41	1.40
2.4	46.32	86.12	1.86
4	53.86	127.59	2.37
5	75.41	191.38	2.54
6	104.50	265.80	2.54
8	131.43	435.92	3.32
9	147.59	520.98	3.53
10	165.90	754.89	4.55
11	180.98	722.99	3.99
12	202.53	680.46	3.36
14	249.93	627.30	2.51
16	349.04	574.14	1.65

Table 4. 4: Pressure data results for foam and brine injection

Mobility reduction was calculated from the ratio of pressure drop during foam injection and before foam injection (brine injection).

4.3.2 Surfactant foam flow behaviour in sand pack

The four sand pack flood experiments were successfully conducted, three of these focussed on the effect of permeability on foam performance and the fourth on the effect of foaming agent on foam behaviour in porous media. The details of the sand packs and foam formulas used for this part are presented above.

Figure 4.12 shows the results in absolute pressures at three locations during co- injection of CO₂ gas and surfactant solution (F₂: CocoSDS foam) into sand pack SP1. During this co-

injection the same increasing behaviour in absolute pressures was observed. The absolute pressures measured at the four locations (A, B, C and D) during the co-injection into SP5 increased until $t=10$ min and continued to increase uniformly probably due to gas trapping. The total increase in absolute pressure was approximately between 15-30 millibar at different locations in SP1.

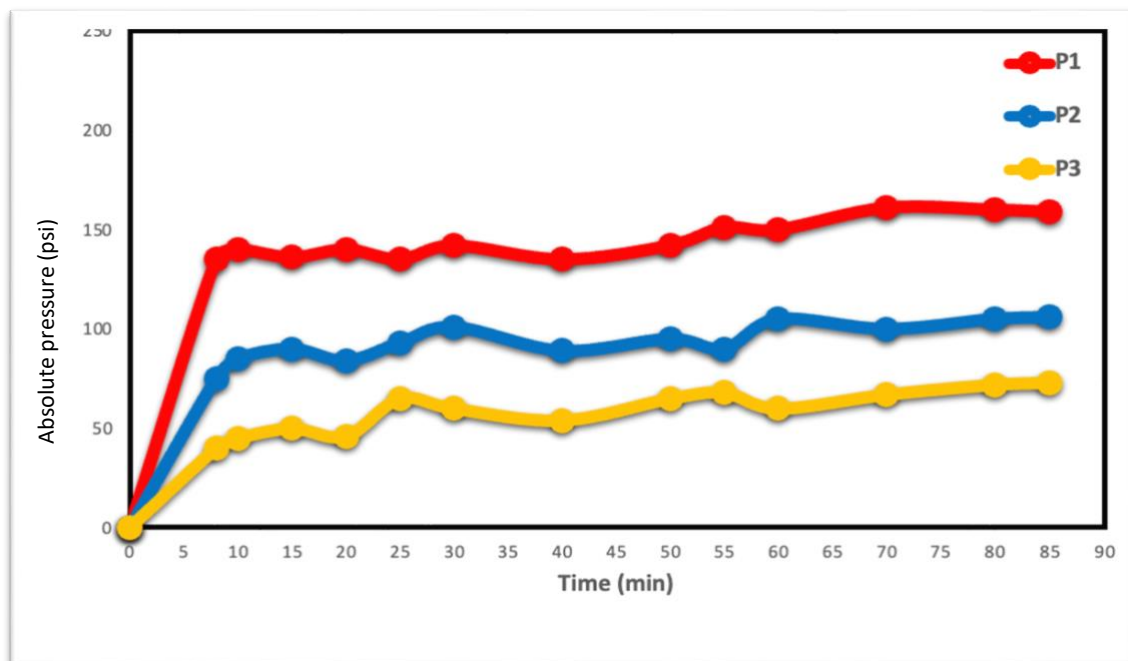


Figure 4. 12: Absolute pressures (millibar) as a function of time (min) in SP1 (injection of F2)

Figure 4.13 shows the calculated pressure gradient across two sections in sand pack SP1 during co-injection of F_2 and CO_2 . Both pressure gradients increased fast before they gradually stabilized. The stabilized pressure gradient across section A was between 4 and 5 millibar/cm around $t=30$ min. The stabilized pressure gradient across section B was between 2 to 3 millibar/cm at around $t=30$ min.

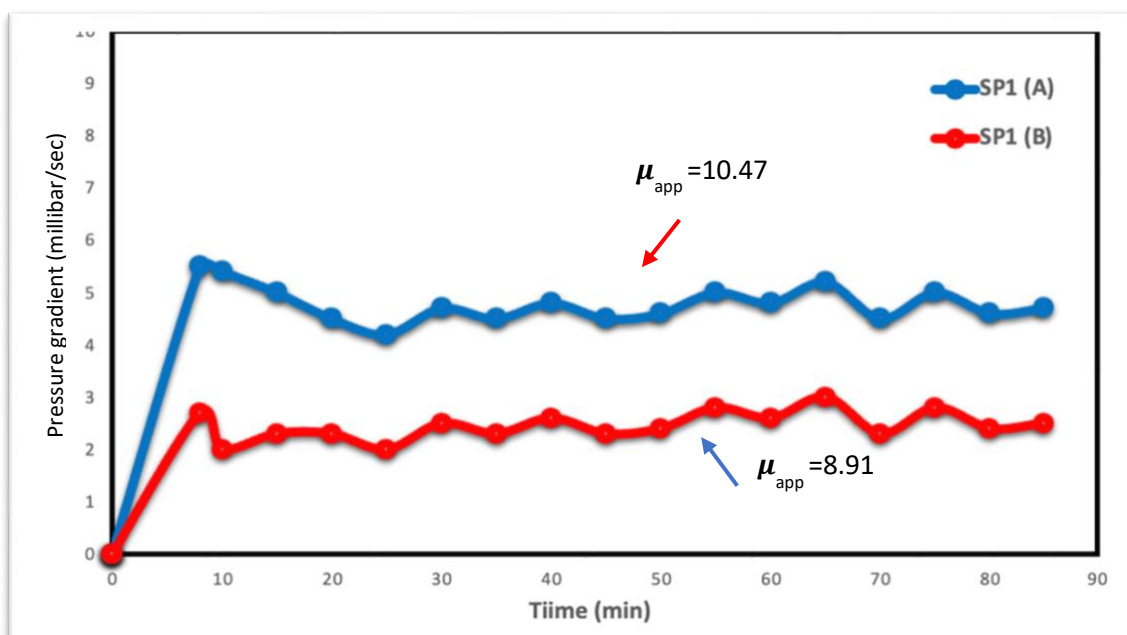


Figure 4. 13: Pressures gradient (millibar/cm) as a function of time (min) in SP1 (injection of F2)

The apparent viscosity for the injected foam was calculated by Darcy’s law (4.6) for SP1 to compare flow and foam ability in different sections. The permeability and the apparent foam viscosity in the two sections across SP1 are listed in Table 4.5.

Sand pack	SP1 (B)	SP1 (A)
K (D)	2.91	1.71
μ_{app} (cp)	8.91	10.47

Table 4. 5: The permeability and the apparent foam viscosity in two sections across sand pack SP1 injecting surfactant foam (F2)

The apparent viscosity in section A was higher than the apparent foam viscosity in section B. This indicates that stronger foam was generated in section A compared to the generated foam in section B. In section B the pressure gradient stabilized at 2 to 3 millibar/cm, the permeability was 2.91D and the apparent foam viscosity was 8.91 cP. In section A the

stabilized pressure gradient was 4 to 5 millibar/cm, the permeability was 1.71D and the apparent foam viscosity was 10.47 cP. This indicates stronger foam was generated in section A compared to section B even though the permeability was higher in section B compared to section A. This is caused by the lower stabilized pressure gradient in section B compared to the higher stabilized pressure gradient in section A. This can be explained using Darcy's law, which shows that, the apparent viscosity is directly proportional to permeability as well as pressure gradient.

4.3.3 Surfactant/polymer foam flow behaviour in sand pack

- **Effect of permeability on the behaviour of polymeric F4 foam (CocoSDS and HPAM)**

Figure 4.14 shows the results in absolute pressures at three locations during co- injection of CO₂ gas and surfactant+polymer solution (F4: CocoSDS foam with HPAM additive) into sand pack SP1. During this co-injection the overall absolute pressures measured at the different locations across the sand pack increased fast within 1 min and gradually increased till t=4 min and continued to increase uniformly probably due to gas trapping. Foam was not observed in the outlet tubing before t=8.5 PV and during the co-injection the CO₂ gas front was observed as a segregated front in the sand pack. The front evolved faster in the uppermost part of the sand pack compared to the lowermost part of the sand pack. In addition, light and dark stripes appeared behind the front. Gas represented light areas and dark areas represented surfactant+polymer solution.

The absolute pressure monitored at P1 increased fast within t=1 min before it decreased and stabilized. At t= 4 min the absolute pressure monitored in P1 increased which was probably caused by the arrival of CO₂ gas front before it decreased and stabilized for some time and slightly increased again. At P3 between t=16 min and t=20 min there was a slight decrease which stabilized at t=22 min onwards. The total increase in absolute pressure was 15 to 20 millibar at different locations in SP5.

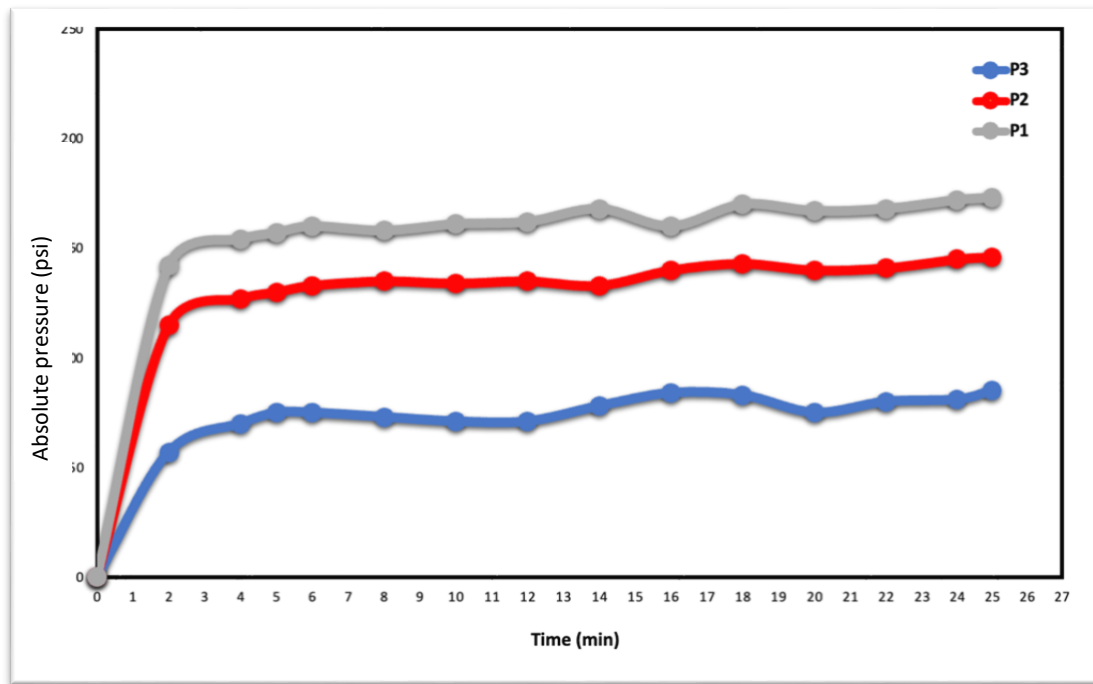


Figure 4. 14: Absolute pressures (millibar) as a function of time (min) in SP1 (injection of F4)

Figure 4.15 shows the calculated pressure gradient across two sections in sand pack SP1 during co-injection of CO₂ and F4 (CocoSDS foam with HPAM additive). The pressure gradient across both sections increased at the onset of co-injection before it decreased around t=1.5 min to a negative pressure gradient which may have been caused by a gas leak. As shown on Figure 4.14 in part B at t=5 min the pressure gradient increased till t= 14 min, before it decreased and fluctuated towards the end of the co-injection. The pressure gradient in section A increased until t=1.5 min and then decreased from 2.5 to 2 millibar/cm and stabilized. The fluctuations observed in the pressure gradients across the two sections might suggest foam generation.

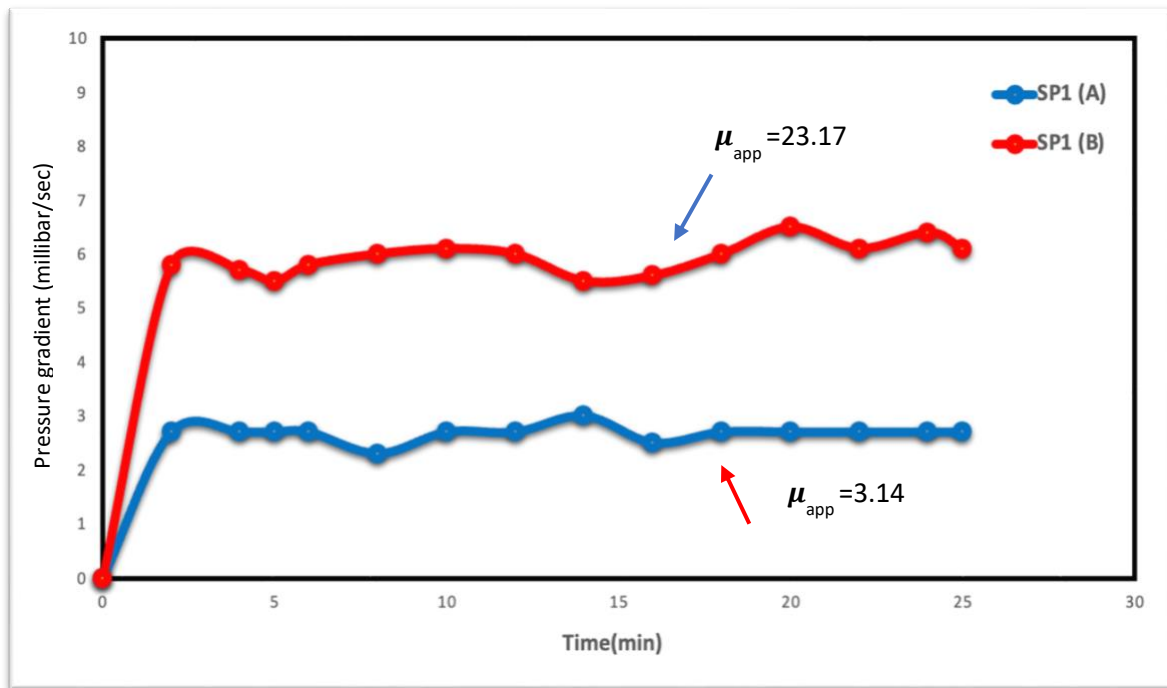


Figure 4. 15: Pressure gradient (millibar/cm) as a function of time (min) in SP1 (injection of F4)

The apparent viscosity for polymer enhanced foam was calculated by Darcy’s law for SP1 to compare flow in the two sections. The permeability and the apparent foam viscosity in the two sections across SP1 are listed in Table 4.6.

Sand pack	SP1 (B)	SP1 (A)
K (D)	2.91	1.71
μ_{app} (cp)	23.17	3.14

Table 4. 6: The permeability and the apparent foam viscosity in two sections across sand pack SP1 using polymeric foam (F4)

The apparent foam viscosity in section B was more than seven times higher than the apparent viscosity in section A. This indicates that stronger foam was generated in section B with higher

permeability compared to section A. In section B although the pressure gradient did not become stable during the co-injection, the trend was increasing. The permeability was 2.91 D and the apparent viscosity was 23.17 cP. In section A the pressure gradient decreased during the co-injection. A decreasing behaviour of pressure gradient indicates generation of unstable foam with apparent foam viscosity as low as 3.14 cP.

- **Effect of permeability on the behaviour of polymeric F6 foam (CocoSDS and PPAM)**

Figure 4.16 shows the results in absolute pressures at three locations during co-injection of CO₂ gas and surfactant+polymer solution (F6: CocoSDS foam with PPAM additive) into sand pack SP2. The absolute pressures increased fast and reached a maximum at t=2 min before they decreased and stabilized. At around t=4 min to t=9 min there was a slight fluctuation. After that the pressure stabilized to the end of the experiment.

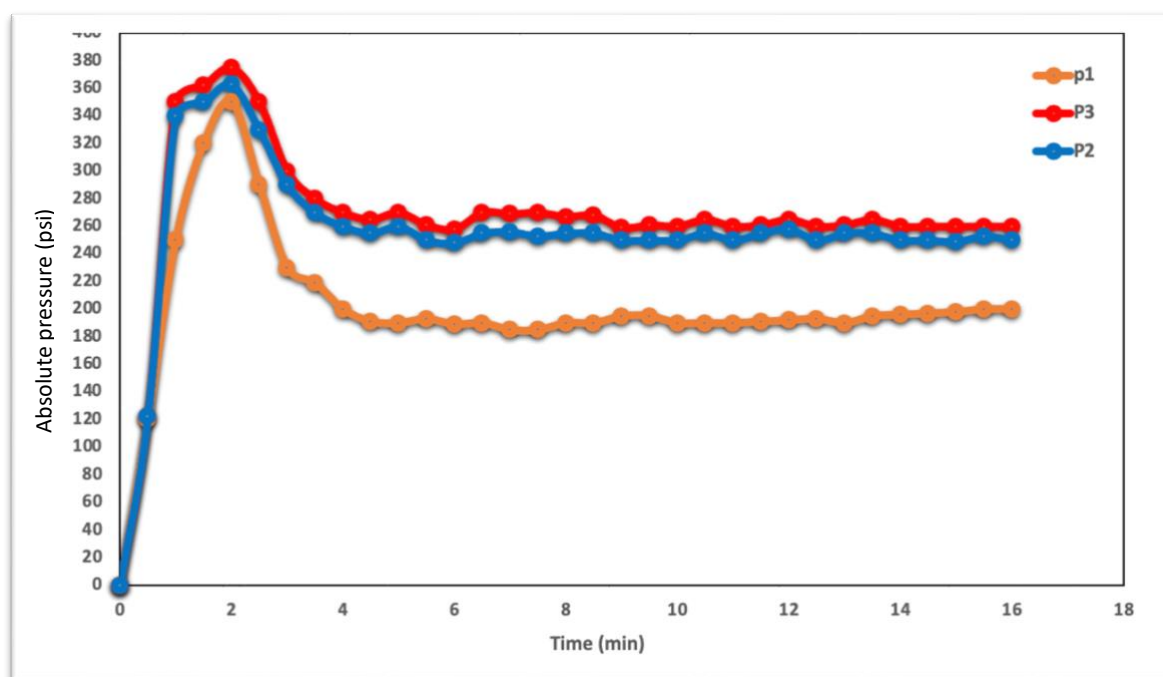


Figure 4. 16: Absolute pressures (millibar) as a function of time (min) in SP2 (injection of F6)

Figure 4.17 shows the calculated pressure gradient across two sections in sand pack SP2 during co-injection of CO₂ and F6 (CocoSDS foam with PPAM additive). The pressure gradient across both sections increased at the onset of co-injection before it decreased around t=2 min to a negative pressure gradient which as explained earlier may have been caused by a gas leak. As shown on Figure 4.16 in part B from t=2 min the pressure gradient increased till t= 5

min, before it decreased and fluctuated towards the end of the co-injection. The pressure gradient in section A increased until t=1.5 min and then stabilized before it increased and fluctuated from t=6 min.

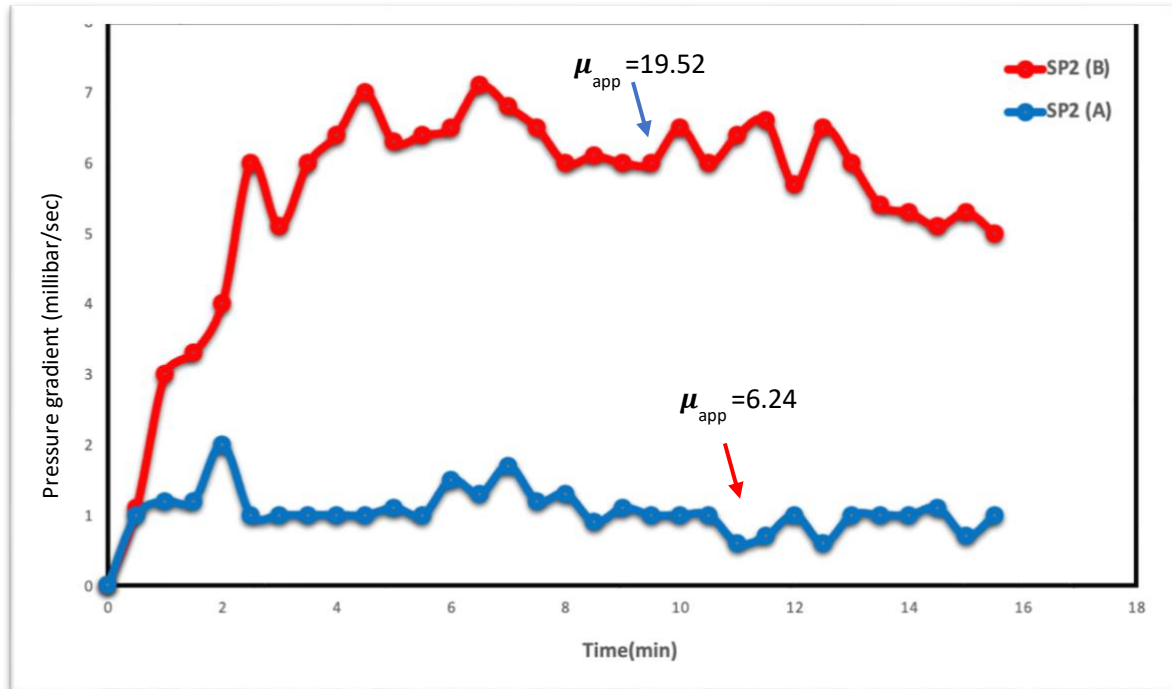


Figure 4. 17: Pressure gradient (millibar/cm) as a function of time (min) in SP2 (injection of F6)

The apparent viscosity for polymer enhanced foam was calculated by Darcy’s law for SP2 to compare flow and foam ability in the two sections. The permeability and the apparent foam viscosity in the two sections across SP2 are listed in Table 4.7.

Sand pack	SP2 (A)	SP2 (B)
K (D)	1.82	2.53
μ_{app} (cp)	6.24	19.52

Table 4. 7: The permeability and the apparent foam viscosity in two sections across sand pack SP2 using polymeric foam (F6)

The apparent foam viscosity was higher in section B compared to the apparent viscosity in section A. This indicates that a stronger foam was generated from the middle towards the outlet, whereas a weaker foam was generated closer to the inlet. In section B the permeability was 2.53 D and the apparent foam viscosity was 19.52 cP. In section A the permeability was 1.82 D and the apparent foam viscosity was 6.24 cP. This indicates that the apparent foam viscosity did vary with the permeability. However, based on previous observations the apparent foam viscosity increased with higher permeability, see Table 4.7.

4.3.4 Surfactant Foam versus Polymer Enhanced Foam

The effect of surfactant foam and polymer enhanced foam by co-injection on the absolute pressure in SP3 and the pressure difference across the sand pack is presented in this part.

The general trend observed in the absolute pressures during the 3 co-injections was:

- Injection 1- surfactant foam: Absolute pressures increased and stabilized.
- Injection 2 – polymer (PPAM) enhanced foam: Absolute pressure increased uniformly.
- Injection 3 - polymer (HPAM) enhanced foam: Absolute pressure increased, stabilized, and decreased and stabilized.

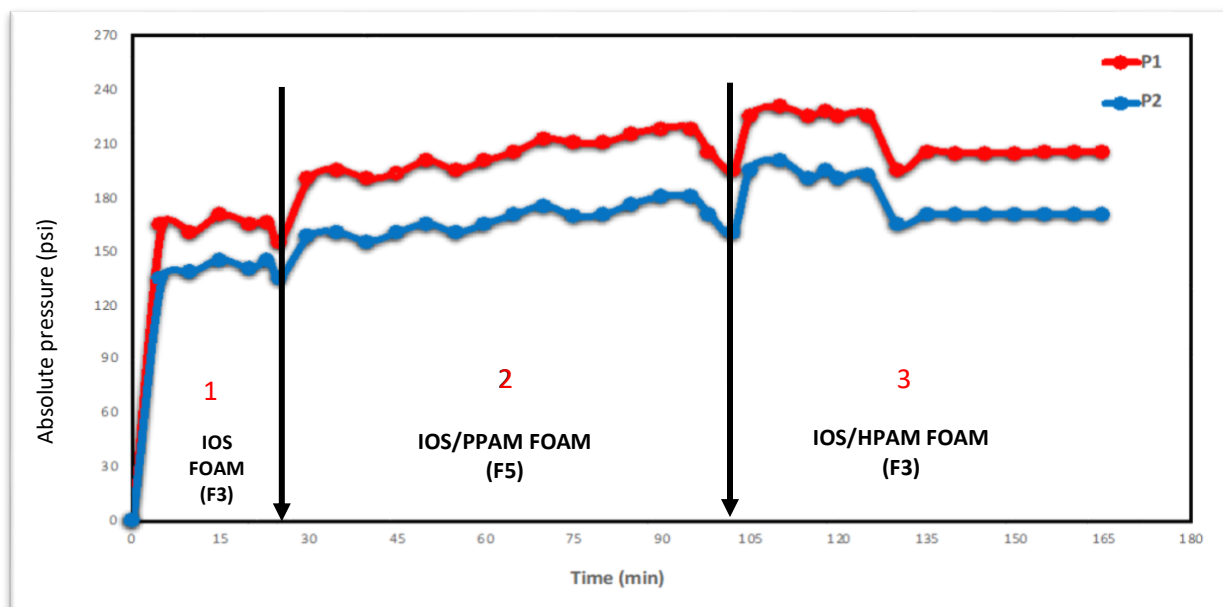


Figure 4. 18: Absolute pressure (millibar) as a function of time (min) in SP3 (injection of F1, F3 and F5)

Chapter 4: Results and discussions

Injection 1: As the co-injection of surfactant foam (IOS) started the pressure started to increase until $t=5$ min, then stabilized till $t=25$ min where the co-injection of polymer enhanced foam began.

Injection 2 - polymer enhanced foam (PPAM) by co-injection started at $t=25$ min and was ended at $t=102$ min. During the co-injection of CO_2 gas and surfactant+polymer solution a uniform increasing trend in the absolute pressures was observed and the total increase in absolute pressures was 30-50 millibar at each location in SP3. The uniform increasing trend in the absolute pressures was probably caused by gas trapping. Fluid samples were taken during the co-injection and may have caused the fluctuations in the absolute pressure. Alternating production of gas and foam was observed at the production end in this experiment, thus gas- foam slugs may have influenced the absolute pressures.

Injection 3- polymer enhanced foam (HPAM) was started at $t=102$ min and was ended at $t=165$ min. During the co-injection of CO_2 gas and surfactant+polymer solution the absolute pressures increased till $t=105$ min and became stable at $t=128$ min, before a sudden drop in absolute pressures was observed. At $t=131$ min the absolute pressures reached a stable trend again. Alternating production of gas and foam was also observed at the production end in this experiment, thus gas-foam slugs may have influenced the absolute pressures like the previous part.

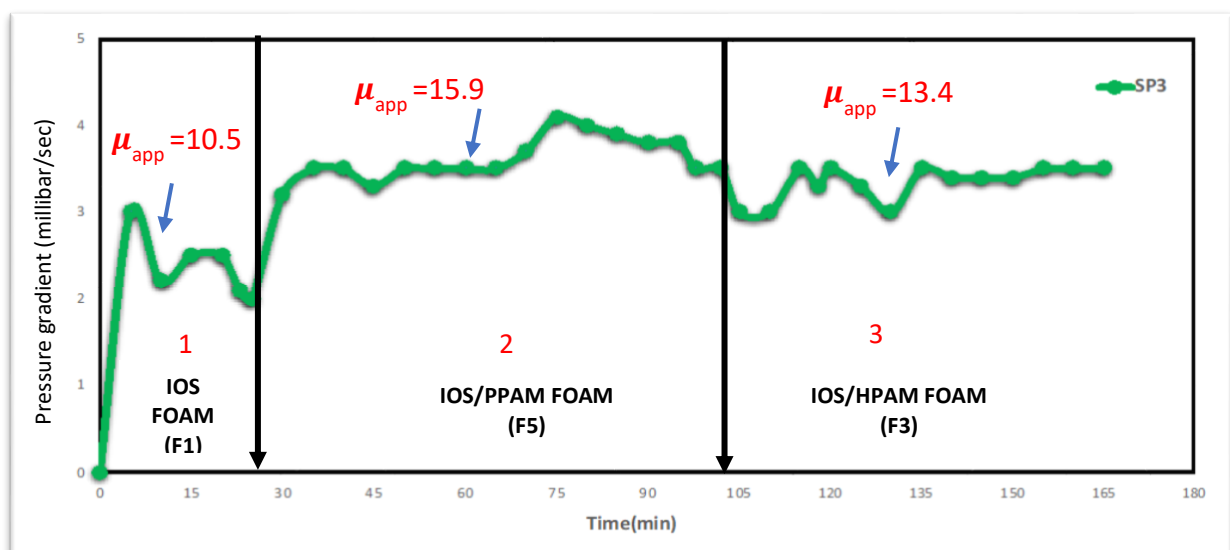


Figure 4. 19: Pressure gradient (millibar/cm) as a function of time (min) in SP3 (injection of F1, F3 and F5)

Chapter 4: Results and discussions

Figure 4.19 shows the calculated pressure gradient across sand pack SP3 during co-injection of CO₂ and F1, F3 and F5 (IOS, PPAM and HPAM foam).

The general behavior of the pressure gradient across the SP3 during the co- injections was:

- Injection 1 - surfactant foam: Pressure gradient increased before it decreased and became stable.
- Injection 2 - polymer enhanced foam (PPAM): Pressure gradient increased before it became stable.
- Injection 3 - polymer enhanced foam (HPAM): Pressure gradient increased before it decreased and became stable.

However, all the pressure gradients were fluctuating with varying degrees after stabilization during the 3 different injections. The pressure gradients across SP3 were more stable during the co-injection of PPAM foam.

The apparent foam viscosities were calculated by Darcy's law for the three co-injections to compare flow in the sand pack SP3. The permeability and the apparent foam viscosity across SP3 during the three co-injections are listed in Table 4.8.

Sand Pack	SP3
K(D)	3.1
μ_{app} (cp)	10.5
Inj.1	
μ_{app} (cp)	15.9
Inj.2	
μ_{app} (cp)	13.4
Inj.3	

Table 4. 8: Permeability and apparent foam viscosity for SP3

The apparent foam viscosity of the injected foam across the sand pack was calculated. It was observed that the apparent viscosity during injection of PPAM foam was significantly higher than the apparent foam viscosity during the other two injections. This indicates that a stronger foam was generated during run 2 (Figure 4.19) compared to the calculated apparent viscosity during run1 and run 3. As the permeability is the same for all the co-injections, the effect of the foaming agent can be discussed. Figure 4.18 confirms that a stronger foam is generated during run 2 (PPAM foam) compared to the other two injections due to the higher apparent viscosity ($\mu_{app}=15.9$ cP). To compare the generated foam during run 1 (surfactant (IOS) foam) and run 3 (polymeric (HPAM) foam) according to the apparent viscosity presented in table 4.8 the apparent foam viscosity is much higher during run 3 ($\mu_{app}=13.4$ cP) compared to the apparent viscosity during run 1 ($\mu_{app}=10.5$ cP) which indicates that a stronger foam was generated during run 3 compared to run 1 which as previously discussed can be explained using Darcy's law.

4.3.5 Oil displacement tests using foam

The following sections describe a series of core flood tests for oil displacement. Generally, the main purpose of this part of the study was to observe the effect of polymeric foam on oil recovery performance. The experiments utilized both HPAM and PPAM at concentrations of 4000 ppm in surfactant solution. The comparative analysis included the pressure differential and oil recovery data with respect to injection throughput. The main core sample properties are given in Table 4.9. The absolute permeabilities of the cores were provided by the supplier but the rest of the properties were measured in the lab. Fresh core samples were used for most of the tests to ensure the repeatability and precision of the experiments, however for very few experiments the used core was employed, therefore after each experiment the core was properly cleaned and reused.

The pore volume of the cores was measured by the saturation method. The cores were saturated in distilled water for 24 hours. The difference between the dry and wet weight of the core sample is the total mass of water in pore the space of the core divided by the density of distilled water (1g/ml) and gives the volume of water in the core sample (pore volume).

Core sample	Test							
	1	2	3	4	5	6	7	8
Absolute permeability (mD)	500				100			
Length (cm)	10.10	10.02	10.16	9.91	9.96	10.12	9.89	9.95
Diameter (cm)	2.52	2.54	2.50	2.55	2.54	2.57	2.48	2.51
Area (cm ²)	4.98	5.06	4.91	5.10	5.06	5.18	4.83	4.95
Pore volume (cm ³)	7.43	7.38	7.51	7.32	8.75	8.70	8.63	8.66
Porosity (%)	14.8 (±0.3)	14.6 (±0.3)	15.1 (±0.3)	14.5 (±0.3)	17.4 (±0.3)	16.6 (±0.3)	18.1 (±0.3)	17.6 (±0.3)

Table 4. 9: Core samples (Benthemier sandstone)

4.3.5.1 Oil Injection (drainage)

Table 4.10 shows the results from flooding the core samples with crude oil which is already saturated with brine.

Absolute Permeability (mD)	Crude oil injection (drainage process)							
	500				100			
Core sample	1	2	3	4	5	6	7	8
Initial oil volume (cm ³)	6.5	6.4	6.4	6.3	7.5	7.2	7.3	7.3
Initial oil saturation (S _{oi})	0.88	0.87	0.85	0.86	0.86	0.83	0.85	0.84

Table 4. 10: Crude oil injection

To achieve this, Initial oil saturation (S_{oi}) in core samples was measured by recording the volume of the brine that was pushed out of the core during the injection period. Initial oil saturation was calculated from the ratio of initial oil volume to pore volume. The saturation of crude oil in each core slightly varied due to differences in each of the cores, such as the permeability or connectivity between the pore spaces. The oil flow within the cores would have also differed in each core. This would potentially alter the volume of the core sample

that would have come in to contact with the oil. However, the levels of saturation were sufficient for use of studying the oil volumes recovered in the steps that followed.

4.3.5.2 Brine injection (imbibition)

Brine injection was performed after establishing the initial reservoir condition (drainage) for the cores. Each core varied slightly in the amount of crude oil recovered from the initial oil volumes, varying from 56 % to 60%.

A low flow rate of 0.2 ml/min was applied in order to keep the pressure constant across the core and ensure a homogenous propagation of brine solution in the cores. The amount of oil recovered during time injection is higher than the average oil recovered in a typical reservoir, which is around 35%. The high percent of oil recovery by water flooding in core testing may be due to the experimental conditions. Additionally, the small dimensions of the core samples, may result in higher recovery levels in the core. The recovery of the oil with the brine injection was carried out up to the point where only brine was exiting the core for some time and the pressure drop across the core was almost constant. This represents the primary oil recovery.

The injection represented a water flooding process that was completed past the point of being economically feasible. Residual oil saturation (S_{or}) and water saturation in the core samples can be measured by the remaining volume of oil and water in core the sample divided by the pore volume as initial water flooding (IWF) process. At this point, the pressure drop across the core was getting constant and the brine solution bypassed the crude oil (fingering), following a path of least resistance towards the end of the core. This demonstrates the need for a new recovery approach to be implemented in order to keep producing oil more economically.

4.3.6 Continuous Water Injection (CWI) in core A and B

Continuous water injection CWI recovered about 56% of OOIP and 60% of OOIP, after about 8 PV of brine injection (Figure 4.20). The injection was continued up to 16 PV, but there was no more oil production after about 9 PV.

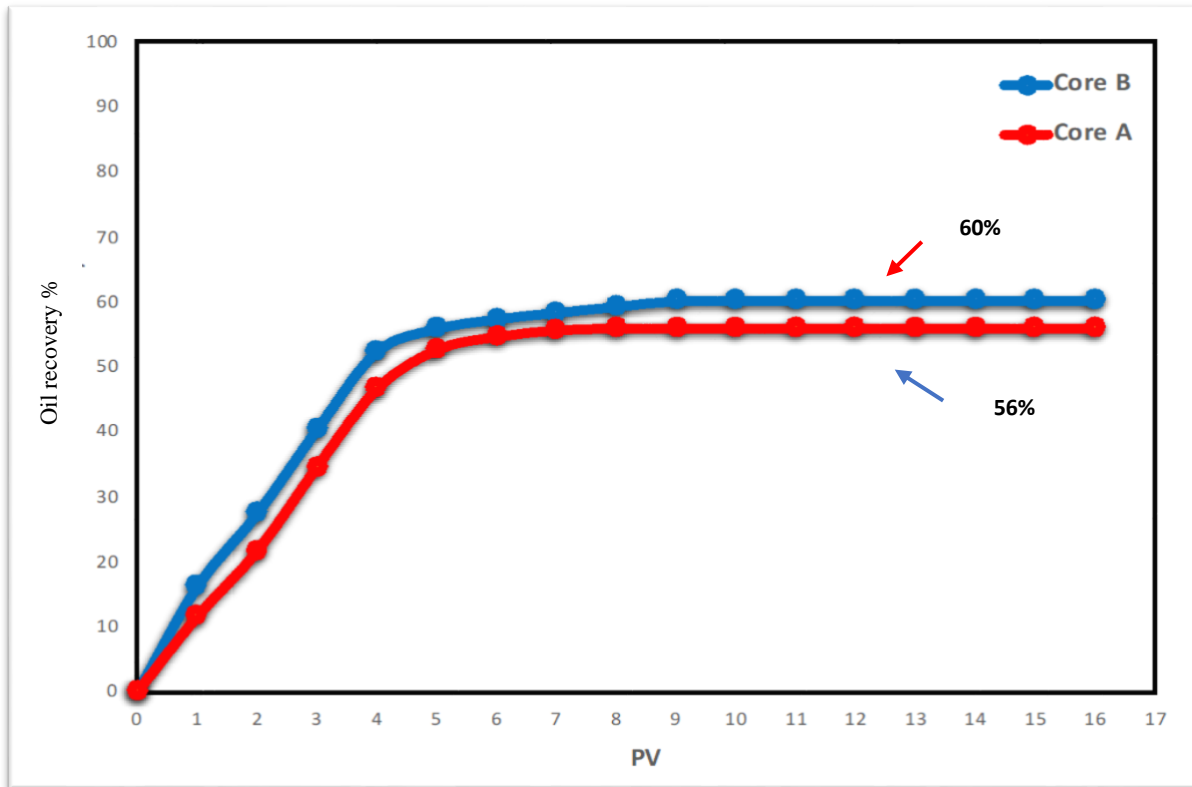


Figure 4. 20: Oil recovery by continuous water injection (CWI)

4.3.7 Minimum miscibility pressure (MMP) measurement using slim tube:

As mentioned previously MMP was calculated using the slim tube to provide the pressure condition so that CO₂ and oil could maintain miscibility. The pressure that was applied in all experiments was kept to 2250 psi.

Immiscible foam was less efficient (30 pore volumes injected) compared to miscible foam (2 pore volumes injected) to reach ultimate recovery. This is explained by the capillary threshold pressure preventing the injected gas from entering the matrix, and the mobilized oil was displaced by the aqueous surfactant or surfactant polymer in the foam. At miscible conditions, there exists no capillary entry pressure between the oil-saturated matrix and the injected CO₂ foam, allowing it to invade the matrix for efficient oil recovery.

In the literature, MMP values have been reported within a range of 1400-5350 psi for different oil compositions, injected gases, and temperatures (Ekundayo and shawket, 2013). MMP values have been reported in a smaller range of 1500-2500 psi for CO₂ and oil with similar density and viscosity to the oil used in this study. As discussed, a pressure increase will

Chapter 4: Results and discussions

not result in miscibility if the oil and injected gas MCM path lie to the left of the critical tie line. Slim tube tests were run at 6 pressure points 1000, 1500, 1750, 2000, 2250 and 2500 psi, at 70° C. The pressure points of 1500 and 2000 psi were repeated to confirm the validity of the data, since the maximum upsurge in oil recovery in response to pressure happened between these two pressures (Table 4.11). For each run, 2 PV of CO₂ was injected.

Meanwhile, oil production was observed at different pressures, the amount of oil produced after 2 PV of CO₂ injection (230 ml) was logged. The experiments repeated at 1500 psi and 2000 psi showed a minor variation in the volume of oil compared to the initial experiments, the results are presented in (Table 4.11).

Pressure (psi)	Produced oil (ml) run 1	Produced oil (ml) run 2	Oil recovery %	Oil recovery %
1000	22		19	
1500	35	29	30	25
1750	50		44	
2000	75	69	65	60
2250	100		88	
2500	102		89	

Table 4. 11: The produced oil vs applied pressure.

From the first series of collected data, MMP was measured at just below 2400 psi, using the method suggested by Amao et al. (2012). The intersection of the two trend lines on the plot of oil recovery versus pressure represents MMP (Figure 4.21).

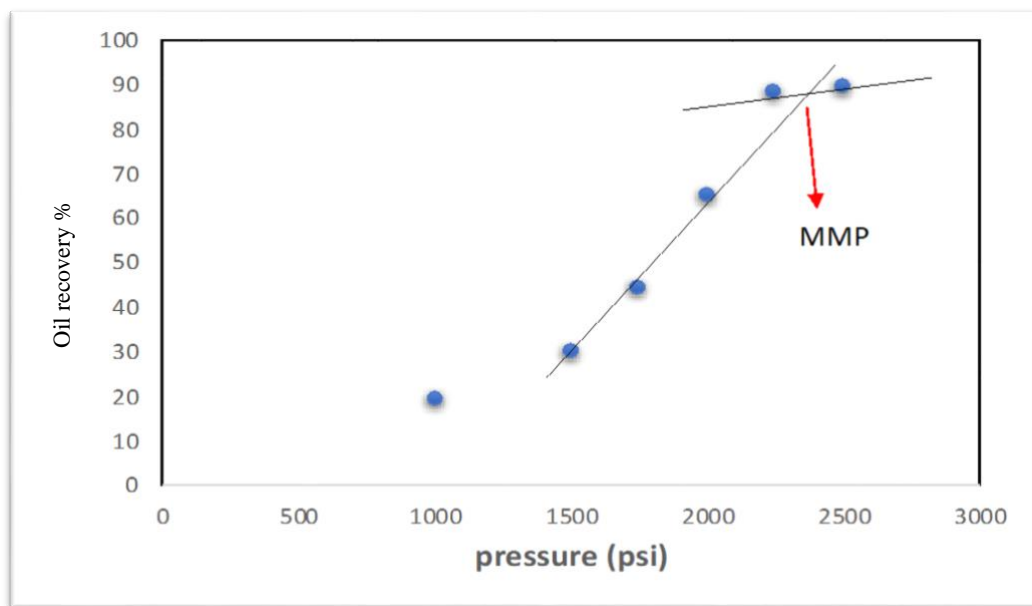


Figure 4. 21: MMP measurement for initial slim tube experiments

Although very precise procedures were used to obtain data, when the experiments were run for a second time at 1500 psi and 2000 psi, the oil recovery was measured slightly differently, which resulted in an MMP determination at slightly below 2500 psi (around 2480 psi). Figure 4.22 shows the measured MMP by using the second series of data at 1500 psi and 2000 psi.

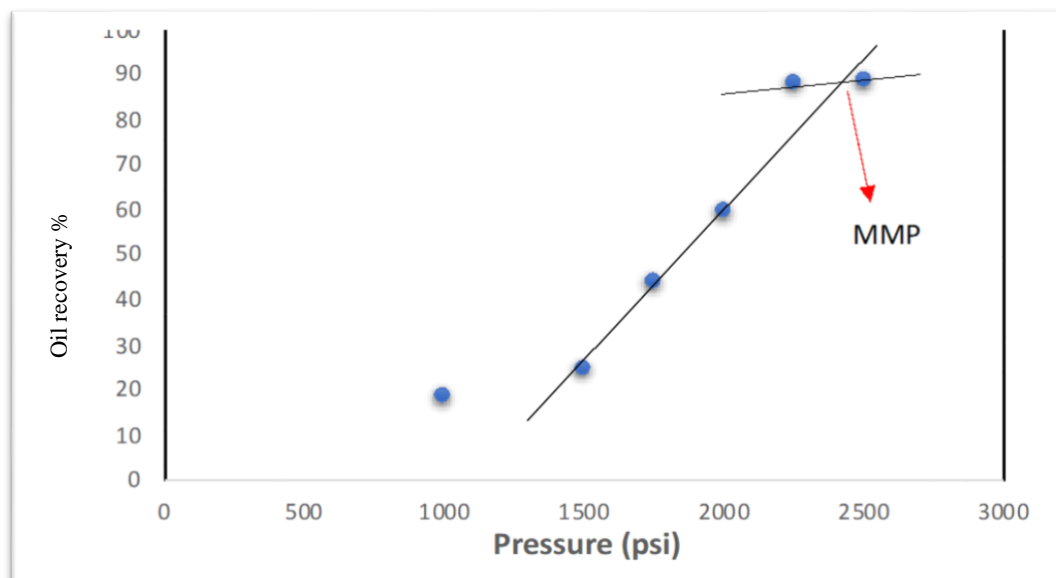


Figure 4. 22: MMP measured by using the oil recovery (run 2)

Chapter 4: Results and discussions

Both measured MMPs are in the range of 2250 psi to 2500 psi. Based on these results, it can be concluded that at 2300 psi, near-miscible displacement was taking place, whilst above 2500 psi full miscibility was achieved. These results were obtained by graphical determination. The presence of a visual cell and a wet gas meter in the slim tube design helped to confirm the credibility of these data visually. Figure 4.23 a) shows the visual cell when it is clean or when a clear (colourless) liquid or gas is flowing through it. Any substance with a colour is detectable via that glass. Figures 4.23 b) and Figure 4.23 c) were taken after the gas breakthrough. Up to 2250 psi, CO₂ and oil were produced separately in an immiscible displacement which can be seen in Figure 4.23 b). This immiscibility was observed from the bubbles that were produced with oil in the visual cell. The dark brown substance is oil, whilst the bubbles (clear area between oil drops) represent CO₂. The last experiment was conducted at 2500 psi, and up to 80 ml one phase was produced (Figure 4.23 c). At the same time, the EL-PRESS pressure meter was detecting gas with no sign of bubbles, which confirmed miscibility.

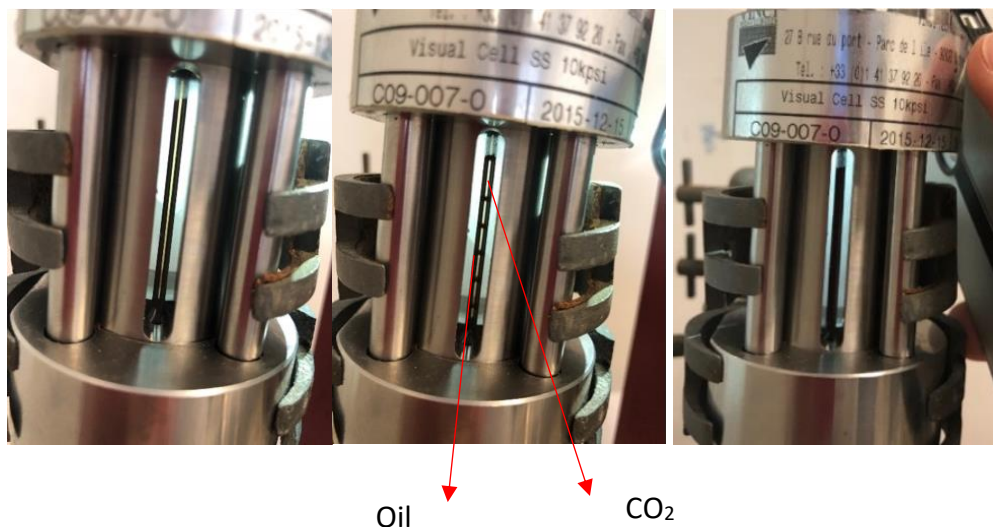


Figure 4. 23: Visual cell: (a) clean/empty state, (b) when oil and CO₂ are present at immiscible pressure and (c) when oil and CO₂ are present at miscible pressure.

4.3.8 Continuous CO₂ injection (CCI)

CO₂ injection was carried out in this part to be compared to the performance of foam flooding.

Chapter 4: Results and discussions

CO₂ injection was started at 2,250 psi from the start of injection. This experiment was used to show the effect of miscibility on oil recovery as well as the amount of CO₂ injection needed to reach S_{or} (Figure 4.24).

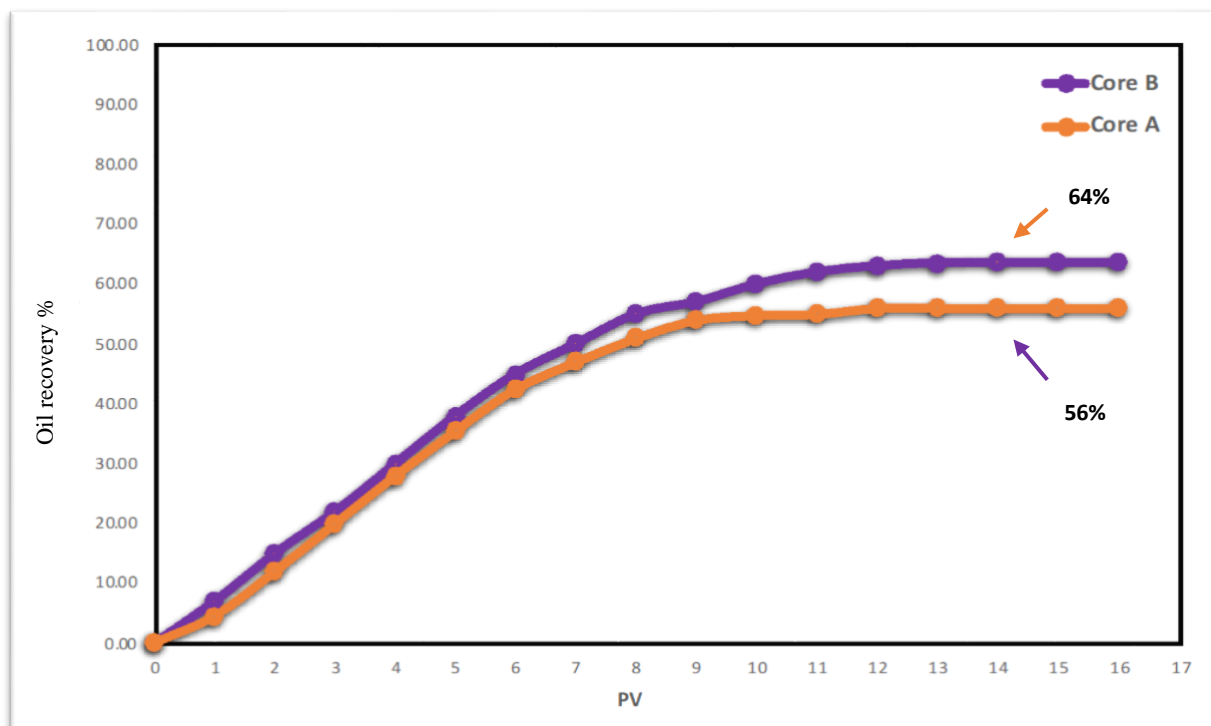


Figure 4. 24: Oil recovery by CCI from core samples A and B.

The recovered oil in core A was 56% of OOIP after 16 PV compared to 64% oil recovery in core B. In this experiment 50% of OOIP was recovered after only 9 PV of CO₂ injection.

Oil recovery by CO₂ injection throughout core flooding was about 24% and 32% less (in core B and A respectively) compared to oil recovery by slim tube at 2,500 psi (88% of OOIP). This oil recovery reduction can be explained by the differences in porosity, permeability, and length of the two systems (sand pack to sandstone core). The presence of high irreducible water saturation in the core samples also reduced the chance of contact between oil and CO₂. On the other hand, the greater diameter and much shorter lengths of the cores caused capillary pressure at the end of the core where oil resisted flowing out of the core into the tubing.

4.3.9 CWI and CCI comparison

Figure 4.25 shows a comparison of oil recovery by miscible CCI and CWI. Both methods failed to recover more than 60–64% of OOIP. However, CCI recovered about 4% more OOIP compared to CWI. The oil recovery response to CWI was much faster, as 52% of OOIP was recovered after only 5 PV of injected water, whilst miscible CCI recovered the same amount of OOIP after 11 injected PV. More than half of the oil recovery by CWI happened after only 2 PV of water injection, but the first two PV of CCI recovered less than a quarter of the total oil recovery.

The structure of the core samples might have caused an early breakthrough for CO₂ but as the time passed and CO₂ saturation increased, MMC took place and reduced IFT. As miscibility needed time to be achieved, oil recovery continued up to 11-12 PV of CO₂ injection. S_{or} was high for both CWI and CCI in the core samples.

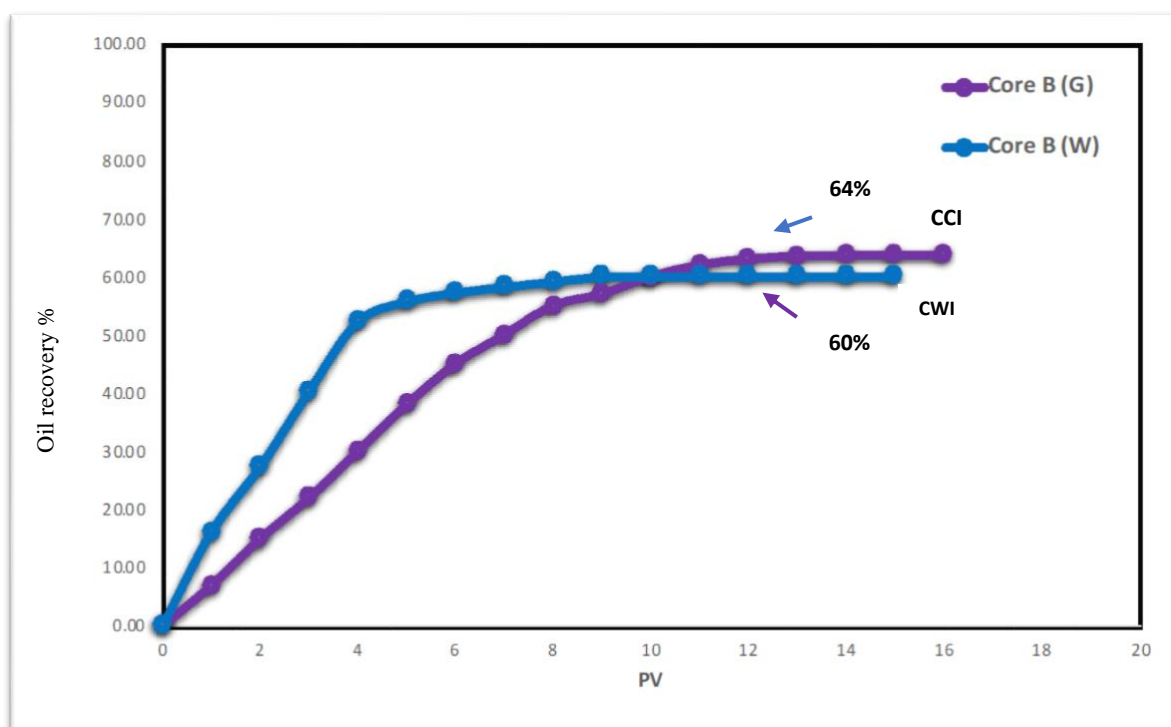


Figure 4. 25: Oil recovery comparison of different methods of CGI and CWI in sandstone core samples.

4.3.10 Foam injection

The foam injection process was conducted after the initial water flooding (IWF) in which the pressure drop became constant across the core sample and no more oil was produced.

4.3.10.1 Surfactant foam injection

The foam injection process was conducted after the initial water flooding (IWF) in which the pressure drop became constant across the core sample and no more oil was produced. To study the effect of surfactant solution on oil recovery two surfactants were employed (CocoSDS and IOS) in a core with a permeability of 500mD. The result will confirm the surfactant type that will be used in surfactant/polymer foam injection.

4.3.10.1.1 Oil displacement experiment using CocoSDS and IOS foam (by co-injection) in 500 mD core B

The pressure drops data, and the oil recovery are shown on Figure 4.26 and Figure 4.27. The first pressure build-up is an indication of initial water flooding (IWF) until it reaches water breakthrough. At this point of displacement, the pressure starts dropping down until it reaches a stabilised value, and no more oil is produced. Foam flooding (FF) was conducted immediately after that point and a second pressure build-up can be observed until foam breakthrough is reached. Extended water flooding (EWF) was conducted after the foam flooding to observe more oil recovery.

Figure 4.26 shows pressure drop for both injections (CocoSDS and IOS foam). Almost 10 PV of brine was injected until the pressure difference was stabilised at 12 psi and 16 psi for CocoSDS and IOS foam respectively. As can be seen on Figure 4.27 oil recovery reached 52% and 53% of initial oil volume for CocoSDS and IOS respectively. Although the 2 cores had permeabilities of 500 mD, there is a very small difference between the oil recovered by IWF. That could have been a result of pressure build up and pressure difference in two cores. Oil saturation in the core sample for both injections decreased from 0.88 to 0.45 for CocoSDS foam, and from 0.87 to 0.46 for IOS foam.

The injection of 18 pore volumes of surfactant solution and CO₂ resulted in a well-stabilized pressure drop of 20 Psi, for CocoSDS and 26 psi for IOS injection, corresponding to a mobility reduction (Resistance factor) of 1.6 for both foams (CocoSDS and IOS). After Foam injection oil recovery increased by 16% of initial oil volume to 68% for CocoSDS foam and to 72%, by 19 % increase of initial oil volume for IOS foam

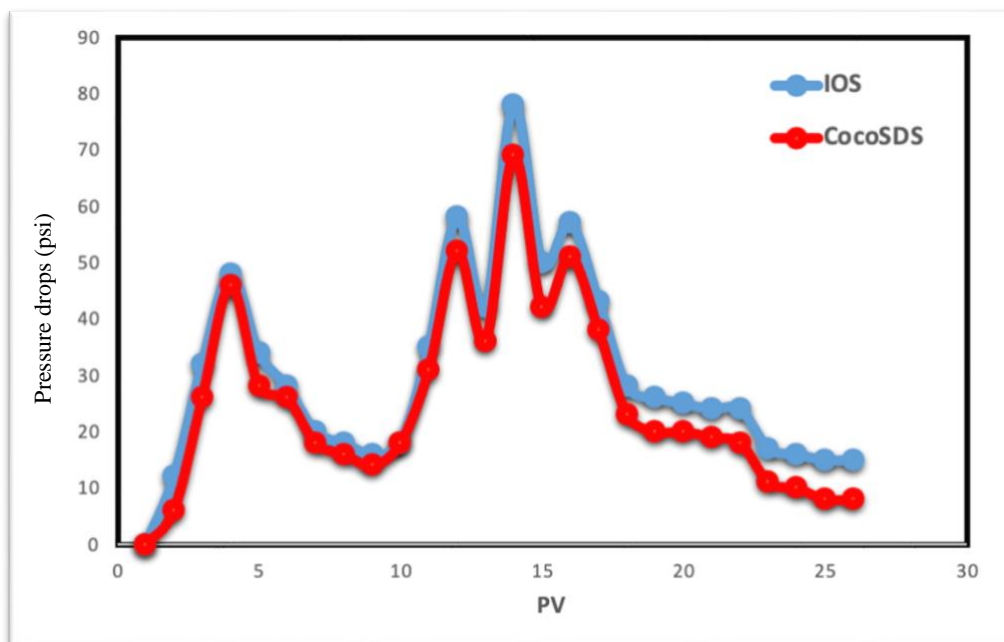


Figure 4. 26: Pressure drop in core B (500mD) using CocoSDS and IOS foam

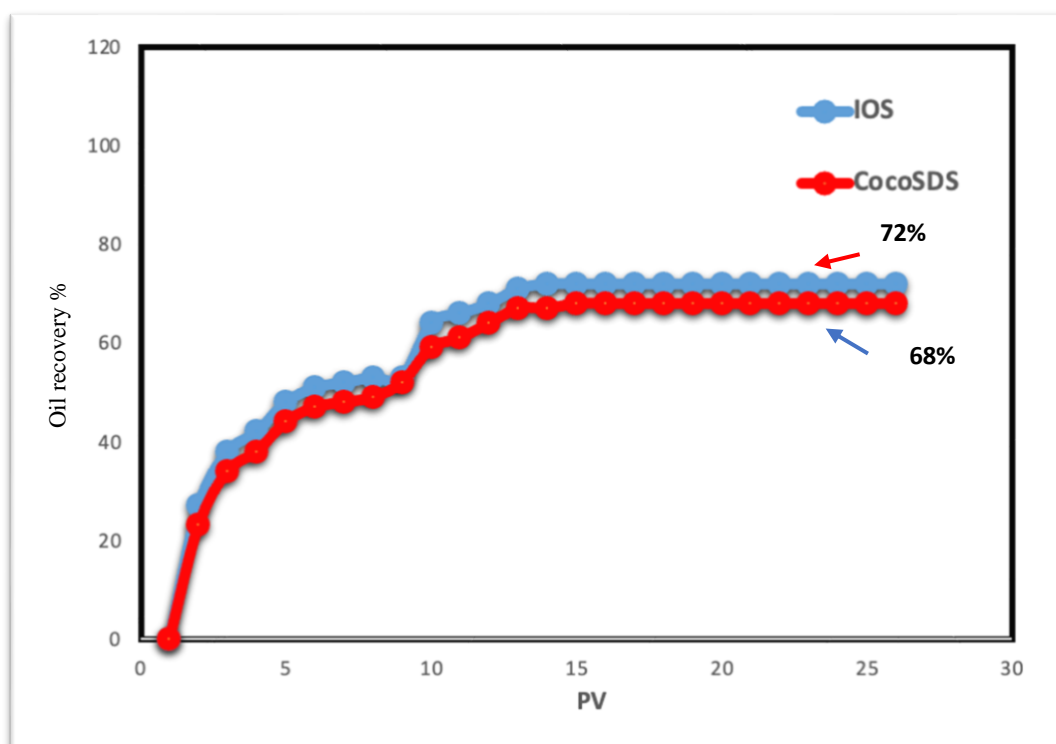


Figure 4. 27: Oil recovery in core B (500mD) using CocoSDS and IOS foam

Extended water flooding (EWF) was carried out after the foam flooding. The final residual oil saturation stayed the same since only less than 1% more oil was recovered after the EWF.

Chapter 4: Results and discussions

4.3.10.1.2 Oil displacement experiment using IOS and CocoSDS foams (alternating injection) in 500 mD core B

Another method of foam flooding is surfactant alternating gas injection. This part discusses the effect of surfactant solution and CO₂ alteration on oil recovery. CocoSDS and IOS were investigated.

Figure 4.28 shows the result of these experiments.

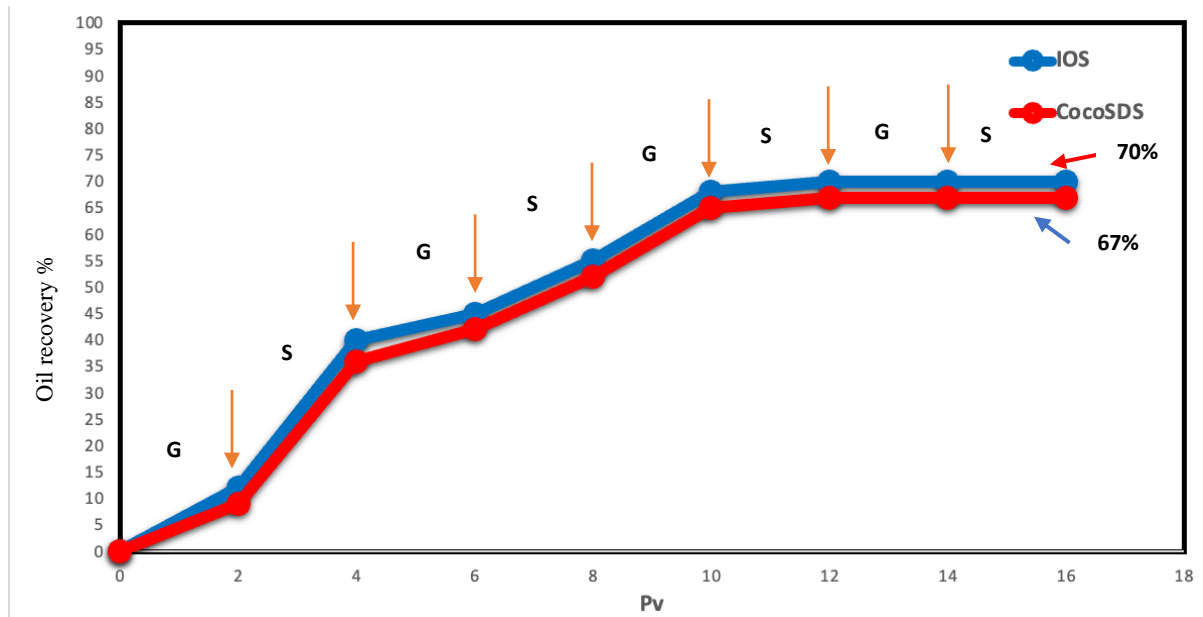


Figure 4. 28: Oil recovery by surfactant IOS and CocoSDS alternating gas injection in core B.

In surfactant alternating gas injection experiment using IOS foam 70% of original oil was recovered compared to 67% of oil recovery by CocoSDS foam. The cumulative oil recovery during the surfactant cycles was slightly more compared to the gas cycles. Due to the higher viscosity of surfactant, more oil was being contacted and pushed towards the injection well. Although more oil production by surfactant was not the case in all cycles.

The oil recovery of surfactant alternating gas injection for IOS foam was 2% less than the oil recovered by co-injection of surfactant (IOS) and gas for the same amount of injected PV. Whereas for CocoSDS foam the oil recovery by alternating method, was 1% less than the oil recovered by co-injection of CocoSDS and gas for the same amount of injected PV.

Due to less oil recovery by surfactant alternating gas injection, the co-injection of gas and surfactant solution was chosen as injection method for the study of the effect of polymer on the performance of foam flooding.

4.3.10.2 Surfactant/polymer foam injection

Pervious pressure drop data and oil recovery results confirm that IOS can recover slightly more oil compared to CocoSDS. Therefore, IOS has been chosen as a foaming agent. In this part the effect of polymer on foam performance is discussed. As mentioned previously in the discussion of sand pack flooding, permeability of the medium has a great impact on foam performance, therefore two cores with different permeabilities have been chosen to study the effect of permeability on the results.

4.3.10.2.1 Oil displacement experiment using IOS foam in presence of HPAM and PPAM (by co-injection) in 500 mD core A

The initial waterflood of the core was conducted to approximately 6 pore volumes of injection at a rate of 0.2 ml/min until it reached a stabilised pressure drop of 15 psi for injection of HPAM foam and 23 psi for PPAM foam as shown on Figure 4.29.

As is clear on Figure 4.30, 53.4% and 53% of original oil was recovered by IWF in both cores (both with same permeabilities) which were used for injection of HPAM and PPAM foam. The oil saturation was reduced from 0.85 to 0.45 (S_{or}) for injecting HPAM foam into the core and decreased from 0.86 to 0.45 (S_{or}) for PPAM foam injection.

Upon switching from IWF to foam injection, an immediate response was observed in the oil recovery followed by an increase in the differential pressure across the core sample for both injections. The stable pressure drop from HPAM foam injection was indicated at 22 psi after injection of almost 10 PV, which gives a mobility reduction (RF) value of 1.5 and the pressure drop for PPAM foam injection was indicated at 37 psi for the same injected PV (10 PV) which gives a mobility reduction (RF) value of 1.6. Oil recovery by HPAM foam increased by 19.6% after IWF to 73% and increased by 26% after IWF to 79% by injection of PPAM foam. The extended water flood was carried out until 15 pore volumes, but the final residual oil saturation almost stayed the same.

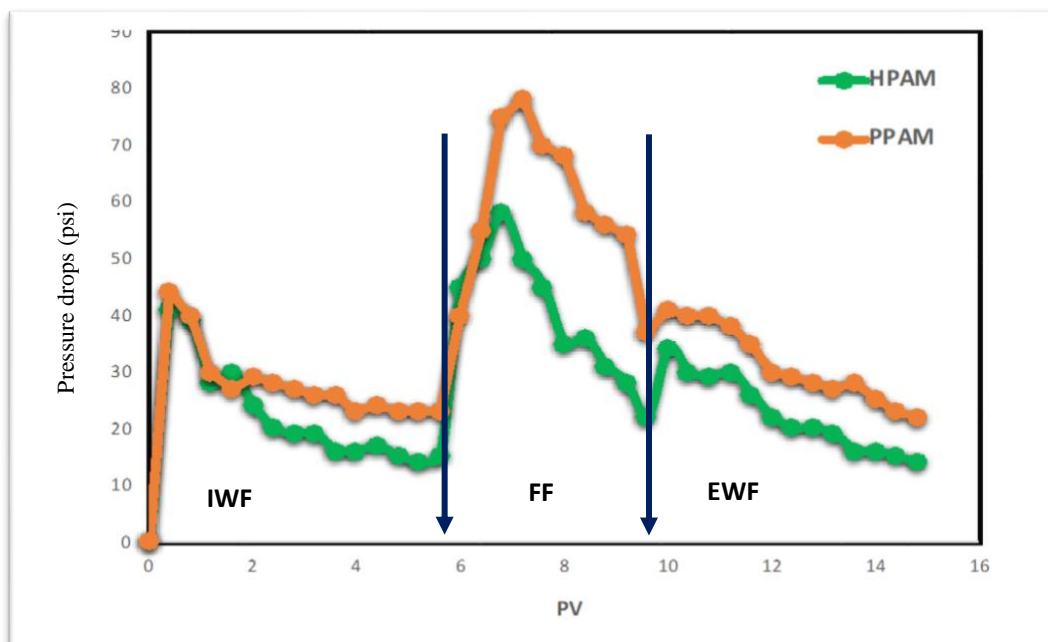


Figure 4. 29: Pressure drop in core A (100mD) using IOS foam in presence of HPAM and PPAM

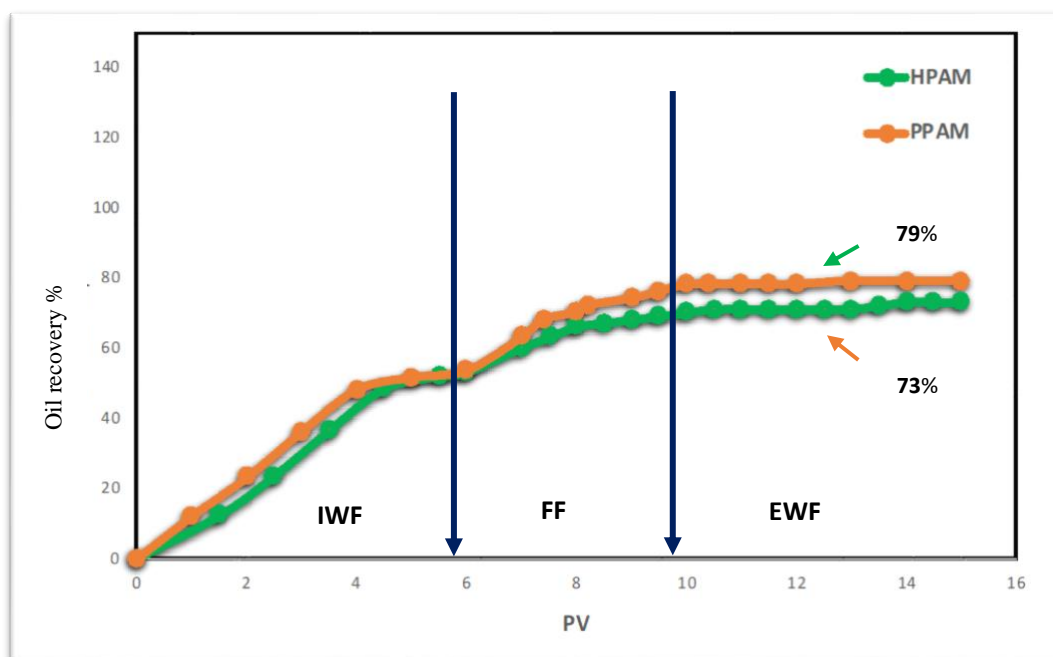


Figure 4. 30: Oil recovery in core A (100mD) using IOS foam in presence of HPAM and PPAM

4.3.10.2.2 Oil displacement experiment using IOS foam in the presence of HPAM and PPAM (by co-injection) in 500 mD core B

The initial waterflood of the core was conducted to approximately 6 pore volumes of injection at a rate of 0.2 ml/min until it reached a stabilised pressure drop at 16 psi in core B before injecting HPAM foam and 16.5 psi for injection of PPAM foam in core B as shown on Figure 4.31.

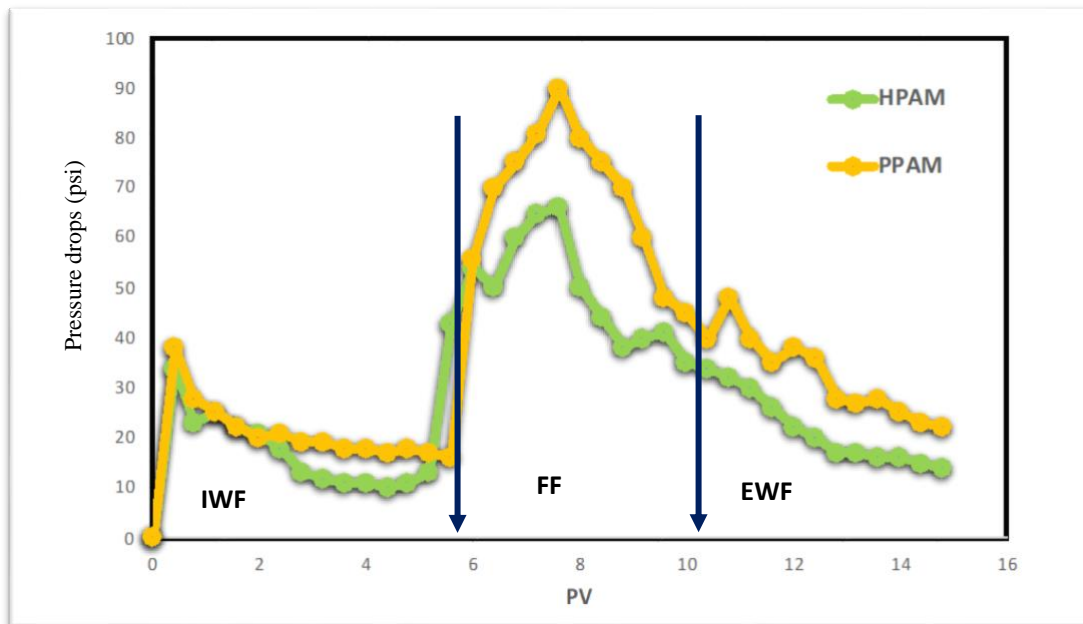


Figure 4. 31: Pressure drop in core B (100mD) using IOS foam in presence of HPAM and PPAM

As is clear on Figure 4.32, 50% of original oil was recovered by IWF in both cores (both with same permeabilities) which were used for injection of HPAM and PPAM foam. The oil saturation was reduced from 0.86 to 0.42 (S_{or}) in the core for injecting PPAM foam and decreased from 0.85 to 0.43 (S_{or}) For HPAM injection. Upon switching from IWF to foam injection, an immediate response was observed in the oil recovery followed by an increase in the differential pressure across the core sample for both injections. The stable pressure drop from HPAM foam injection was indicated at 32 psi which gives a mobility reduction (RF) value of 2 and for PPAM foam injection was indicated at 42 psi which gives a mobility reduction (RF) value of 2.6. Oil recovery by HPAM foam and PPAM increased by 26% to 76% and by 32% to

82% after IWF respectively. The extended water flood was carried out until 15 pore volumes, but the final residual oil saturation almost stayed the same.

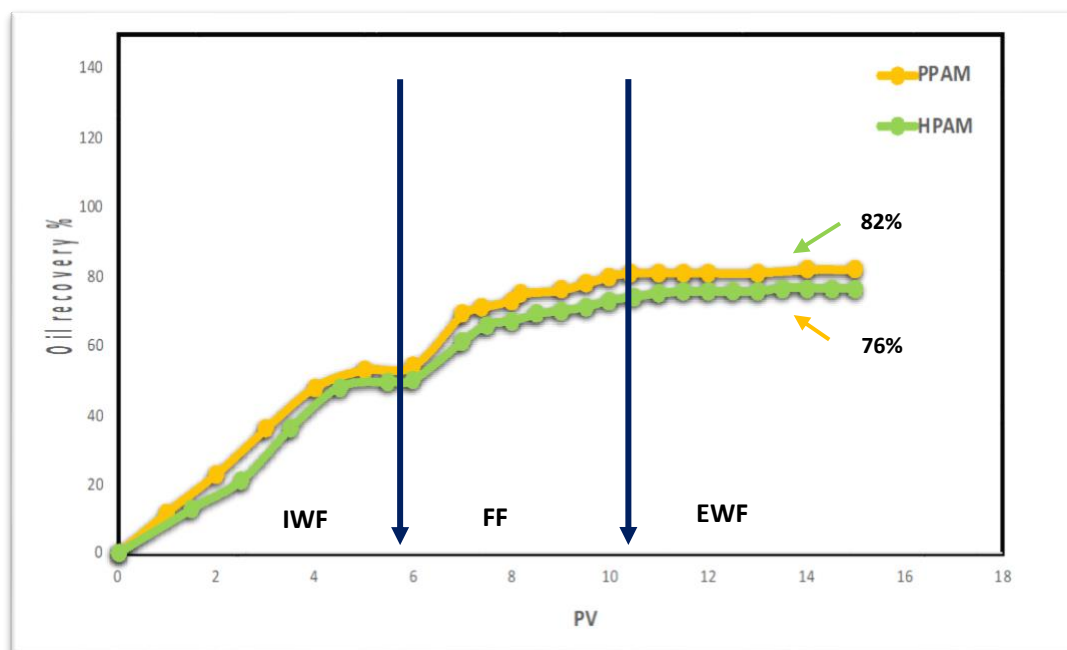


Figure 4. 32: Oil recovery in core B (100mD) using IOS foam in presence of HPAM and PPAM

4.3.10.3 Comparison of oil displacement results of IOS foam in the presence of HPAM (by co-injection) in 100 mD core A and 500 mD core B

As is shown on Figure 4.33 the initial waterflood of the core was conducted to approximately 6 pore volumes of brine injection at a rate of 0.2 ml/min in both cores followed by injection of HPAM foam, until a stabilised pressure drop at 15 psi was reached in core A and 16 psi in core B. Initial waterflood (IWF) performance reached 53.4 % of initial oil volume in core A and 50% of initial oil volume in core B (Figure 4.33), resulting in reduction of oil saturation in core A.

The stable pressure drop from HPAM foam injection in core A with lower permeability (100 mD) was indicated at 22 psi after injection of almost 10 PV, which gives a mobility reduction (RF) value of 1.5, compared to the stable pressure drop from injection of HPAM foam in core B with higher permeability (500 mD) which was indicated at 32 psi that giving a mobility reduction (RF) value of 2.

Chapter 4: Results and discussions

Injection of the same foam in different cores results in different mobility reduction factors as a result of different pressure drops across the cores.

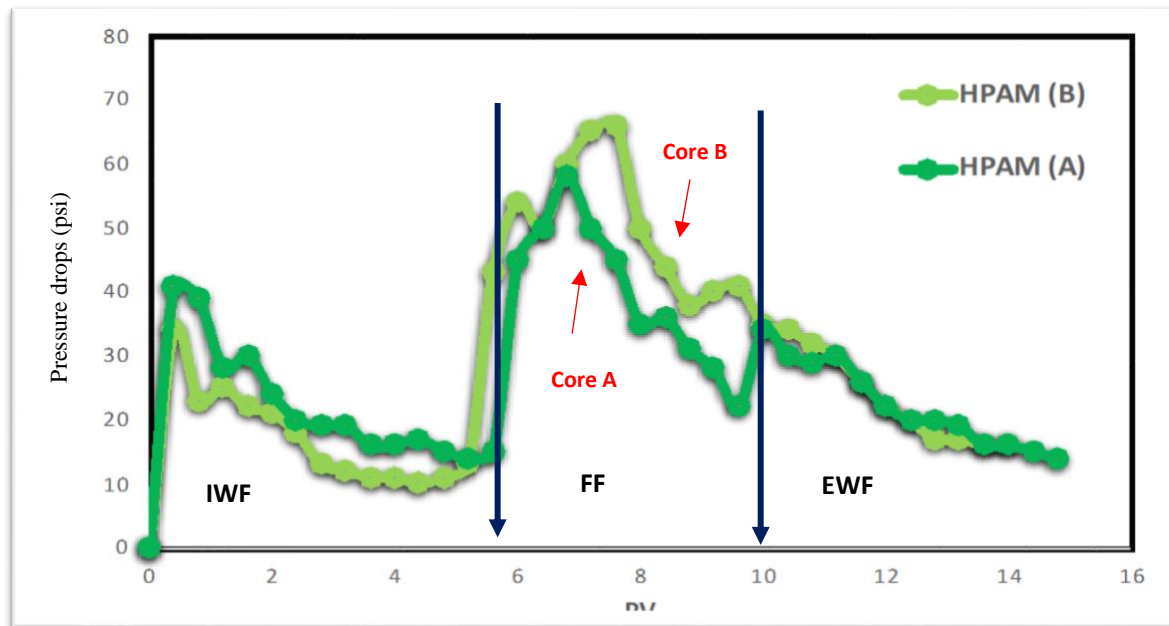


Figure 4. 33: Pressure drop in cores A&B (100mD &500mD) using IOS foam in presence of HPAM

As can be on Figure 4.34, 50% of original oil was recovered by IWF in core A whereas 53.4% of original oil was recovered by IWF in core A, prior to injection of HPAM foam. This was as a result of slightly different amounts of injected water (approximately 6 PV), as well as different permeabilities. The oil saturation was reduced from 0.85 to 0.45 (S_{or}) in core A for HPAM foam injection and decreased from 0.85 to 0.43 (S_{or}) in core B. Oil recovery by HPAM foam increased by 19.6% after IWF to 73% in core A and increased by 26% after IWF to 76% in core B.

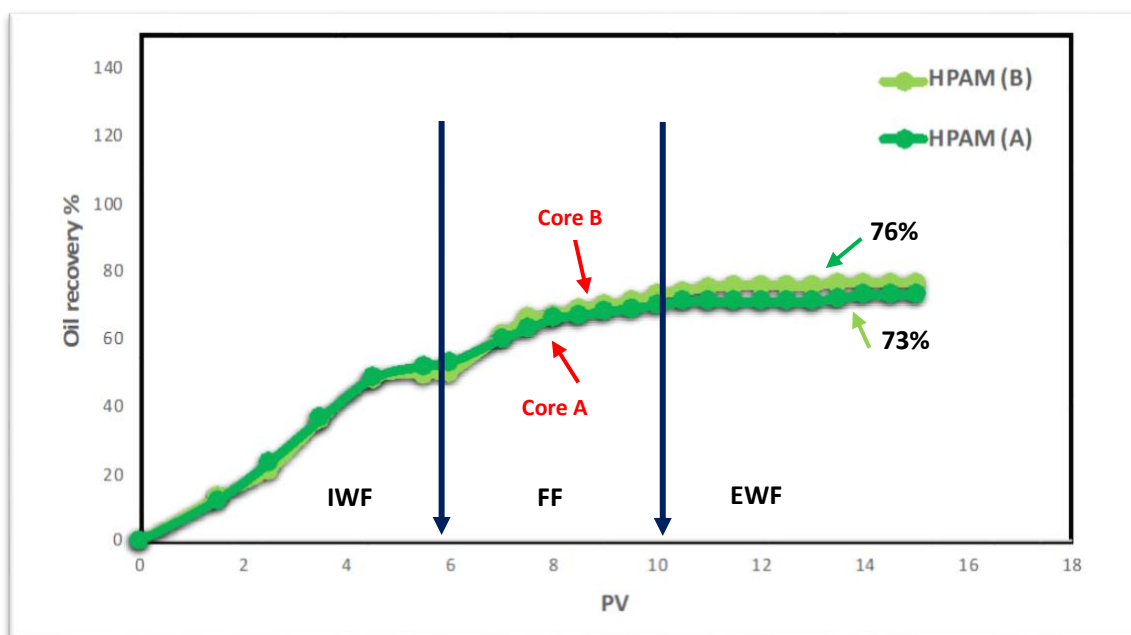


Figure 4. 34: Oil recovery of IOS foam in the presence of HPAM in cores A&B (100mD &500mD)

Although the extended water flood was carried out until 15 pore volumes, the final residual oil saturation almost stayed the same.

4.3.10.4 Comparison of oil displacement results of IOS foam in the presence of PPAM (by co-injection) in 100 mD core A and 500 mD core B

As is clear on Figure 4.35 the initial waterflood of the core was conducted to approximately 6 pore volumes of brine injection at a rate of 0.2 ml/min in both cores and followed by injection of PPAM foam, until a stabilised pressure drop at 15 psi was reached in core A and 16 psi in core B. Initial waterflood (IWF) performance reached 53% of initial oil volume in core A and 50% of initial oil volume in core B (Figure 4.35), resulting in reduction of oil saturation in core A from 0.86 to 0.45 (S_{or}) and 0.86 to 0.42 in core B (S_{or}).

The stable pressure drop from PPAM foam injection in core A with lower permeability (100 mD) was indicated at 37 psi for 10 injected PV which gives a mobility reduction (RF) value of 1.4, compared to the stable pressure drop from injection of PPAM foam in core B with higher permeability (500 mD) which was indicated at 42 psi giving a mobility reduction (RF) value of 2.6.

Chapter 4: Results and discussions

Injection of the same foam in different cores resulted in different mobility reduction factor as a result of different pressure drops across the cores.

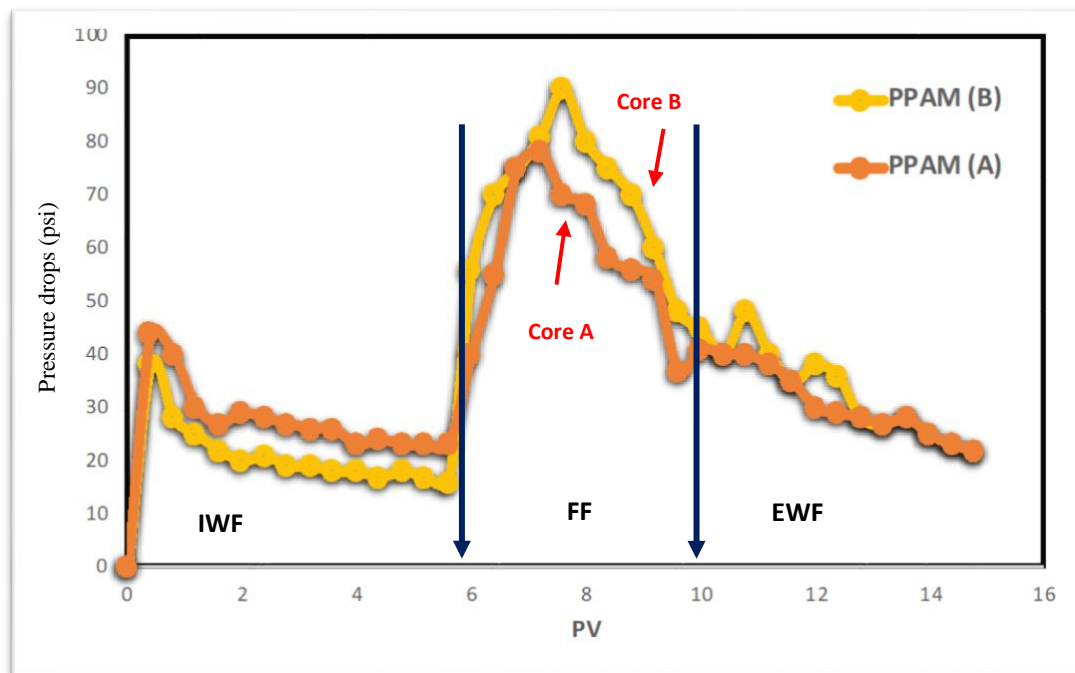


Figure 4. 35: Pressure drop in cores A&B (100mD &500mD) using IOS foam in the presence of PPAM

As can be on Figure 4.36, 50% of original oil was recovered by IWF in core A whereas 53% of original oil was recovered by IWF in core A, prior to injection of PPAM foam. This was as a result of slightly different amounts of injected water (approximately 6 PV), as well as different permeabilities. The oil saturation was reduced from 0.86 to 0.45 (S_{or}) in core A for HPAM foam injection and decreased from 0.86 to 0.42 (S_{or}) in core B. Oil recovery by PPAM foam increased by 26% after IWF to 79% in core A and increased by 32% after IWF to 82% in core B. Although the extended water flood was carried out until 15 pore volumes, the final residual oil saturation almost stayed the same.

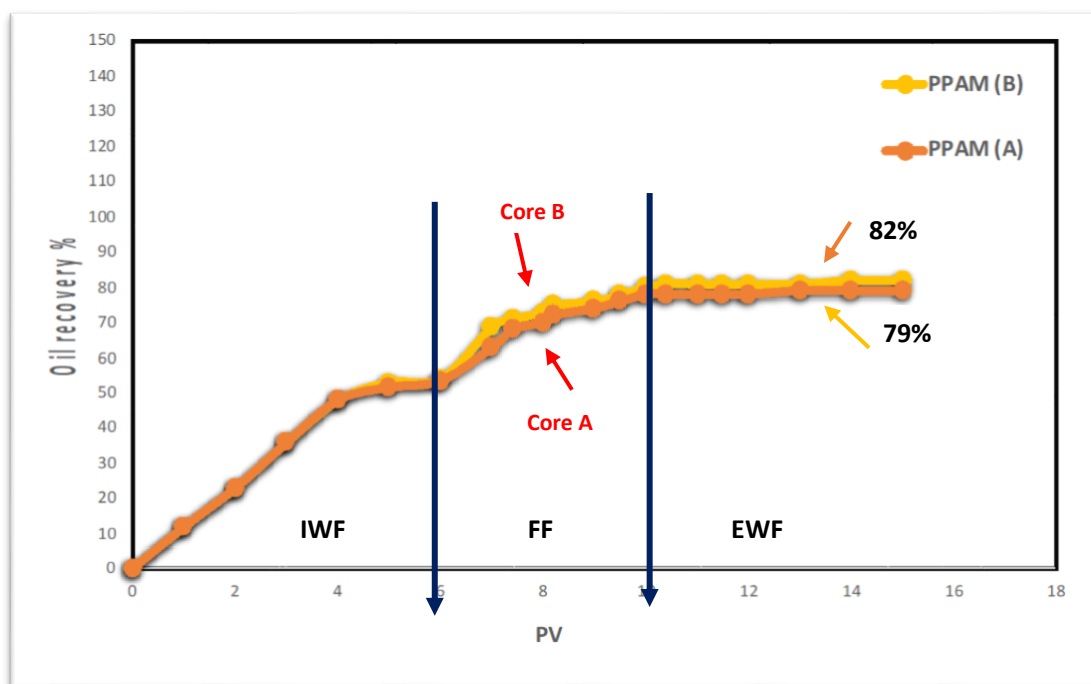


Figure 4. 36: Oil recovery of IOS foam in the presence of PPAM in cores A&B (100mD &500mD)

A Summary of core flooding tests for surfactant foams is shown in Table 4.12.

Summary of core flooding tests for surfactant foams in core B (500 mD)				
Surfactant type	CocoSDS		IOS	
	S_o	S_w	S_o	S_w
Saturation	0.88	0.12	0.87	0.13
IWF	0.48	0.52	0.47	0.53
FF	0.32	0.68	0.28	0.72
EWf	0.32	0.68	0.28	0.72

Table 4. 12: Summary of core flooding tests for surfactant foams

Table 4.12 presents a summary of oil recovery results of surfactant foam injection (CocoSDS and IOS) into core B with 500 mD. It is noticeable that the oil recovery value after the initial water injection (IWF) are very similar, with initial oil volume of 52% for CocoSDS and 53% for IOS. Due to the use of a fresh core for each experiment there was a slightly higher value of oil recovery in the injection of IOS foam experiment which might have been the result of

Chapter 4: Results and discussions

connection of pore spaces. As results show, a greater oil recovery was observed in case of IOS foam injection of 0.72 of original oil volume.

The residual oil saturation (S_{or}) after initial water flooding remains almost constant (0.47 - 0.48) for both tests (Table 4.9). It proves the high level of similarity between the core samples in terms of rock properties such as porosity, permeability, and connected pore spaces.

A Summary of core flooding tests for surfactant/polymer foams is shown in Table 4.13.

Summary of core flooding tests for surfactant/polymer foams in core A & B (100 & 500 mD)								
Surfactant/polymer type	IOS/HPAM				IOS/PPAM			
Core	100 mD		500 mD		100 mD		500 mD	
Parameter	S_o	S_w	S_o	S_w	S_o	S_w	S_o	S_w
Saturation	0.85	0.15	0.85	0.15	0.86	0.14	0.86	0.14
IWF	0.47	0.53	0.50	0.50	0.47	0.53	0.50	0.50
FF	0.27	0.73	0.24	0.76	0.27	0.79	0.27	0.82
EWf	0.27	0.73	0.24	0.76	0.27	0.79	0.27	0.82

Table 4. 13: Summary of core flooding tests for surfactant/polymer foams

As can be seen from table 4.13, four tests were performed by using surfactant/polymer foams (IOS in presence of PPAM and HPAM) in two core samples with different absolute permeabilities of 100 mD and 500 mD. The total volume of brine and polymer solution injected for each experiment was around 15 pore volumes.

A low flow rate of 0.2 ml/min was applied to inject the solutions for all tests, therefore the effect of the shear rate on the solution viscosity is negligible. The viscosity of injected surfactant/polymer solution in the presence of PPAM was higher than for the surfactant/polymer solution in the presence of HPAM. The viscosity of the produced solution reduced slightly in all tests; however, HPAM solution exhibited a slightly larger reduction in viscosity than PPAM solution in all tests. This could be due to the effect of brine salinity. The

presence of Na^+ ion in the brine forms a shield preventing the repulsion between the negative charges on the HPAM molecule, causing less stretching in HPAM polymer. The PPAM molecule structure is on the contrary neutral and therefore shows a higher salinity resistance and therefore a less viscosity reduction. This indicates that PPAM foam is more tolerant to salinity compared to HPAM.

The results from the core flood tests indicate an early breakthrough of water suggesting that viscous fingering mechanisms of displacement appear to be predominant in waterflooding. That is why it is critical to investigate the disadvantage of the fingering effect, especially when the addition of water-soluble polymers to foam can reduce the susceptibility of this displacement.

These tests confirm that presence of PPAM in surfactant solution in high permeable core sample can have a great impact on oil recovery.

Mobility reduction in core B (500 mD)				
Foam type	CocoSDS	IOS	IOS/HPAM	IOS/PPAM
MRF (RF)	1.6	1.6	2.0	2.5

Table 4. 14: Mobility reduction (RF) results in core B for surfactant foams

As can be seen on Table 4.14 In the case of surfactant solution, the mobility reduction (RF) was the same for both CocoSDS and IOS foam, as a result of very similar pressure drop across the core for both injections. For surfactant/polymer solutions, PPAM foam demonstrated higher mobility reduction (RF) compared to HPAM foam which showed higher mobility reduction (RF) than both surfactant foams. The high mobility reduction (RF) of PPAM foam could be due to the larger size of the PPAM molecule as a result of hydrophobic aggregation in the copolymer (Panthi 2014).

Chapter 4: Results and discussions

Mobility reduction in core A&B				
Core	Core B (100 mD)		Core B (500 mD)	
Foam	IOS/HPAM	IOS/PPAM	IOS/HPAM	IOS/PPAM
MRF (RF)	1.5	1.6	2.0	2.5

Table 4. 15: Mobility reduction (RF) results in core A&B for surfactant/polymer foams

As is shown in Table 4.15 for both cores, PPAM foam resulted in a higher mobility reduction (RF) than the HPAM foam in both cores (100mD and 500mD). However, as can be seen from the results, the mobility reduction (RF) was higher in core B with 500 mD.

Chapter 5: Conclusions

5. Chapter 5 Conclusions

5.1 Conclusions

The following conclusions can be drawn from this research:

- CO₂ foam was generated using purely anionic surfactant or a mixture of anionic and cationic surfactants in a chromatography column. Stability of the generated foam was then investigated by measuring of each foam's half-life.
- The effect of presence of polymer and oil in the foaming solution on foam stability was studied.
- Foam that consists of bubbles of large sizes and with a wide range of bubbles size distribution are expected to become unstable.
- Based on foam coalescence tests without oil two general observations were obtained: Foam column have constant height during foam decay and foam decay is caused by liquid drainage indicated by a gradually development of dryer foam.
- The results (in absence of oil) show great stability for IOS and COCOSDS foam in presence and absence of polymer.
- In presence of oil foam was raised with a slower rate as the amount of oil increased and foam column was divided into several parts.
- The foam texture was characterized with non-uniform bubble size distribution in areas where crude oil was spreading on the lamellae and a narrower bubble size distribution in the areas with no or less crude oil present.
- For foam stability experiments in presence of polymers, both HPAM and PPAM have significantly increased foam stability by increasing the foam solution viscosity and decreasing the rate of liquid drainage.
- The results (in presence of oil) show great stability for IOS and COCOSDS foam in presence and absence of polymer.
- IOS and CocoSDS were used in sand pack flooding and core flooding to investigate the effect of using polymeric foam on oil displacement in porous media
- The effect of permeability on foam generation and its strength through its rheological behaviour was investigated through sand pack flooding. Apparent foam viscosity of polymer free and polymer enhanced CO₂ foams was studied. Three sand packs were employed for this purpose.

- The results show that as permeability increased, pressure gradient increased. As a result, a higher apparent viscosity was achieved, which indicated a stronger foam was generated in high permeable zone.
- The sand pack flooding confirms that PPAM foam showed an interesting result. Both the apparent viscosity and foam stability were found to be significantly higher compared to foam free polymer (CocoSDS and IOS) and HPAM foam.
- In this research, for core flooding, the core samples that are used for the experimental investigation on enhanced oil recovery are homogeneous sandstone with small dimensions as a representative of reservoir rocks, however, actual reservoir conditions need to be studied more in details to have a better understanding of polymer enhanced foam flooding. Factors such as heterogeneity of reservoir, long duration of foam injection from injection wells until producer wells and type of reservoir rock are key elements that reduce the viscoelasticity of foam/polymer enhanced foam significantly.
- In the presence of foam, gas mobility in porous media is reduced by gas trapping and viscous resistance of flowing lamellas to gas flow.
- PPAM foam at polymer concentration of 4000 ppm gives a better oil recovery than HPAM foam at the same condition. This could be due to higher viscosity achieved by PPAM compared to HPAM. Sandstone cores with absolute permeabilities of 100mD and 500mD were used for oil recovery. The data collected and compared to each other. This can be due to lower permeability of core which affect the ease movement of fluid.
- mobility reduction (RF) tests were also carried out for both PPAM foam and HPAM foam in core samples. Greater mobility reduction was observed for PPAM foam. This can be due to its larger molecular structure in solution which increases polymer viscosity.
- The results from the core flood tests indicate an early breakthrough of water suggesting that viscous fingering mechanisms of displacement appear to be predominant in waterflooding.

- Viscosity reduction for HPAM foam in core flood tests was slightly greater than PPAM foam in core sample at the same shear rate. This could be due to presence of monovalent cation in brine which affect the viscosity of HPAM more than PPAM.
- The synthesised PPAM foam shows a better viscosity enhancement at the same experimental condition compared to HPAM foam. Viscosity reduction of PPAM foam in core flood test for sandstone was lower than HPAM foam at the same conditions. Therefore, it can be considered as a good candidate for EOR at reservoir condition.

***Chapter 6: Recommendation for future
work***

6. Recommendation for future work

This project has studied the effect of polymer enhanced foam stability on enhance oil recovery. Although the gained results using the hydrophobically modified polymer were very promising, more experimental work such as heterogeneity of reservoir rock, mechanical and microbial degradation of polymers need to be done to ensure the capability of PPAM usage for oilfield application.

The following recommendations are based on the experimental lab work that was carried out in this study:

- A standard procedure for sand packing could be developed to obtain homogenous sand packs. An advantage with respect to homogenous sand packs is that direct comparison of foam generation and flow behavior can be established.
- Polymer enhanced foam injections for EOR in unconsolidated sand pack could be performed in sand packs with larger dimensions. Both cross sectional area and length of the sand packs could be changed because this could yield results more representative for a reservoir.
- In addition, the pressure gradient could be measured across several different intervals of the longer sand pack to evaluate the foam generation.
- More experimental work such as heterogeneity of reservoir rock, mechanical and microbial degradation of polymers need to be done to ensure the capability of PPAM usage for oilfield application
- Oil with different properties can be tested for further investigation.
- During the course of core flood experiments, fluid displacement was conducted in a horizontal direction which reduced the effect of gravitational forces. To understand the effect of gravity on fluid segregation, vertical core flood experiments are recommended.
- A comparison between PPAM with other extensively used polymers in oilfield such as xanthan can be carried out.
- Investigation of parameters such as polymer retention, viscosity of polymer solution in porous media and oil displacement efficiency could be covered.

Chapter 6: Recommendation for future work

- History matching of the experimental data with the use of simulators such as CMG or Eclipse could be carried out.

Chapter 7: References

7. References

Ahmed, S., Elraies, K., Tan, I. and Hashmet, M., (2017) 'Experimental investigation of associative polymer performance for CO₂ foam enhanced oil recovery', *Journal of Petroleum Science and Engineering*, 157, pp.971-979.

Alfakher, A. (2019) 'Carbon Dioxide Mobility and Sweep Alteration Using Surface-Coated Silica Nanoparticles', PhD thesis, The University of Texas at Austin.

Al-Manasir, N., Kjøniksen, A. and Nyström, B., (2009) 'Preparation and characterization of cross-linked polymeric nanoparticles for enhanced oil recovery applications', *Journal of Applied Polymer Science*, 113(3), pp.1916-1924.

Almossawy, M. I., Demiral, B. and Raja, D. M. A. (2011) 'Foam Dynamics in Porous Media and Its Applications in Enhanced Oil Recovery: Review', *Ijrras*.

Alshuaibi, M., Farzaneh, S., and Sohrabi, M. (2018) 'An experimental and simulation investigation on the effect of different gas mixtures on performance of miscible CO₂ injection in HPHT Abu Shabi reservoir', Society of petroleum engineers: SPE, Annual Technical Conference and Exhibition, Dallas, Texas, USA. 24-26 September. pp.1-20.

Alvarez, J.M., Rivas, H., and Rossen, W.R. (2001) 'A Unified Model for Steady-State Foam Behavior at High and Low Foam Qualities', *SPE J.* 6: 325-333

Alwahaibi, Y.M. and Al Hadhrami, A.K. (2011) 'The influence of high permeability lenses on immiscible, first-and multi-contact miscible injection', *Journal of Petroleum Science and Engineering*, 77(3), pp. 313-325.

Chapter 7: References

Amao, A., Siddiqui, S. and Menouar, H. (2012) 'A new look at the minimum miscibility pressure (MMP) determination from slim tube measurements', Society of petroleum engineers: SPE Improved Oil Recovery Symposium, Oklahoma, USA. 14-18 April. pp.1-13.

Andrianov, A. et al. (2012) 'Immiscible foam for enhancing oil recovery: Bulk and porous media experiments', Industrial and Engineering Chemistry Research. doi: 10.1021/ie201872v.

Aronson, A.S., Bergeron, V., Fagan, M., et al. (1994) 'The Influence of Disjoining Pressure on Foam Stability and Flow in Porous Media', Coll. Surf. A.: Physicochem. Eng. Aspects **83**: 109-120.

Ashoori, E., Marchesin, D. and Rossen, W. R. (2011) 'Roles of transient and local equilibrium foam behavior in porous media: Traveling wave', Colloids and Surfaces A: Physicochemical and Engineering Aspects. doi: 10.1016/j.colsurfa.2010.12.042.

Aveyard, R. et al. (1994) 'Aspects of aqueous foam stability in the presence of hydrocarbon oils and solid particles', Advances in Colloid and Interface Science. doi: 10.1016/0001-8686(94)800057.

Balan, B.S., M.S. (2013) 'Dynamics of Foam Mobility in Porous Media', PhD thesis The University of Texas at Austin.

Basheva, E. S. et al. (2000) 'Role of betaine as foam booster in the presence of silicone oil drops', Langmuir. doi: 10.1021/la990777.

Beygi, M. R. et al. (2013) 'A New Approach to Model Hysteresis and Its Impact on CO₂-EOR Processes with Mobility Control Strategies', in SPE Western Regional & AAPG Pacific Section Meeting 2013 Joint Technical Conference. doi: 10.2118/165324-MS.

Chapter 7: References

- Blaker, T. et al. (2002) 'Foam for Gas Mobility Control in the Snorre Field: The FAWAG Project', SPE Reservoir Evaluation & Engineering. doi: 10.2118/78824-PA.
- Brame, S.D. (2019) 'The Effect of Rock Morphology on Steam Foam Rheology', PhD thesis. The University of Texas at Austin.
- Bureiko, A., Trybala, A., Kovalchuk, N. and Starov, V. (2015) 'Current applications of foams formed from mixed surfactant–polymer solutions', *Advances in Colloid and Interface Science*, 222, pp.670–677.
- Caram, Y. (2006) 'On the rheological modelling of associative polymers', *Article in Rheological Act* 46(1):45-57.
- Cavalcante, F. (2016) 'Mobility Control of Gas Injection in Highly Heterogeneous and Naturally Fractured Reservoirs', PhD thesis. The University of Texas at Austin USA.
- Chang, H. L. (1978) 'Polymer flooding technology yesterday, today, and tomorrow', *Journal of Petroleum Technology*, 30, 1,113-1,128.
- Chambers, K.T. and Radke, C.J., (1990). *Capillary Phenomena in Foam Flow Through Porous Media. Interfacial Phenomena in Petroleum Recovery.*
- Chen, M., Rossen, W.R., and Yortsos, Y.C. (2005). *The Flow and Displacement in Porous Media of Fluids with Yield Stress.* Chem. Eng. Sci.
- Delshad, M. et al. (2006) 'Modeling Wettability Alteration in Naturally Fractured Reservoirs', in *Proceedings of SPE/DOE Symposium on Improved Oil Recovery*. doi: 10.2118/100081-PA.
- Dicksen, T., Hirasaki, G. J. and Miller, C. A. (2002) 'Mobility of Foam in Heterogeneous Media: Flow Parallel and Perpendicular to Stratification', *SPE Journal*. doi: 10.2118/78601-PA.

Chapter 7: References

Dupuis, G., Rousseau, D., Tabary, R. and Grassl, B. (2010) 'How to get the Best out of Hydrophobically Associative Polymers for IOR? New Experimental Insights.', SPE Improved Oil Recovery Symposium. doi: 10.2118/129884-MS.

Ekundayo, J.M. and Shawket, G.G. (2013) 'Minimum Miscibility Pressure Measurement with Slim Tube Apparatus – How Unique is the Value?', SPE Reservoir Characterisation and Simulation Conference and Exhibition. Abu Dhabi, UAE. 16-18 September, pp. 1-10.

Ettinger, R. A. and Radke, C. J. (1992) 'Influence of Texture on Steady Foam Flow in Berea Sandstone', SPE Reservoir Engineering. doi: 10.2118/19688-PA.

Exerowa, D., and Kruglyakov, P.M. (1998) '*Foam and Foam Films: Theory, Experiment , Application*', eds. Mobius, D., and Miller, R.S., Amsterdam, the Netherlands: Elsevier Science.

Falls, A. H. et al. (1988) 'Development of a Mechanistic Foam Simulator: The Population Balance and Generation by Snap-Off', SPE Reservoir Engineering. doi: 10.2118/14961-PA..

Falls, A. H., Musters, J. J. and Ratulowski, J. (1989) 'The Apparent Viscosity of Foams in Homogeneous Bead Packs', SPE Reservoir Engineering. doi: 10.2118/16048-PA.

Farajzadeh, R. et al. (2012) 'Foam-oil interaction in porous media: Implications for foam assisted enhanced oil recovery', *Advances in Colloid and Interface Science*. doi: 10.1016/j.cis.2012.07.002.

Farajzadeh, R., Muruganathan, R., Rossen, W. and Krastev, R., (2011) 'Effect of gas type on foam film permeability and its implications for foam flow in porous media', *Advances in Colloid and Interface Science*, 168(1-2), pp.71-78.

Farajzadeh, R., Andrianov, A. and Zitha, P. (2021) 'Foam assisted oil recovery at miscible and immiscible conditions. SPE

Chapter 7: References

Farajzadeh, R., Krastev, Y., and Zitha, P.L.J. (2008) 'Foam Film Permeability: Theory and Experiment', *Adv. in Colloid and Interface Sci.* **137**: 27-44.

Farn, R.J. (2006) '*Chemistry and technology of surfactants*', Oxford, Blackwell Publishing, ISBN-13: 978-1-4051-2696-0

Friedmann, F., Chen, W. H. and Gauglitz, P. A. (1991) 'Experimental and Simulation Study of High-Temperature Foam Displacement in Porous Media', *SPE Reservoir Engineering*. doi: 10.2118/17357-PA.

Garrett, (2013). *The Science of Defoaming: Theory, Experiment and Applications*.

Ghosh, (2016) 'Study of alternating anionic surfactant and gas injection in carbonate core', PhD thesis. The University of Texas at Austin USA

Gauglitz, P. A. et al. (2002) 'Foam generation in homogeneous porous media', *Chemical Engineering Science*. doi: 10.1016/S0009-2509(02)00340-8.

Gauglitz, P. A. et al. (2002) 'Foam Generation in Porous Media', in *SPE/DOE Improved Oil Recovery Symposium*. doi: 10.2118/75177-MS.

Ghosh, P. and Mohanty, K.K. (2018) 'Novel Application of Cationic Surfactants for Foams with Wettability Alteration in oil-wet Low-permeability carbonate rocks', *SPE Journal*, **23**(6), pp. 2218-2231.

Green, D. W. and Willhite, G. P. (1998) 'Enhanced Oil Recovery-Society of Petroleum Engineers Textbook Vol. 6, Soc', *Petroleum Eng.*, Houston, TX.

Grigg, Yi Liu, Baojun Bai, (2005) 'Salinity, pH and Surfactant Concentration Effects on CO₂-Foam.

Chapter 7: References

- Liu, Y., Grigg, R. B. and Svec, R. K. (2005) 'CO₂ Foam Behavior: Influence of Temperature, Pressure, and Concentration of Surfactant', in SPE Production Operations Symposium. doi: 10.2118/94307-MS.
- Gupta, R. and Mohanty, K. K. (2008) 'Wettability Alteration of Fractured Carbonate Reservoirs', in SPE Symposium on Improved Oil Recovery. doi: 10.2118/113407-MS.
- Hadjiiski, N.D. Denkov, S. Tcholakova, I.B. Ivanov, (2003). Role of entry barriers in the foam destruction by oil drops.
- Hahn E., (2015) 'Novel cationic surfactants for CO₂-Foam flooding in carbonate reservoir.
- Haugen, Å., Mani, N., Svenningsen, S., Brattekkås, B., Graue, A., Ersland, G. and Fernø, M., (2014) 'Miscible and Immiscible Foam Injection for Mobility Control and EOR in Fractured Oil-Wet Carbonate Rocks', *Transport in Porous Media*, 104(1), pp.109-131.
- Hematpur, H., Mahmood, S. M., Nasr, N. H., & Elraies, K. A. (2018) '*Foam flow in porous media: Concepts, models and challenges*', *Journal of Natural Gas Science and Engineering*, 53, 163-180. doi:10.1016/j.jngse.2018.02.017
- Hiraski, G., (1989) 'The Steam-Foam Process. *Journal of Petroleum Technology*, 41(05), pp.449-456.
- Hirasaki, G.J., Miller, C. A. and Puerto, M (2011) 'Recent Advances in Surfactant EOR', *SPE Journal*, 16(4), pp. 889-907.
- Hirasaki, G. J. and Lawson, J. B. (1985) 'Mechanisms of Foam Flow in Porous Media: Apparent Viscosity in Smooth Capillaries', *Society of Petroleum Engineers Journal*. doi: 10.2118/12129-PA.

Chapter 7: References

- Hirasaki, G. J., Miller, C. A., Szafranski, R., Tanzil, D., Lawson, J. B., Meinardus, H., Wade, W. H. (1997) 'Field Demonstration of the Surfactant/Foam Process for Aquifer Remediation. Society of Petroleum Engineers. doi:10.2118/39292-MS
- Hadjiiski, N.D. Denkov, S. Tcholakova, I.B. Ivanov, (2003) 'Role of entry barriers in the foam destruction by oil drops.
- Hutchins, R. D. and Miller, M. J. (2005) 'A circulating foam loop for evaluating foam at conditions of use', SPE Production & Facilities. doi: 10.1128/AEM.67.8.3450.
- Jones, S. A. et al. (2016) 'Surfactant screening for foam EOR: Correlation between bulk and core-flood experiments', Colloids and Surfaces A: Physicochemical and Engineering Aspects. doi: 10.1016/j.colsurfa.2016.03.072.
- Kamari, E., Shadizadeh, S. and Rashtchian, D., (2013) 'IMPROVEMENT OF FRACTIONAL FLOW MODEL FOR MISCIBLE DISPLACEMENT PROCESS: AN EXPERIMENTAL INVESTIGATION IN SINGLE FRACTURED POROUS MEDIUM. Journal of Porous Media, 16(3), pp.255-266.
- Kasimbazi G, 2014. Polymer flooding, Norwegian university of Science and Technology.
- Kil, R. A., Nguyen, Q. P. and Rossen, W. R. (2011) 'Determining Trapped Gas in Foam from Computed-Tomography Images', SPE JOURNAL. doi: 10.2118/124157-PA.
- Khatib, Z.I., Hirasaki, G.J., and Falls, A.H. (1988). Effects of Capillary Pressure on Coalescence and Phase Mobilities in Foams Flowing Through Porous Media. *SPE Reservoir Eng.* **3**(3): 919-926.
- Koczko, K., Lobo, L. A. and Wasan, D. T. (1992) 'Effect of oil on foam stability: Aqueous foams stabilized by emulsions', Journal of Colloid And Interface Science. doi: 10.1016/0021-9797(92)90218-B.

Chapter 7: References

- Kornev, K.G., Neimark, A.V., and Rozhkov, A.N. (1999) 'Foam in Porous Media: Thermodynamic and Hydrodynamic Peculiarities', *Adv. in Colloid and Interface Sci.* **82**: 127-187.
- Kovscek, A.R. and Radke, C.J. (1994) 'Fundamentals of Foam Transport in Porous Media, in Foams: Fundamentals and Applications in the Petroleum Industry', ACS Advances in Chemistry Series. 3.
- Kutay, S. and Schramm, L., 2004. Structure/Performance Relationships for Surfactant and Polymer Stabilized Foams in Porous Media. *Journal of Canadian Petroleum Technology*, 43(02).
- Lake, L. W., Russell, J. and Rossen, B., (2014) 'Fundamentals of Enhanced Oil Recovery, Society of Petroleum Engineers', doi: 10.1111/j.1540-8159.2008.01126.x.
- Land,S., (2016) 'Polymer enhanced foam in unconsolidated sand. University of Bergen.
- Lake, L. W., Russell, J. and Rossen, B. (2014) 'Fundamentals of Enhanced Oil Recovery, Society of Petroleum Engineers', doi: 10.1111/j.1540-8159.2008.01126.x.
- Lara-Ceniceros, A., Rivera-Vallejo, C. and Jiménez-Regalado, E., (2007) 'Synthesis and characterization of telechelic polymers obtained by micellar polymerization', *Polymer Bulletin*, 59(4), pp.499-508.
- Lawson, J. B. and Reisberg, J. (1980) 'Alternate Slugs Of Gas And Dilute Surfactant For Mobility Control During Chemical Flooding', in SPE/DOE Enhanced Oil Recovery Symposium. doi: 10.2118/8839-MS.
- Lee, H. O. and Heller, J. P. (1990) 'Laboratory Measurements of CO₂-Foam Mobility', SPE Reservoir Engineering. doi: 10.2118/17363-PA.
- Lee, H. O., Heller, J. P., & Hoefler, A. M. W. (1991). Change in Apparent Viscosity of CO₂ Foam With Rock Permeability. Society of Petroleum Engineers. doi:10.2118/20194-PA

Chapter 7: References

- Li, Q., & Rossen, W. R. (2005) 'Injection Strategies for Foam Generation in Homogeneous and Layered Porous Media. Society of Petroleum Engineers. doi:10.2118/96116-MS
- Li, R. F., Le Bleu, R. B., Liu, S., Hirasaki, G. J., & Miller, C. A. (2008) 'Foam Mobility Control for Surfactant EOR. Society of Petroleum Engineers. doi:10.2118/113910-MS
- Li, R. F. et al. (2012) 'Wettability Alteration and Foam Mobility Control in a Layered , 2D Heterogeneous Sandpack', SPE Journal. doi: 10.2118/141462-MS.
- Liu, Y., Grigg, R. B. and Svec, R. K. (2005) 'CO₂ Foam Behavior: Influence of Temperature, Pressure, and Concentration of Surfactant', in SPE Production Operations Symposium. doi: 10.2118/94307-MS.
- Liu, M., Andrianov, A., & Rossen, W. R. (2011) 'Sweep Efficiency in CO₂ Foam Simulations with Oil. Society of Petroleum Engineers. doi:10.2118/142999-MS
- Liu, R., Liu, H., Li, X., & Fan, Z. (2008) 'The Reservoir Suitability Studies of Nitrogen Foam Flooding in Shengli Oilfield. Society of Petroleum Engineers. doi:10.2118/114800-MS
- Ma, K. et al. (2012) 'Visualization of improved sweep with foam in heterogeneous porous media using microfluidics', Soft Matter. doi: 10.1039/c2sm25833a.
- Mannhardt, K., Novosad, J. J., & Schramm, L. L. (1998) 'Foam/Oil Interactions at Reservoir Conditions. Society of Petroleum Engineers. doi:10.2118/39681-MS
- Mansri, A., Tennouga, L. and Desbrières, J. (2007) 'Viscosimetric behaviour of hydrolyzed polyacrylamide-poly(4-vinylpyridine) [AD37-P4VP] mixture in aqueous solution', European Polymer Journal. doi: 10.1016/j.eurpolymj.2006.10.031.
- Marsden, (1986) 'Foam in porous media. United Estate Department of Energy',.
- Masalmeh, S.K., and Wei, L. (2010) Impact of Relative Permeability Hysteresis, IFT dependent and Three Phase Models on the Performance of Gas Based EOR Processes. Abu Dhabi

Chapter 7: References

International Petroleum Exhibition and Conference. Society of Petroleum Engineers. 1-4 November, UAE. DOI: <https://doi.org/10.2118/138203-MS>

Myers, D. (2005) *Surfactant Science and Technology: Third Edition*, Surfactant Science and Technology: Third Edition. doi: 10.1002/047174607X.

Nguyen, D., Wang, D., Oladapo, A., Zhang, J., Sickorez, J., Butler, R., & Mueller, B. (2014)' Evaluation of Surfactants for Oil Recovery Potential in Shale Reservoirs. Society of Petroleum Engineers. doi:10.2118/169085-MS

Nguyen, T., Rommerskirchen, R., Fernandez, J., & Nguyen, Q. P. (2018). Surfactants As Steam Foam Additives for Thermal EOR Processes. Society of Petroleum Engineers. doi:10.2118/190473-MS

Nguyen, Q. P. et al. (2007) 'Mapping of foam mobility in porous media', *Journal of Petroleum Science and Engineering*. doi: 10.1016/j.petrol.2006.12.007.

Nguyen, Q. P., Currie, P. K. and Zitha, P. L. J. (2004) 'Motion of foam films in diverging-converging channels', *Journal of Colloid and Interface Science*. doi: 10.1016/j.jcis.2003.12.010.

Pandey, A. et al. (2008) 'Chemical Flood Simulation of Laboratory Corefloods for the Mangala Field: Generating Parameters for Field-Scale Simulation', *Proceedings of SPE/DOE Symposium on Improved Oil Recovery*. doi: 10.1007/978-3-540-88655-6-2.

Pope, G., Tsaur, K., Schechter, R. and Wang, B., 1982. The Effect of Several Polymers on the Phase Behavior of Micellar Fluids. *Society of Petroleum Engineers Journal*, 22(06), pp.816-830.

Chapter 7: References

Osei-Bonsu, K., Shokri, N. and Grassia, P. (2015) 'Foam stability in the presence and absence of hydrocarbons: From bubble- to bulk-scale', *Colloids and Surfaces A: Physicochemical and Engineering Aspects*. doi: 10.1016/j.colsurfa.2015.06.023.

Osei-Bonsu, K., Grassia, P. and Shokri, N. (2017) 'Relationship between bulk foam stability, surfactant formulation and oil displacement efficiency in porous media', *Fuel*. doi: 10.1016/j.fuel.2017.04.114.

Osterloh, W.T., and Jante, M.J. (1992). Effects of Gas and Liquid Velocity on Steady State Foam Flow at High Temperature. SPE Paper 24179 presented at the SPE/DOE Eight Symposium on Enhanced Oil Recovery, Tulsa, OK, 22-24 April.

Ransohoff, T. C. and Radke, C. J. (1988) 'Mechanisms of Foam Generation in Glass-Bead Packs', *SPE Reservoir Engineering*. doi: 10.2118/15441-PA.

Rossen, W. R. et al. (2010) 'Injection Strategies To Overcome Gravity Segregation in Simultaneous Gas and Water Injection Into Homogeneous Reservoirs', *SPE Journal*. doi: 10.2118/99794-PA.

Ramadhan, G., Hirasaki, G., & Nguyen, Q. P. (2018, April 14). Foaming Behavior of CO₂-Soluble, Viscoelastic Surfactant in Homogenous Porous Media. Society of Petroleum Engineers. doi:10.2118/190302-MS.

Ren, G., Zhang, H., and Nguyen, Q.P. (2011) 'Effect of Surfactant Partitioning between CO₂ and Water on CO₂ Mobility Control in Hydrocarbon Reservoirs', presented at SPE Enhanced Oil Recovery Conference, Kuala Lumpur, Malaysia, 19-21 July. Paper SPE 145102

Chapter 7: References

Sagir, M. et al. (2014) 'Synthesis of a New CO₂ Philic Surfactant for Enhanced Oil Recovery Applications', Journal of Dispersion Science and Technology. doi: 10.1080/01932691.2013.803253.

Sandersen, S. (2012) 'Enhanced oil recovery with surfactant flooding', PhD thesis, Denmark, Technical University of Denmark.

Schramm, L.L. (1994). Foams: Basic Principles. In Foams: Fundamentals and Applications in the Petroleum Industry, ed. L.L. Schramm, Washington, DC: ACS Advances in Chemistry Series, American Chemical Society.

Schramm, L. L. and Green, W. H. F. (1995) 'The influence of marangoni surface elasticity on gas mobility reductions by foams in porous media', Colloids and Surfaces A: Physicochemical and Engineering Aspects. doi: 10.1016/0927-7757(94)02997-7.

Shaohua G, Yang H, (2015), An anti-biodegradable hydrophobic sulfonate- based acrylamide copolymer containing 2,4-dichlorophenoxy for enhanced oil recovery. New J. Chem, 39, 9265-9274.

Shen, C. et al. (2006) 'Does Polymer Stabilize Foam in Porous Media?', in Proceedings of SPE/DOE Symposium on Improved Oil Recovery. doi: 10.2523/99796-MS..

Sheng, J. (2013) Modern Chemical Enhanced Oil Recovery Theory and Practice, Journal of Chemical Information and Modeling. doi: 10.1016/B978-1-85617-745-0.00013-9.

Sheng, J. J. (2011) Modern Chemical Enhanced Oil Recovery, Modern Chemical Enhanced Oil Recovery. doi: 10.1016/C2009-0-20241-8.

Chapter 7: References

- Sheng, J. J. and Chen, K. (2014) 'Evaluation of the EOR potential of gas and water injection in shale oil reservoirs', *Journal of Unconventional Oil and Gas Resources*. doi: 10.1016/j.juogr.2013.12.001.
- Shokrollahi, A., Ghazanfari, M. H. and Badakhshan, A. (2014) 'Application of foam floods for enhancing heavy oil recovery through stability analysis and core flood experiments', *Canadian Journal of Chemical Engineering*. doi: 10.1002/cjce.22044.
- Shramm, L. (2000) 'Surfactants: Fundamentals and applications in the petroleum industry', Cambridge, Cambridge University Press, ISBN 0-521- 640679.
- Simjoo, M. et al. (2013) 'CT scan study of immiscible foam flow in porous media for enhancing oil recovery', *Industrial and Engineering Chemistry Research*. doi: 10.1021/ie300603v.
- Sochi T, 2010, Flow of non-newtonian fluids in porous media, *journal of polymer science*, Volume 48, 2437–2767.
- Sorbie, K. S. (2013) 'Polymer-improved oil recovery, Springer Science & Business Media.
- SYDANSK, R. 1994a. Polymer-enhanced foams part 1: laboratory development and evaluation', *SPE Advanced Technology Series*, 2, 150-159.
- Srivastava, M. et al. (2009) 'A Systematic Study of Alkaline-Surfactant-Gas Injection as an EOR Technique', *Society of Petroleum Engineers Journal*. doi: 10.2118/01110-0042-JPT.
- Tang, G. Q. and Kovscek, A. R. (2006) 'Trapped gas fraction during steady-state foam flow', *Transport in Porous Media*. doi: 10.1007/s11242-005-6093-4.
- Tanzil, D., Hirasaki, G. J., & Miller, C. A. (2000)' Mobility of Foam in Heterogeneous Media: Flow Parallel and Perpendicular to Stratification. Society of Petroleum Engineers. doi:10.2118/63228-MS

Chapter 7: References

Vassenden, F. and Holt, T. (2000) 'Experimental Foundation for Relative Permeability Modeling of Foam', in conference. doi: 10.2118/62506-PA.

Vikingstad, A. K. et al. (2005) 'Foam-oil interactions analyzed by static foam tests', *Colloids and Surfaces A: Physicochemical and Engineering Aspects*. doi: 10.1016/j.colsurfa.2005.02.034.

Vitasari, D., Grassia, P. and Martin, P. (2013) 'Surfactant transport onto a foam lamella', *Chemical Engineering Science*. doi: 10.1016/j.ces.2013.08.041.

Wever, D. A. Z., Picchioni, F. and Broekhuis, A. A. (2011) 'Polymers for enhanced oil recovery: A paradigm for structure-property relationship in aqueous solution', *Progress in Polymer Science (Oxford)*. doi: 10.1016/j.progpolymsci.2011.05.006.

Xu, X., Saeedi, A. and Liu, K. (2016) 'Laboratory studies on CO₂ foam flooding enhanced by a novel amphiphilic ter-polymer', *Journal of Petroleum Science and Engineering*. doi: 10.1016/j.petrol.2015.10.025.

Xu, X., Saeedi, A. and Liu, K. (2017) 'An experimental study of combined foam/surfactant polymer (SP) flooding for carbone dioxide-enhanced oil recovery (CO₂-EOR)', *Journal of Petroleum Science and Engineering*. doi: 10.1016/j.petrol.2016.11.022.

Zhang, Y. et al. (2000) 'New and Effective Foam Flooding To Recover Oil in Heterogeneous Reservoir', in *SPE/DOE Improved Oil Recovery Symposium*. doi: 10.2118/59367-MS.

Zhou, Z.H., and Rossen, W.R. (1995). Applying Fractional-Flow Theory to Foam Processes at the Limiting Capillary Pressure. *SPE Adv. Tech. Series* **3**(1): 154- 162.